THE REPRESENTATION OF SPACE IN MAMMALS

Resolution of Stochastic Place and Grid Codes

Alexander Mathis

Dissertation at the
Graduate School of Systemic Neuroscience at the
Ludwig-Maximilians-Universität München

Graduate School of
Systemic Neurosciences
LMU Munich

Dissertation at the
Graduate School of Systemic Neuroscience at the
Ludwig-Maximilians-Universität München

THE REPRESENTATION OF SPACE IN MAMMALS

Resolution of Stochastic Place and Grid Codes

Submitted by
Alexander Mathis
München, 13th of June 2012

First Supervisor / Reviewer
Prof. Andreas Herz
Second Supervisor / Reviewer
Dr. Martin Stemmler

Date of Oral Defense:
July 30, 2012

Für Opi.

ABSTRACT

Animals require cognitive maps for efficiently navigating in their natural habitat. Cognitive maps are a neuronal representation of their outside world. In mammals, place cells and grid cells have been implicated to form the basis of these neuronal representations. Place cells are active at one particular location in an environment and grid cells at multiple locations of the external world that are arranged in a hexagonal lattice.

As such, these cell types encode space in qualitatively different ways. Whereas the firing of one place cell is indicative of the animal's current location, the firing of one grid cell suggests that the animal is at any of the lattice's nodes. Thus, a population of place cells with varying parameters (place code) is required to exhaustively and uniquely represent an environment. Similarly, for grid cells a population with diverse encoding parameters (grid code) is needed. Place cells indeed have varying parameters: different cells are active at different locations, and the active locations have different sizes. Also, the hexagonal lattices of grid cells differ: they are spatially shifted, have different distances between the nodes and the sizes of the nodes vary in their magnitude. Hence, grid codes and place codes depend on multiple parameters, but what is the effect of these on the representation of space that they provide?

In this thesis, we study, which parameters are key for an accurate representation of space by place and grid codes, respectively. Furthermore, we investigate whether place and grid codes provide a qualitatively different spatial resolution.

OVERVIEW

The research is presented in the form of articles; two accepted papers and two manuscripts. The complete articles are included as single chapters, each preceded by a brief summary and a clarification of my specific contribution. In addition, the following paragraphs provide a brief overview of the organization of the thesis.

In the introduction, we recapitulate the spatial behavior of animals, which suggests that they have cognitive maps, and the

neuronal basis of spatial representations in mammals. In particular, we review experimental results on place and grid cells. Then we state our research questions.

In the first paper, grid codes and place codes that represent a one dimensional environment, called linear track, are compared (chapter 2). We show that a typical grid code outperforms a place code. Specifically, we derive optimal parameter regimes for both codes. For place codes, the analysis reveals that the resolution is optimized by a population of place cells with constant sizes, and that varying sizes are not advantageous. For grid cells, however, the different spatial scales of the hexagonal lattices *can* substantially improve the coding accuracy. We demonstrate that nested grid codes, where the spatial periods are staggered, offer the highest resolution.

These nested grid codes have a resolution that scales exponentially in the number of neurons, rather than linearly as for place codes. Therefore, even for small population sizes, nested grid codes offer substantially more resolution. Neuronal representations with unimodal tuning curves, like place codes, are abundant in the brain and encode various stimulus spaces with varying dimensions. We generalize the nested coding strategy to codes that represent spaces of arbitrary dimensions and verify the better scaling properties for this case too. This suggests that nested, periodic neuronal representations could also be used for other stimulus variables than space 3.

In all the preceding articles the neurons are statistically independent in their firing. In chapter 4, we treat grid codes and place codes with noise correlations. As we point out, noise correlations do not affect the qualitative scaling of the resolution.

In the last study, we derive the optimal characteristics for grid codes representing a planar environment. These optimal characteristics are then compared to the measured properties of grid cells. We point out the similarities, and argue that the grid code indeed appears to be optimized for its presumed task: accurately encoding space (chapter 5).

Finally, these results are discussed jointly and some future research questions are stated.

CONTENTS

1 INTRODUCTION

> Ich bin. Aber ich habe mich nicht.
> Darum werden wir erst.
>
> Ernst Bloch, [10].

We start by describing certain spatial behaviors of animals, which indicate that they possess cognitive maps of their environment. As we will then show, in mammals these maps are believed to be supported by place and grid cells. Studying the spatial resolution of such maps, formed by populations of place or grid cells, is at the heart of this thesis. In particular, we investigate the characteristics of place and grid cells that affect the resolution of such spatial representations.

1.1 SPACE AND SPATIAL BEHAVIOR

Philosophers position themselves in different paradigms regarding the matter of *space*. Some regard it as an entity in itself, others as a framework for holding relations among entities or as an apriori structure waiting to be filled by a posteriori experience [68, 103]. While classical Physics resided in three-dimensional space, Einstein transferred it to the continuum of space-time [85]. Similarly, in Mathematics space came a long way from Euclid's elements, via Descartes' analytic geometry to non-Euclidean geometries and finally, the notion of topological spaces [133].

Here, however, we take a much more pragmatic stance. Space is merely considered as the *physical arena* of our behavior, where we live in, navigate through, plan, and defend ourselves [103]. Most animals are motile and their abilities to move in space are astonishing. For instance, many types of open-ocean predatory fish choose their foraging strategy as either Brownian or Lévy motion depending on the abundance of food. When food is scarce animals move according to Lévy flights, a class of random walks with jumps distributed like a power-law. Then the trajectories of animals remind of fractal curves. It has been argued that such movements are the most efficient ones for catching patchy

prey that occurs in low concentrations. Brownian motion, on the other hand, feeds the animal well enough when food is abundant [61].

Another staggering ability beside foraging is exemplified by the behavior of digger wasps, which was eloquently described by Gallistel [46]:

> "Digger wasps dig nest burrows in which they lay an egg. They cover the burrow entrance with pebbles, making it all but invisible, then fly off in search of insect prey. They sting their prey to paralyze it, carry it back to the burrow, open the burrow, drag the prey inside, exit the burrow and close it up again. The larva that hatches from the egg eats the paralyzed, still living prey."

How can digger wasps remember the location of their invisible nest? Tinberger and Kruyt established that the configuration of landmarks near the nest guides the wasp, rather than a *sensory trace*. If such landmarks, like pine cones and sticks are moved together, the wasp looks for the nest at the corresponding point in the moved configuration, rather than at the unaltered location of the nest [46]. In order to remember these features wasps systematically orbit around their nest to update their visual memory about the goal location, before leaving to catch prey [151]. Yet, such a "snapshot" of a goal relative to landmarks is a *map*, which more specifically, if it is stored in the brain, is called *cognitive map* [46, 103, 137]. With this notion in mind, the wasp's behavior can be summarized by stating that the wasp forms a cognitive map of the nest's neighborhood that is later used to find the nest [46]. Such behavior is widespread among animals, including mammals. And as one might expect, not just the close vicinity of the nest is captured in a cognitive map, but the large-scale environment as well [46, 89, 90, 103, 137]. This navigation strategy is called *piloting* [46].

As we have seen for digger wasps, when animals pilot, they orient themselves according to comparisons of their current environment to spatial memories. The salient cues, which are decisive for storing snapshots and comparing those to the current environment, vary of course from species to species. Typical landmarks can be mundane objects like pine cones, sticks, or larger objects like trees, hills or gas stations, but also the stars, the sun, odor traces or geomagnetic field lines [103]. For instance, pigeons are capable of orienting based on both the position of the sun and their magnetic sense [103].

Navigation is not solely based on orienting according to landmarks, however. A standard taxonomy of navigation classifies the strategies of animals into *piloting* and *dead reckoning* [46, 110]. Dead reckoning is a complementary strategy of integrating speed and heading-direction over time, such that the current position can be known from a past position plus the movements afterwards [36, 46, 110]. Desert ants can return directly after foraging over hundreds of meters through unfamiliar, seemingly identical territory. Bees are even adept of homing after kilometers of tortuous flights [143]. The internal position estimate can be the result of counting steps, as in desert ants [149], or of integrating optic flow, like in honeybees [34, 130]. Another name for dead reckoning is path integration, and mammals also employ this method, as shown by their ability to head home straightly after a circuitous route [36, 92]. Meticulously controlled experiments demonstrated that they achieve this by integrating head-direction and speed. Mammals have a vestibular organ that measures angular and linear acceleration by the semicircular canal system and the otoliths, respectively [143]. These signals are supported by somatosensory information and motor efference copy [35, 92, 110, 143]. Together they allow the mammal's brain to internally compute its position. As one might expect, similar mechanisms can be used when navigating towards a goal rather than the nest [37]. However, path integration is, due to its nature of adding up small motion increments an inherently noisy process [7, 38]. As such, especially for long-range navigation, it has to be supplemented by other non-self-generated signals that correct the errors in the internal representation, like landmarks, etc. [36, 143]. Bees, for instance, return to Lévy flights, when they have completely lost track of their hive – which is the most efficient search strategy to find their hive [115], because from a random position the hive can be considered as "scarcely distributed", as the prey for for predatory fish.

So far we have seen ethological observations about how animals navigate through *physical space* and how navigation is supported by cognitive maps that are updated by both self-motion signals and sensory cues. As the examples indicate, the importance of spatial memory for spatial behavior cannot be underestimated. Where these maps reside in the brain was not addressed, however. Thus in the next section we will have a look at this topic and from now on focus on mammals. We will mostly concentrate on rats, as they are the predominating experimental model system for mammalian spatial cognition [36].

1.2 THE NEURONAL REPRESENTATION OF SPACE

A broad corpus of anatomical, physiological, and lesion evidence supports the hypothesis that the hippocampus and adjacent structures are involved in the representation of space [36, 88, 96, 103, 110]. The hippocampal formation is a compound structure that encompasses the hippocampus proper as well as the dentate gyrus and the subiculum. Superficial layers of the entorhinal cortex (EC) project to the hippocampal formation, while deep layers receive hippocampal feedback ([141, 148], figure 1). These structures receive multimodal sensory input, including head-direction and proprioceptive signals [141].

Two fundamental observations brought the *hippocampus* to the forefront of research about space and more generally memory [110]:

- In 1971 O'Keefe and Dostrovsky found cells, basically in the middle of the *rodents'* brain, far away from all sensory areas that had an obvious correlate. These cells have a high elevated firing rate at one location and are practically silent elsewhere. For this reason they are called *place cells* [102].

- In humans lesions of the hippocampus, and more broadly of the temporal lobe, cause severe loss of recent *declarative memory*.[1] Lesioned subjects, like H.M., fail to transfer content from their short-term memory to the long-term memory – they suffer an anterograde amnesia [119].

Both insights had a profound impact on theories of the hippocampus, each inspiring one of the prevailing theories: On the one hand, that place cells are the building blocks of the cognitive map [103], and, on the other hand, that the hippocampus associates episodes to form memories, which are transferred to the cortex [31, 73, 80, 128]. Similarly to humans, the spatial memory of rats is impaired, when their hippocampus is lesioned [94]. The human hippocampus has also been implicated in navigation, as for instance the hippocampi of London's taxi drivers are significantly larger than those of controls [79], and place cells in humans have been reported by brain imaging [78] and physiological recordings [33]. As we will see in the next section, place cells indeed provide a spatial map, and their memory component cannot be disregarded [32, 99, 103].

1 Memory can be divided in declarative and procedural memory. While *procedural memory* keeps skills learned through practice, declarative memory holds facts, events, knowledge and episodes. Thus, another name for declarative memory is episodic memory [110, 128].

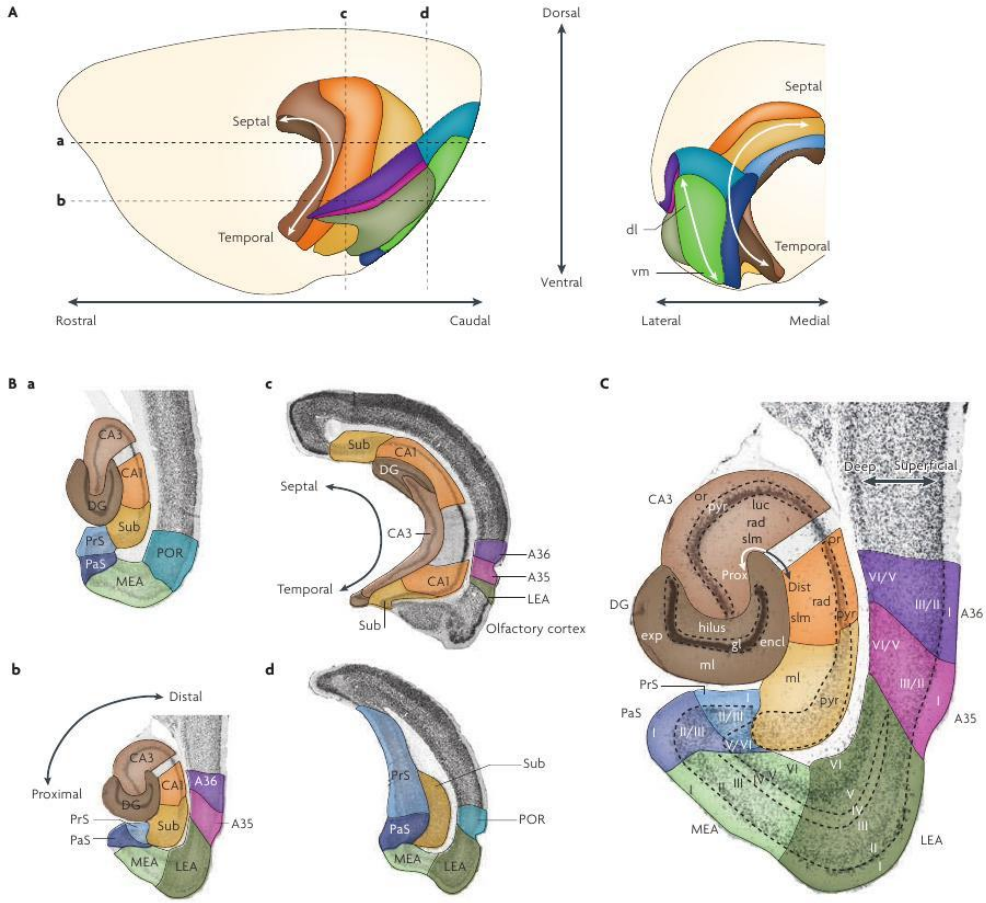

Figure 1: Illustration of the hippocampal formation and parahippocampal region in the rat. **A:** Lateral (left) and caudal (right) views of hippocampal formation and parahippocampal region in the rat. The *hippocampus proper* comprises the dentate gyrus (DG; dark brown), CA3 (medium brown), CA2 (not indicated), and CA1 (orange); together with the subiculum (Sub; yellow)) it is called *hippocampal formation*. The parahippocampal region consists of the presubiculum (PrS; medium blue), parasubiculum (PaS; dark blue), and the entorhinal cortex, which has a lateral (LEA; dark green) and a medial (MEA; light green) part, the perirhinal cortex (A35; pink and A36; purple) and the postrhinal cortex (POR; blue-green). The dashed lines in the left panel mark the planes of two horizontal sections (a,b) and two coronal sections (c,d). These sections are depicted with the same color code in **B**. **C:** A nissl-stained horizontal cross section (expanded from **B**b). The cortical layers are labeled with Roman ciphers. For the layers in the hippocampus the following abbreviations are used: *gl*, granule cell layer; *luc*, stratum lucidum; *ml*, molecular layer; *or*, stratum oriens; *pyr*, pyramidal cell layer; *rad*, stratum radiatum; *slm*, stratum lacunosum-moleculare. Figure reprinted with permission from [141].

1.2.1 Place cells

Place cells in the hippocampus proper and dentate gyrus typically code a single location in the environment by a high firing rate when the animal is at that location, and remain silent elsewhere [102, 103]. For a place cell, the region of space that corresponds to active firing is called the place field. The centers of place fields are distributed all over the experimental environment ([146], Fig. 2a) and the diameter of place fields increases along the dorsoventral axis of the hippocampus from values of 20cm up to at least 10m [70]. In larger environments, a single place cell sometimes exhibits more than one place field [74, 107].

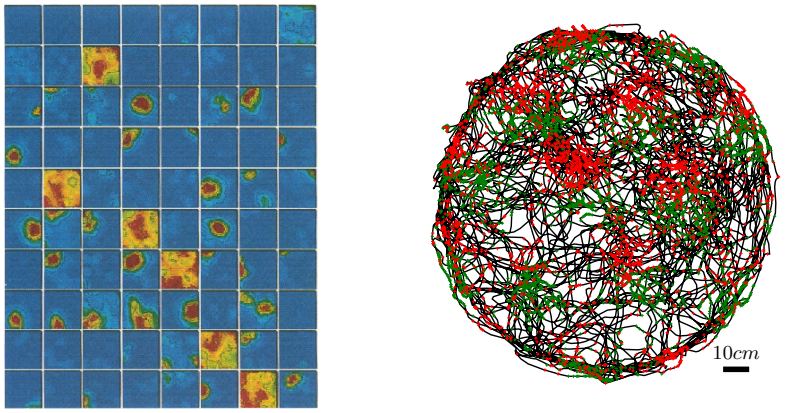

(a) (b)

Figure 2: (a) Firing maps of 80 simultaneously recorded pyramidal and inhibitory neurons of the rat hippocampus. Each panel represents the spatial firing rate of one cell, averaged over the whole recording session within a quadratic box. High firing rates are depicted in red, medium rates in yellow and low firing rates in blue. Inhibitory cells show rather spatially unspecific firing and have high firing rates all over the environment. The centers of the place fields are distributed all over the environment. Reprinted with permission from [146]. (b) The trajectory of a foraging rat within a circular arena is depicted in black. The spatial positions of spikes from two grid cells in red and green are shown. Both units were extracted from one tetrode recordings and are therefore anatomically close. Both cells exhibit multiple firing fields that are arranged like a hexagonal lattice. Their lattices are similar, yet spatially translated; they represent different spatial phases. Figure generated from publicly available data (`http://www.ntnu.no/cbm/moser/gridcell`, [55]).

Already a moderately large population of place cells, like the ones depicted in Fig. 2a, can be used to accurately reconstruct

the rat's position [146]. The firing of place cells is determined by both allocentric cues [101] and idiothetic variables [103, 140]. All this merely implies a correlation of place cell firing and position. Indeed, the causality has not been proven conclusively, but sophisticated experiments suggest that the firing of place cells appear to mirror the internal position estimate of the rat.[2]

Place cell firing is stable in familiar environments [41, 95]. Furthermore, it has been pointed out that the spatial representation of place cells could be innate, as neurons with place cell activity appear just days after rat pups open their eyes [72, 145]. However, place cells do not *simply* form a spatial map: firstly, the firing rate of place cells is contextually modulated.[3] Secondly, the spatial map that place cells provide is not topographic, i.e. the proximity relationships of place cells change drastically across environments.[4] Thirdly, path integration and external cues compete for updating the place map in the case of a contradictory situation.[5] All these findings emphasize the spatial memory aspect

2 For instance, Kubie et al. tested this hypothesis by a task in which rats have to pause at an unmarked, fixed site to obtain a food reward [71]. This task was carried out in a circular environment with certain, controlled distal cues. During the experiment the distal cues were systematically moved in a continuous fashion. It was observed that the rats paused at, apparently, random positions within the circular environment - not at the learned, fixed site. Earlier Fenton et al. had determined, how *distal cue configurations* influence the firing of the place cells [40]. From this understanding and the changes of the distal cues during the experiment the authors could precisely predict the pause locations of the animal. Hence, the position estimate of the hippocampus appears to be closely related to the rat's estimate [71]. Conclusive experiments, maybe along the lines of optogenetic methods that allow to selectively alter the state of neurons and circuits [91], should soon shed more light on this issue.

3 Their firing rates can alter significantly after small modifications of the environment, like changing the color of a wall [25, 75]. This has been called *rate remapping*. They can even be responsive to odors in odor discrimination tasks or training rules [25]. As such, this could be important for associating locations with certain stimuli and therefore allow episodic memory [25, 31, 32].

4 Completely different place cells can be active even in similar environments with different distal cues. Even if a cell has a place field in both environments the peak firing rates, and the centers are unrelated. This tendency has been named *global remapping*, and can even happen within the same environment, if salient properties alter drastically [25, 75, 98, 111, 112].

5 In an experiment by Gothard et al. rats had to run from a home location at the beginning of a linear track to a goal location at the end. They were familiar with the environment. When the length of the linear track was changed between sessions, it became clear that the rats had home-aligned and goal-aligned place maps. In all cases, the place cells *close* to the home, fired at the same distance from the home and the place cells *close* to the goal location fired at the same distance from the goal — despite different track lengths. In case of large track length changes, a sudden transition from home-aligned to goal-aligned place cells could be observed somewhere along the linear track. This indicates that initially path integration drives the firing until external cues align the place cells firing to the goal location [51, 112]. This frame switching

of the spatial maps in the hippocampus [25, 41, 57, 58, 64, 65]. Other spatially modulated cells, which on a population level resemble an internal compass, are also known and will be presented next.[6]

1.2.2 Head-direction cells

A crucial ingredient to the path integration system was found in the form of head-direction cells [135, 136]. They code the rat's heading direction in an allocentric way. These cells exist in several brain areas including the postsubiculum and entorhinal cortex. Vestibular and proprioceptive signals generate and update their firing. Some head-direction cells are additionally tuned to angular head-accelerations and thus update the activity too. Their direction preference remains stable over multiple sessions in the same, familiar environment. Their initial preference however, depends on allocentric cues, that are mostly visual [134]. One of the more important roles of some head-direction cells is providing their input to grid cells, cells that we describe next.

1.2.3 Grid cells

In 2004 Fyhn et al. discovered neurons in the most ventral portion of the medial entorhinal cortex (mEC) that exhibited multiple firing fields [45].[7] These fields are arranged in a regular,

---

can occur on the order of a tenth of a second, as it was shown in the *teleportation* experiment by Jezek et al. For this experiment rats were extensively trained in *one* box with *two* different light cues that were only presented separately. So the animal learned two independent place maps. After the learning period of both environments, the effect of "instantly transferring" the rat from one room to the other by changing the light stimulus could be studied. Thereby rapid transitions from the one frame to the other could be observed [65].

6 One cannot introduce the hippocampus without remarking that when rats are running, the local field potential (LFP) shows a strong theta rhythm (6-11Hz). This rhythm might serve as an organizing clock in the hippocampal formation [20]. For instance, when a rat transverses a place field, the theta phase of the spikes shifts systematically. The spikes tend to progressively happen at earlier theta phases – a phenomenon called *phase precession* [104, 118].

7 Over the years prior to 2004 much evidence for the existence of spatially modulated cells projecting to the hippocampus had been accumulated. Anatomically it was known that head-direction cell signals are relayed to the hippocampus via the mEC [88, 134, 148] and modeling studies suggested that the *path integrator* might be located upstream of the hippocampus [87, 140]. Additionally, it had been reasoned that the huge number of independent, unique place maps that would have to be stored in the hippocampus could severely constrain the storing capacity, a problem that could be circumvented by a universal map that underlies these place maps [103, 124, 140]. Further evidence for

periodic fashion. The extend of these fields is not confined to the recording arena: when the enclosure is expanded, cells have additional firing fields in the novel part [55].[8] The pattern of these fields resembles a hexagonal lattice or grid, which coined their name: *grid cells* ([55], see Fig. 2b). More recently grid cells have also been found in the pre- and parasubiculum [12].

The firing pattern of grid cells can be characterized by the (firing) peak-to-peak distance, called spatial period, the field size, the (angular) orientation of the lattice and the position of one of the lattice's vertices, called the (spatial) phase. Grid cells have many topographic properties. Anatomically neighboring grid cells share similar spatial periods, field sizes and orientations. The spatial period grows from about 20 centimeters up to several meters along the dorsoventral axis of the mEC [16, 45, 55]. The field sizes grow too and it appears that the ratio of grid field width to spatial period remains constant [16, 55]. The phases of anatomically neighboring grid cells are uniformly distributed, without any apparent topography. Yet, even a modest number of grid cells covers the entire recording arena [55]. Deeper layers of the mEC, in particular layer III and V, contain grid cells too, and their lattice properties are similar across layers [55, 116]; Together these observations suggest a modular organization of the mEC, which is supported by anatomical findings [19, 147] – reminiscent to the columnar structure in other cerebral cortex areas [97].

Crucially, the position of the grid fields is stable across recording sessions in the same environment, while the peak firing rates of grid fields vary moderately. This suggests that the exact position of a grid lattice is determined by allocentric reference points, and indeed rotating distal cue cards rotates grids accordingly. Yet, even after cue removal, like switching off the light, the grid

such cells came from experiments; the localized firing of CA1 and CA3 cells persisted after blocking dentate gyrus input [86] and CA1 place cells remained to fire in place, even after blocking CA3 [15]. All this pointed to the existence of spatially modulated cells in the mEC, yet, only faintly modulated cells had been found earlier [96].

8 Hence, it was initially reported that the density of grid fields stays the same in an expanded environment and thus also the spatial period [55]. Later experiments by Barry et al. revealed that rescaling the box leads to a corresponding rescaling of the grid pattern – these contractions or expansions of the grid pattern were most pronounced at the first exposure to the new shape. When both the initial and the alternative shapes were known to the animal no rescaling took place. Interestingly, after a substantial time in the rescaled environment the grid pattern seems to return to the initial scale. Hence the spatial period appears to be shaped by an interplay of intrinsic, self-motion estimates and learned associations to environmental cues [6].

firing pattern persists; leaving the spacing and the average firing rate unaltered [55].

This robustness of the grid pattern to sensory changes points to *idiothetic signals* as the likely mechanism for updating their firing, which predisposes the grid cells as the path integrator [55]. This claim has not been proven conclusively, but the anatomical, functional and behavioral knowledge strongly lends strong support for this interpretation [96]. *Homing* and spatial search performance of rats with lesions to the dorsal pole of the mEC is strongly impaired [108, 131]. Grid cells that are additionally modulated by idiothetic signals, like running speed and head-direction, have later been found and were termed *conjunctive cells* [116]. They are believed to play a key role in updating the animal's internal position estimate, as they combine the current estimate with the current velocity [88].

For the aforementioned binding of grid cells to allocentric cues two independent and compatible mechanisms have been suggested: firstly, grid cells might be anchored by feedback from hippocampal place cells. As place cells have spatial memory properties it is conceivable that their activity initializes the grid cells consistently in known environments [88, 96]. Secondly, there are cells that represent the border of environments and therefore could serve for anchoring the brain's spatial representation.[9]

Grid cells have also been discovered in mice [44] and more recently in Egyptian fruit bats [150]. For the latter finding the bats were crawling for food pellets, so these grid patterns are also planar lattices. Whether bats' grid cells also have three dimensional grids during flight is still unresolved. Furthermore, there is evidence from fMRI that grid cells are present in humans as well [27].[10]

1.2.4 Summary

The gist of the matter is that grid cells are believed to constitute the path integrator, by integrating head-direction and speed

9 The firing rate of *boundary vector cells* is modulated by the shortest distance to the closest boundary in the environment. The running direction and properties of the boundary barely have an effect on their firing rate. These cells have been reported in the subiculum [76]. Cells with similar properties have been found in the entorhinal cortex too and are called *border cells* [117, 127]. If one rotates distal cue cards that serve as landmarks, the spatial representation of these cells moves as well; thus these cells might be indeed instrumental in anchoring the firing of grid cells by setting the spatial phase [127].

10 Finally, like for place cells also grid cells show phase precession in each field as observed by analyzing pooled data [54] and single-runs [114].

signals. The firing of the grid cells network might be anchored to specific landmarks by border cells or hippocampal place cells. The feedback of hippocampal place cells re-calibrates the entorhinal path integrator in case of accumulated position estimate errors [88, 96].

1.3 AIM OF THIS THESIS

As we have seen, many details about the building blocks of cognitive maps in mammals have been found. Particularly interesting properties are the hexagonality and the self-similarity of the grid cell's firing patterns as well as the the multiple scales of spatial representation in both place and grid cells. Hence, while much is known about the cells that encode space, an answer why particular designs have evolved remains elusive [50]. In light of these cell properties, three key questions arise:

- How do grid and place cells represent space?
- Which characteristics contribute to the spatial resolution of such codes?
- Is the population of grid cells, which has been implicated as the path integrator and therefore should be precise, optimized for resolution?

The work presented in this thesis translates these *vague* questions into well-defined mathematical problems and studies those. The first two questions are treated in chapters 2-4, the last one in chapter 5. In the final part of the introduction we will provide more details regarding these questions. They are dependent on each other, as if we do not know how these codes represent space, we cannot discuss which parameters improve the resolution.

How do populations of grid cells (grid code) and place cells (place code) represent space? – apparently in completely different ways. While place cells give sparse responses: if one cell fires the animal is already as uniquely localized as the place field. However, if a grid cell fires, then the rat could be in any of the grid fields. Hence, although grid cells are allegedly specialized in the representation of space, and place cells have other functions too, naively it appears as if place cells offer a more useful spatial code than grid cells.

This intuition is plainly wrong, if one considers the population level. To see this, let us consider a fictive population of binary

place cells. How many different states can 9 neurons provide? There can at most be $2 \cdot 9$ states.[11]

What about 9 grid cells? Figure 3 shows a particular arrangement of the grid cells that we call *nested grid code*. As explained in the figure caption this code with 9 grid cells can have $3^3 = 27$ states. Thus, the same number of binary grid cells can provide more states. This advantage becomes more pronounced the more neurons one considers. By the same argument as above 99 place cells can provide at most 198 states, yet 99 grid cells with, for instance, 3 phases per module can provide a baffling number of 3^{33} states. Much more states than neurons contained in the human brain. This simple counting argument shows that the number of states a population of grid cells can provide can dwarf those of a population of place cells.

This argument has of course only limited explanatory power for the brain. Just let us consider one obvious problem. Real neurons are noisy, in the sense that the identical stimulus condition might elicit a different number of spikes. Grid cells and place cells are no exception. So what happens if a certain neuron accidentally fires, or fails to fire? In figure 3 let us assume that instead of phase 1 in module 1, it is actually phase 2 in module 1 that fires. This noisy code word would correspond to a state that is almost half the width of the linear track away. But how likely is that, and what happens under realistic neuronal noise conditions, and what effect do other parameters have? Neural coding theory offers the tools to rigorously tackle such questions.

1.3.1 Neural coding theory

We alluded to codes a couple of times. Formally, a code is a rule of translating one signal into another. These signals can be physical variables, letters, bits, spikes, etc. For instance, our senses translate physical variables into spike trains. Also between brain areas signals are transferred and possibly recoded.

11 By state we mean a vector $v = (v_1, v_2, \ldots, v_9)$ of ones and zeros that signifies the activity of the 9 neurons at position v. For instance, if $v_1 = 1$, the first neuron is active, and if $v_1 = 0$ it is inactive. Now let us assume that these states are spatially ordered $a, b, c, d, \ldots$. This means that state a is a neighbor of b, b of c, etc. Because a and b are different states, at least one neuron has to have a different state: for instance, $a_3 \neq b_3$ meaning neuron 3 is active at a, but inactive at b or vice versa. So, either neuron 3 turns off or on, when traversing from a to b. Crucially, each neuron is a place cell. Hence, along this sequence of positions $a, b, c, d, \ldots$ it can at most only once turn on and only once turn off, because it has only one place field. Thus, any neuron can at most twice change its state. Consequently, there can be at most $2 \cdot 9$ different code words.

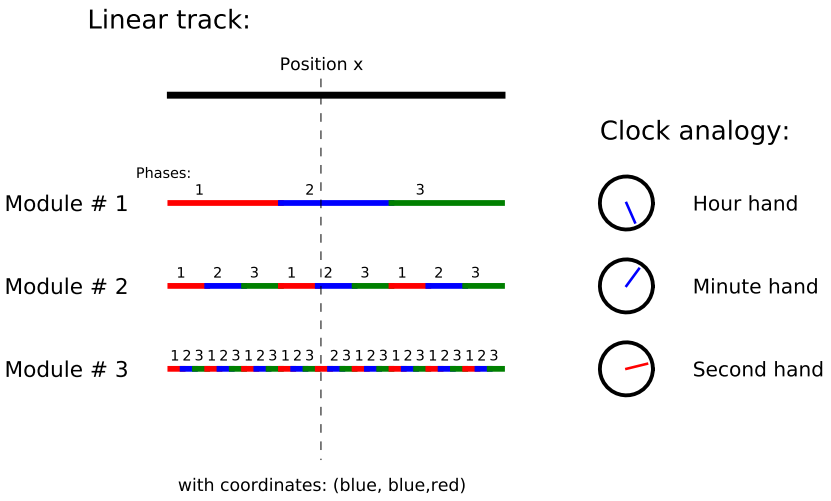

Figure 3: Illustration nested coding scheme. Example with three different spatial periods with three discrete phases each. The different cells with the same spatial period comprise a module. For instance, phase 1 of module 1 is active in the first third of the linear track, phase 2 of module 2 in the second third, and etc. The first module gives coarse spatial information, that is further subdivided by the other two modules. By themselves the other modules provide ambiguous spatial information; together they effectively subdivide the linear track. In particular, each phase of module 1 is subdivided by the three phases of module 2, and they themselves are again subdivided by the 3 phases of module 3. All in all that makes $3^3 = 27$ states. This coding strategy is analogous to the principle of a clock, where each hand further refines time. All three hands code a twelve-hour span down to second precision.

Figuring out the code book of these transformations is one of the major quests of Neuroscience [28, 142].

In the brain many stimulus variables are encoded by population codes, where the elicited spikes of many neurons represent the stimulus in a distributed way. The nobel-prize-winning example is the encoding of the edge orientation in images by simple cells in the visual system [59, 60]. Evidence for similar encoding strategies exists across the brain, from lower and higher sensory areas to motor areas and even in between, as exemplified by the place and grid cell populations [28, 48, 49, 152]. Neuronal responses, like the number of spikes, are often noisy in the sense that the repeated presentation of identical stimuli results in variable spike counts [23]. The stimulus-response function together with the statistical distribution mathematically define the *encoding* step of a population. Given a certain population code, like a place code or a grid code, which translate positions into vectors of spike counts, the spatial resolution of such a code can be computed [23, 120]. Intuitively, the resolution is the average encoding precision of such a code (formally defined in chapter 2).

Within this framework we establish the qualitatively different scaling of a nested grid code and place codes, *despite* neuronal noise. This result is presented in chapter 2 for the linear track and higher dimensional stimulus variables in chapter 3. There we show that the resolution of nested grid codes can scale exponentially in the number of neurons, whereas place cells can only scale linearly in the number of neurons. This framework also allows us to study multiple other dependencies: What is the effect of the different spatial scales of place cells? What about other sets of spatial periods than the nested arrangement? Such questions are treated in chapter 2.

The first two chapters consider place and grid codes with statistically independent neurons. The effect of correlations on the resolution are elucidated in chapter 4.

The remaining key question is whether the grid code in the medial entorhinal cortex is optimal for encoding space. In the following section we introduce a principle that has been put forward as a theoretical model for the connection between function and form.

1.3.2 Optimal coding hypothesis

> Form follows function.
>
> Louis Henry Sullivan.

As noted in a recent review article by Simoncelli and Olshausen [125], the evolution and development of any neuronal system is hypothesized to be sculpted by the following three factors:

1. "the tasks that the organism must perform,
2. the computational capabilities and limitations of neurons (this would include metabolic and wiring constraints),
3. the environment in which the organism lives" [125].

The last, ecological factor has a pronounced impact on sensory systems. Therefore, Attneave and Barlow proposed the *efficient coding hypothesis* as a theoretical framework for sensory coding [4, 5]. They observed that an important factor for neural systems are information bottlenecks, like the optic nerve. Therefore, from an information theoretical point of view it is efficient to have a neuronal code that matches the environmental and neuronal response characteristics. Thus sensory systems should excel at processing sensory signals that manifest themselves most frequently in the environment [4, 5, 125]. Indeed, the efficient coding hypothesis has been applied to successfully predict the structure of receptive fields, tuning curves in the cochlear, and the sparseness of neuronal representations in sensory cortices [2, 3, 77, 105]. However, the efficient coding hypothesis does not mention the accuracy of the coding [125].

Like the third factor, also the first two factors, namely the *task* together with *computational capabilities* exert a dominating influence on neural systems. In the task of path integration the challenge has been presented earlier: the neuronal representation has to store the current position as precisely as possible, despite neuronal noise. Otherwise small intrinsic deviations of the position estimate accumulate over time to huge errors and subsequently render path integration useless. As the accuracy, presumably, has such a prevailing effect on the path integration system, we ask if these factors can explain the observed features of the grid code in the mEC. Taken together, and due to our emphasis on the accuracy, we call this the *optimal coding hypothesis*. It was in light of this framework that we ask in chapter 5, what are the parameters of a grid code that optimize its resolution. Thereby we formalize the second and third factors in the

following way (chapter 5 for details). As second factor we consider a fixed number of grid cells with a limited peak firing rate (power constraint). Furthermore, we require that the size of the environment is bounded and that the spatial resolution within this environment should be equally high at all positions. This is assumed, because a path integration system should be spatially invariant [63]. In that sense, our study design also mirrors certain ecological factors.

Hence, we investigate the optimality of a population of grid cells under the constraints just presented. We show which features of the grid code endow it with the highest spatial resolution and compare these optimal properties to the properties of grid cells in the mEC. This work is presented in chapter 5.

2 GRID CELLS OUTPERFORM PLACE CELLS

2.1 SUMMARY

Rodents possess two neuronal coordinate systems for representing their position that are known: place cells in the hippocampus and grid cells in the medial entorhinal cortex. While place cells typically fire at one particular location in space, grid cells spike at numerous sites that are arranged periodically.

We study the spatial resolution of these two coding schemes and find that a generic set of modular grid cells[1] typically outperforms even the optimal set of place cells with the same number of cells, when encoding an interval. A one dimensional interval can be seen as the abstraction of a linear track. The two dimensional case is treated in chapter 5.

Furthermore, we derive optimal parameter regimes for populations of place cells (place code) and populations of grid cells (grid codes) in this one dimensional case. Optimality here refers to the resolution an ideal observer can achieve. We compute the resolution analytically by Fisher information and numerically by maximum likelihood estimation; this study also sheds light on when and why these measures differ.

For place codes the analysis shows that a heterogeneous population of place cells with varying tuning widths gives no qualitative improvement over a homogeneous population. In particular, the resolution is maximized by a constant optimal tuning width. For grid cells, however the different spatial scales *can* significantly improve the coding accuracy. The study of a large set of grid codes reveals that nested grid codes, where the spatial periods are staggered, offer the highest resolution. As presented in the paper there are also parameter regimes, where grid codes offer only poor spatial resolution.

1 As specified in the paper. Basically generic means that the spatial periods are uniformly picked random numbers, which are smaller than the size of the environment.

2.2 REFERENCE

This work was carried out under the supervision of Andreas Herz and Martin Stemmler; AM, AH and MS conceived and designed the research. AM performed research. AM, AH and MS discussed the results and wrote the paper. Preliminary results of this article were presented in two conference talks: one at the *Annual Computational Neuroscience meeting* in San Antonio in June 2010 and the other one at the *Bernstein Conference on Computational Neuroscience* in Berlin in September 2010 [81, 83].

The paper has been accepted in *Neural Computation* under the following reference:

A Mathis, AVM Herz, and M Stemmler: "Optimal Population Codes for Space: Grid Cells Outperform Place Cells". *Neural Computation*, accepted February 7, 2012.

Optimal Population Codes for Space: Grid Cells Outperform Place Cells

Alexander Mathis[1, 2], **Andreas VM Herz**[1, 2], **Martin Stemmler**[1, 2]
[1] Bernstein Center for Computational Neuroscience Munich, 82152 Martinsried, Germany.
[2] Graduate School of Systemic Neuroscience and Division of Neurobiology, Ludwig-Maximilians-Universität München, 82152 Martinsried, Germany.

Keywords: Grid Cell, Entorhinal Cortex, Place Cell, Hippocampus, Population Coding, Fisher Information, Maximum Likelihood Estimator, Navigation

Abstract

Rodents use two distinct neuronal coordinate systems to estimate their position: place fields in the hippocampus and grid fields in the entorhinal cortex. Whereas place cells spike at only one particular spatial location, grid cells fire at multiple sites that correspond to the points of an imaginary hexagonal lattice. We study how to best construct place and grid codes, taking the probabilistic nature of neural spiking into account: which spatial encoding properties of individual neurons confer the highest resolution, when decoding the animal's position from the neuronal population response? For grid codes, the periodic pattern of firing fields introduces ambiguities in the position estimate. The solution to this problem requires grid cells with different spacings, and the spatial resolution crucially depends on choosing the right ratios of these spacings across the population. We compute the expected error in estimating the position both in the asymptotic limit, using Fisher information, and for low spike counts, using maximum likelihood estimation. Achieving high spatial resolution and covering a large range of space in a grid code leads to a trade-off: the best grid code for spatial resolution is built of nested modules with different spatial periods, one inside the other, whereas maximizing the spatial range requires distinct spatial periods that are pairwisely incommensurate. Optimizing the spatial resolution predicts two grid cell properties that have been experimentally observed. First, short lattice spacings should outnumber long lattice spacings. Secondly, the grid code should be self-similar across different lattice

spacings, so that the grid field always covers a fixed fraction of the lattice period. If these conditions are satisfied and the spatial "tuning curves" for each neuron span the same range of firing rates, then the resolution of the grid code easily exceeds that of the best possible place code with the same number of neurons.

1 Introduction

An animal's position and heading in world coordinates is reflected in coordinated neural firing patterns within different subnetworks of the brain, most notably the hippocampus, subiculum, and entorhinal cortex (O'Keefe and Dostrovsky, 1971; O'Keefe, 1976; Taube et al., 1990b,a; Fyhn et al., 2004; Hafting et al., 2005; Boccara et al., 2010). In rodents, these subnetworks have evolved at least two distinct representations for encoding spatial location: in the hippocampus proper, place cells fire only at a single, specific location in space, whereas in the medial entorhinal cortex (mEC), grid cells build a hexagonal lattice representation of physical space, such that each cell fires whenever the animal moves through a firing field centered at a cell-specific lattice point.

How accurately can an animal determine its location using one of these two distinct encoding schemes for space? Most neurons in cortex spike irregularly and unreliably (Softky and Koch, 1993; Shadlen and Newsome, 1998) and cells in the hippocampal-entorhinal loop are no exception (Fenton and Muller, 1998; Kluger et al., 2010). As the animal moves through space, it spends only a brief moment in each firing field of a grid cell or the firing field of a place cell, eliciting no more than a handful of unreliable spikes: grid cells, for instance, often spike only once or twice during a single pass through a firing field (Reifenstein et al., 2010). Hence, for both codes precise information about position can only be gained from a population of grid and place cells, respectively. If all grid cells share the same lattice length scale the same pattern of spikes across the population corresponds to different locations in space, leading to catastrophic errors in estimating position. How different lattices can be combined to resolve the ambiguity introduced by the multiplicity of firing fields is crucial for navigation and might explain the variation of the spatial periods along the dorso-ventral axis for the mEC (Brun et al., 2008).

The goal of this paper is to answer the question of how grid codes should be constructed and relate these to the resolution of population codes. Single-peaked place fields are analogous to the tuning curves for orientation in visual and motor cortices, for which the questions of neuronal coding and optimal tuning widths have been investigated extensively (Paradiso, 1988; Seung and Sompolinsky, 1993; Brunel and Nadal, 1998; Zhang and Sejnowski, 1999; Pouget et al., 1999; Bethge et al., 2002; Brown and Bäcker, 2006; Bobrowski et al., 2009). Theoretical studies on the coding properties of grid cells (Burak et al., 2006; Fiete et al., 2008) have dealt with the spatial range encoded by populations of grid cells, without assuming an explicit noise model. Here, our focus will neither be on the spatial range, nor on how grid-like firing patterns arise (Fuhs and Touretzky, 2006; McNaughton et al., 2006; Burgess et al., 2007; Kropff and Treves, 2008; Burak and Fiete, 2009; Remme et al., 2010; Zilli and Hasselmo, 2010;

Mhatre et al., 2010), nor how grid fields can lead to place fields (Fuhs and Touretzky, 2006; Solstad et al., 2006; Rolls et al., 2006; Franzius et al., 2007; Si and Treves, 2009; Cheng and Loren, 2010). Rather we extract general observations about grid and place cells from experimental findings and relate these to the resolution of population codes. In addition to comparing grid and place codes quantitatively, we derive optimal parameter regimes for both codes. Using the hypothesis that neuronal populations code efficiently (Attneave, 1954; Barlow, 1959), we can then make predictions about grid cell properties in the mEC.

The comparison will be carried out in the framework of Poisson rate coding for the position of an animal along a one-dimensional path, typically a linear track (Hafting et al., 2008; Brun et al., 2008). A place cell is characterized by a single firing field with a given spatial center and width; for grid cells, one measures the spatial period and phase of the regularly spaced lattice of firing fields. These parameters define families of tuning curves for population models of spatial coding. Based on maximum likelihood decoding, we estimate the distortion, or average error, in recovering the animal's position. Asymptotically, given enough neurons and a long enough time to observe the firing rate, the distortion becomes analytically calculable. The Cramér-Rao bound states that the inverse of the Fisher information yields the minimum achievable square error, provided the estimator is unbiased; furthermore, maximum likelihood decoding attains this bound (Lehmann and Casella, 1998). In the context of neural population coding, many authors have calculated the Fisher information (Paradiso, 1988; Seung and Sompolinsky, 1993; Brunel and Nadal, 1998; Zhang and Sejnowski, 1999; Pouget et al., 1999; Eurich and Wilke, 2000; Wilke and Eurich, 2002; Bethge et al., 2002; Brown and Bäcker, 2006). However, it is also known that no such estimator will attain the lower bound if the neurons have Poisson spike statistics and the expected number of spikes is low even when a neuron is firing at its maximal rate (Bethge et al., 2002). In other words, if the product of the firing rate $f_{\max}$ and the time window T for counting spikes obeys $f_{\max}T \approx 1$, the Fisher information greatly exaggerates the true spatial resolution of the population code. If one takes the time window for read-out to be one cycle of the on-going $7-12$ Hz theta rhythm during movement, the natural time-scale for grid and place cells is short compared to the typical firing rates in these cells. Under these conditions, the asymptotic error and the true error can diverge, so that the parameters for an optimal grid or place code are only to be found numerically. Maximum likelihood decoding is computationally expensive, so we treat the case of populations encoding a one-dimensional stimulus in detail. Multiple stimulus dimensions correspond to a product space in the mathematical sense; under ideal conditions, the errors across stimulus dimensions add. Hence, studying the one-dimensional case will be illustrative for how general grid codes should be constructed, as we will discuss.

Some of the results here have been presented in a briefer format Mathis et al. (2010).

2 Grid Code Schemes

The place code is a classical instance of a population code (Wilson and McNaughton, 1993), wherein each position in space is represented by the activity of a large number of place cells (Fig. 1a) with intersecting place fields. The set of well-localized place fields forms a dense cover of the explored space, so that the set of simultaneously active place cells yields an accurate estimate of the animal's position. Additional precision in estimating the position can be gained from the spatial profile of how individual place cells map position into a firing rate—the place cell's "tuning curve" (Paradiso, 1988; Seung and Sompolinsky, 1993; Zhang and Sejnowski, 1999). Early models considered cells with single fields and a standard tuning curve for each cell. Yet the width of the place fields grows along the dorso-ventral axis (Kjelstrup et al., 2008), and ventral CA3 cells are more likely to have more than one place field (Leutgeb et al., 2007; Fenton et al., 2009). As we will show, both of these properties can improve the resolution, but only marginally.

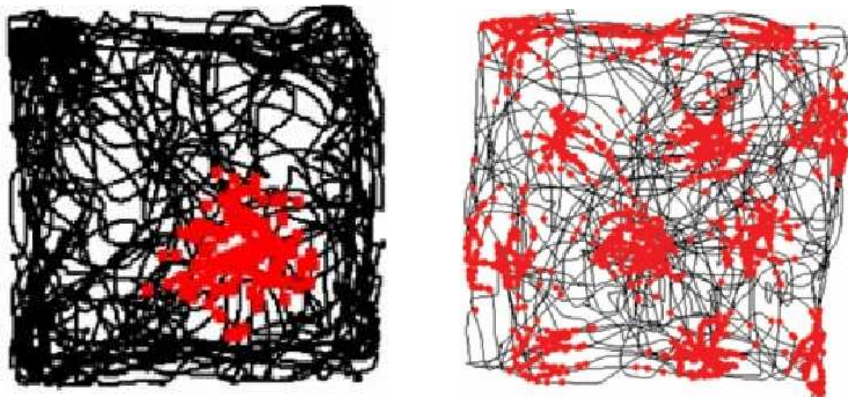

(a) (b)

Figure 1: Firing patterns for a place and grid cell. (a) A place cell spikes only when the animal is within a single region of space called the place field. Black lines depict the trajectory of a rat in a square arena. The superimposed red dots mark the rat's location when this CA1 cell in hippocampus fired a spike. Figure adapted from (Jeffery, 2008) with permission. (b) In contrast, a grid cell from entorhinal cortex fires at multiple spatial locations, which form a hexagonal lattice. Three neighboring firing fields span a nearly equilateral triangle. Figure adapted from (Hafting et al., 2005) with permission.

A grid code, in contrast, is harder to read out. The firing of a single grid cell (Fig. 1b) implies that the animal could be at any one of a range of different locations, without specifying which one. A clear-cut estimate of position becomes possible by taking into account the properties of neighboring grid cells, each of which is characterized by a regular lattice of locations at which the cell fires. For neighboring grid cells, the lattices share similar spatial periods and orientations, but are spatially translated (Hafting et al., 2005; Sargolini et al., 2006; Doeller et al., 2010). A single grid cell thus signals the spatial phase of the animal's location relative to the lattice. Taking a subset from the local

grid cell population that spans all phases is tantamount to discretizing the spatial phase and forms the basis for defining a grid module: an ensemble of grid cells that share the same lattice properties, but have different spatial phases. Along the dorsolateral axis of the mEC, the typical spatial period grows from values of around 20 centimeters up to several meters (Fyhn et al., 2004; Giocomo et al., 2007; Brun et al., 2008), while the ratio of grid field width to spatial period remains constant (Hafting et al., 2005; Brun et al., 2008).

The range and precision of the grid code's representation of space crucially depends on how the spatial periods of different modules are arranged. In the most extreme case, the combination of spatial periods could yield a population code with a high resolution, but a short range, or vice versa. Many grid codes will have mixed properties, implying no hard trade-off between range and precision, but we first compare and contrast two radically different grid coding schemes: in the first, the spatial periods themselves span a wide range, effectively subdividing space; in the second, the spatial periods are similar, yet incommensurate, so that the phases represented in the population response are unique for each position across a wide range of space. We will call the first scheme the 'nested interval scheme', illustrated in Figure 2a. Imagine that the spatial periods λ_i are ordered, $\lambda_1 > \lambda_2 > \ldots > \lambda_L$. For each λ_i, assume that there are M grid cells that share this spatial period, but have lattices that are shifted relative to each other. The M cells will represent the equidistant phases $2\pi j/M$ with $j \in \{0, 1, \ldots, M-1\}$. Such a grid codes positions smaller than λ_1 precisely and effectively in a step-by-step fashion: Module 1 only provides coarse information about the position estimate, with a resolution of λ_1/M. Module 2, although itself ambiguous within the range $[0, \lambda_1]$, adds resolution within each of the M subintervals of length λ_1/M. Likewise, module 3 adds further precision and so forth. An analog clock works the same way: within a twelve-hour span, the minute and second hand are ambiguous *per se*. While the hour hand could, in principle, encode the time of the day down to microsecond precision, there is a limit to the angular resolution of the human eye, whereas the combination of all hands is easy to read. Similarly, the nested interval scheme can resolve the position with high accuracy, even though the individual modules either lack spatial precision or lack spatial range. Unlike the clock, the periods λ_i are not necessarily integer multiples of each other, *i.e.* $\lambda_i \nmid \lambda_{i-1}$. In this case, the range, which is the longest distance that is unambiguously coded by the modules, can be much larger than the largest spatial period λ_1. Extending the range beyond the largest spatial period is the key idea behind the 'modular arithmetic scheme' (Fiete et al., 2008), which is the alternative to nested interval coding.

Consider two one-dimensional modules with spatial periods 12 and 17. One can represent each module as a circle S^1, whose circumference matches the period. Geometrically, spatial positions are mapped onto the product of these two circles, which is a torus $T^2 = S^1 \times S^1$. The mapping of spatial position is unique up to the point at which

$$\begin{aligned} \Pi\colon [0,\infty) &\rightarrow T^2 \\ x &\mapsto (\mathrm{mod}\,(x,12), \quad \mathrm{mod}\,(x,17)) \end{aligned} \tag{1}$$

closes in on itself for the first time, *i.e.* $\min_{x>0} \Pi(x) = \Pi(0)$. As the integers 12 and

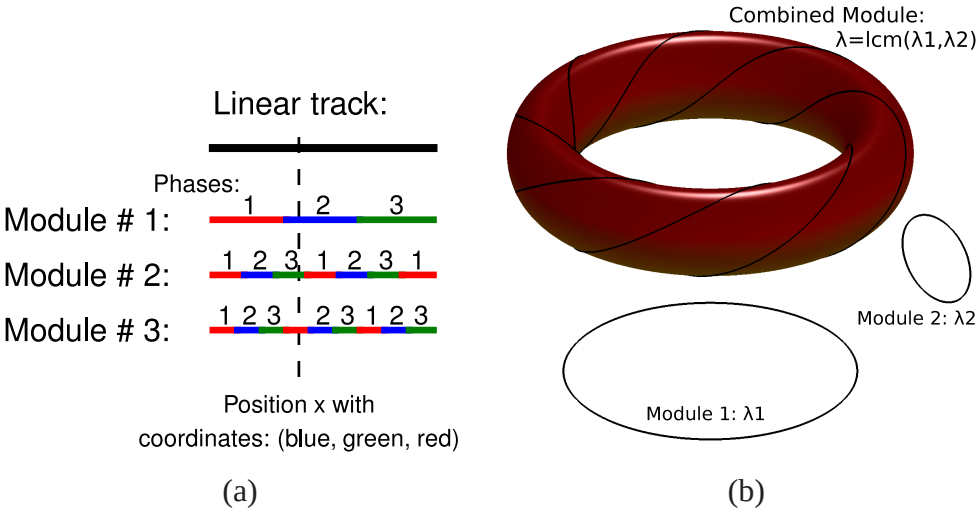

(a) (b)

Figure 2: (a) **Nested Interval Scheme.** Example with three clearly different spatial periods and three discrete phases each. The first module gives coarse spatial information, that is further refined by the other two modules. By themselves the other modules provide ambiguous spatial information on the range, together they effectively subdivide the unit interval. (b) **Modular Arithmetic Scheme.** The two periodic variables depicted by the circles with different spatial periods λ_1 and λ_2 can lead to an elongation of the coding range. Geometrically this can be seen by considering a particle wandering with the same increment in each variable on the Cartesian product of the two circles, which is a torus. The trajectory of this particle will close after length $lcm(\lambda_1, \lambda_2)$, the least common multiple as described in the text.

17 have no common divisor, the period is $204 = 12 \cdot 17$, the least common multiple of the two spatial periods.[1] This principle is illustrated in Figure 2b. By induction, one can show that the range of a sequence of spatial periods $\{\lambda_1, \lambda_2, \ldots \lambda_L\}$ is given by the least common multiple of this sequence $lcm(\lambda_1, \lambda_2, \ldots \lambda_L)$.

At best, an ideal, noiseless grid code with integer periods has a range that is the product of the spatial length scales (Fiete et al., 2008). A small change in the periods, however, can lead to a dramatic reduction in the range: for instance, changing the periods from 12 and 17 to 12 and 18 reduces the range from 204 to merely 36, the least common multiple of 12 and 18. In general, for two positive real numbers representing the spatial periods, the combined period is given by:

$$lcm(x, y) = \begin{cases} \infty & x/y \notin \mathbb{Q} \\ n \cdot x & x/y \in \mathbb{Q} \text{ with } x = \frac{m}{n} \cdot y, \\ & \text{for } m, n \in \mathbb{N}, \text{without common divisor.} \end{cases} \quad (2)$$

[1] In contrast to the watch example, the two periods should not have a common divisor. Since a second divides a minute and a minute divides an hour, a standard analog watch does not represent more than the maximal 12-hour period.

This function is highly discontinuous. For every pair of periods $(\lambda_1, \lambda_2) \in \mathbb{Q}$, one can find an arbitrarily close pair of rational spatial periods with an arbitrarily large lcm. In contrast, within any vicinity (λ_1, λ_2), a smallest least common multiple exists.

An even more severe problem than the sensitivity of the range lurks. For the spatial periods from the example above, $\lambda_1 = 12$ and $\lambda_2 = 17$, changing the modular coordinates from $(0, 0)$ to $(1, 0)$ implies a jump in position from 0 to 85, which is almost half of the range. Small errors in the phase can thus lead to huge mistakes in the position estimate. Choosing more closely spaced periods limits the magnitude of the such an error, yet a unit step in any one coordinate represents a shift in the position by at least one spatial period.

In principle, the grid lattice need not be regular, nor need a grid cell share the same lattice spacing with other grid cells. We will not consider the most general case here, but make the prior assumption of both periodicity and modularity, two features that could facilitate the downstream read-out of the neuronal population's response. We will construct both nested interval and modular codes by sampling from the space of different possible spatial periods in several ways:

1. **Deterministic Ensembles:** Given N cells, assign an equal number of cells to a set of modules whose spatial periods are defined as follows: starting with an initial module with spatial period $\lambda = 1$, let each successive module have a smaller period, such that $\lambda_{n+1} = s\lambda_n$, where $s < 1$ is a constant contraction factor. The set of spatial periods forms a geometric sequence. Such grid codes consist of nested intervals, by design, and are unsuited for modular arithmetic.

2. **Stochastic Ensembles:** For N cells, a divisor $L|N$ is chosen randomly. Then the spatial periods are drawn identically from one of two distributions: in the first case, from the uniform distribution $[0, 1]$; in the second case, from the uniform distribution $[(1 - A) \cdot \mathrm{s}, A + (1 - A) \cdot \mathrm{s}]$, where s is a random shift variable, and A a random amplitude, both drawn uniformly from $[0, 1]$. Either case is applied in 70% or 30% of the realizations, respectively. The second case results in more densely spaced spatial periods, all of which lie within $\pm(1 - A) \cdot \mathrm{s}$ of the period with length A, which tends to favor decoding based on modular arithmetic. In general, drawing from the stochastic ensemble can yield spatial periods that fit either the nested interval or modular arithmetic scheme; the resulting grids embody generic modular codes consisting of periodically spaced tuning curve peaks.

The choice of spatial periods for the grid affects both the range and the resolution of the code. In the absence of noise, a well-designed grid code could simultaneously span large distances and discriminate fine differences in position; however, intrinsic variability introduces trade-offs between these two properties of the code. While the modular arithmetic scheme does not require closely spaced spatial periods *a priori*, the close spacing becomes important in the presence of noise. Hence, the nested interval and the modular arithmetic schemes become distinct if one insists that the spatial range in the latter scheme be robust. We now submit both schemes to the crucial test: can one

reliably estimate the position by counting the spikes from a finite set of neurons within a limited time window? We start by contrasting the resolution of grid and place codes for populations of neurons.

3 Population Coding Model

We consider a population of N stochastically independent Poisson neurons (similar to Paradiso, 1988; Seung and Sompolinsky, 1993; Salinas and Abbott, 1994; Bethge et al., 2002; Pouget et al., 2003; Huys et al., 2007, for instance). The firing rate of each neuron depends on the one-dimensional position x on the unit interval $X = [0, 1]$. A priori, each position is equally likely, resulting in a flat prior $P(x) = 1$.

The firing rate of neuron i is described by its tuning curve $\{\alpha_i(x)\}_{i\leq N}$. Given a position $x \in [0, 1]$, the conditional probability of observing the N-dimensional spike pattern $K = (k_1, \ldots, k_N) \in \mathbb{N}^N$ in a time interval of length T is:

$$P(K|x) = \prod_{i\leq N} \text{Poisson}(k_i, T \cdot \alpha_i(x)) = \prod_{i\leq N} \frac{(T \cdot \alpha_i(x))^k}{k!} \cdot \exp(-T \cdot \alpha_i(x)). \quad (3)$$

The maximal firing rate $f_{max} = \max_{x\in X, i\leq N}(\alpha_i(x))$ is assumed to be constant across the population. Periodic tuning curves $\alpha_i(x)$ correspond to grid codes, whereas single-peaked, aperiodic $\alpha_i(x)$ correspond to place codes.

The tuning curves of place cells are taken as Gaussian functions with centers distributed equidistantly over $X = [0, 1]$:

$$\alpha_i(x) = f_{max} \cdot \exp\left(-\frac{(x - \frac{i}{N-1})^2}{2\sigma^2}\right) \text{ with } 0 \leq i < N. \quad (4)$$

The free parameters are the maximal firing rate f_{max}, the tuning width σ, and the number of neurons N. Figure 3a illustrates this family of tuning curves for $N = 12$ cells with tuning width $\sigma = 0.1$.

In contrast, the tuning curves for grid cells are defined as periodic functions with Gaussian-like bumps of the type $\exp\left(-\frac{(-\frac{\lambda}{2} + \mod(\frac{\lambda}{2}+x,\lambda))^2}{2\sigma^2}\right)$. Here $\mod(z, \lambda)$ stands for the remainder after dividing z by the spatial period λ.

To construct a family of grid cell tuning curves, we vary the spatial periods and the spatial phases. Each spatial period $\{\lambda_l\}_{l<L}$ defines a grid module; each of the L modules contains $M = N/L$ equidistantly arranged phases within its periodic domain. Hence, for each module λ_i, with $0 \leq i < L$, there are equidistant spatial phases $\varphi_j = \frac{j\cdot\lambda_i}{M}$ $0 \leq j < M$ per module λ_i and tuning curves:

$$\alpha_{i,j}(x) = f_{max} \cdot \exp\left(-\frac{(-\frac{\lambda_i}{2} + \mod(\frac{\lambda_i}{2} + x - \varphi_j, \lambda_i))^2}{2\sigma_i^2}\right). \quad (5)$$

Figure 3b illustrates a grid code for 12 cells with two spatial periods. After fixing f_{max} and N, the only remaining free parameter for the place code is the spatial tuning

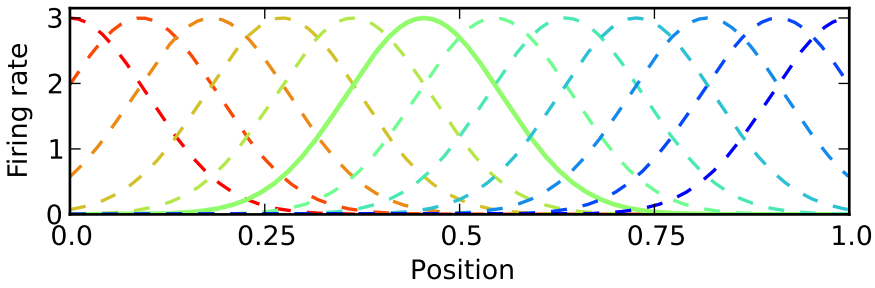

(a)

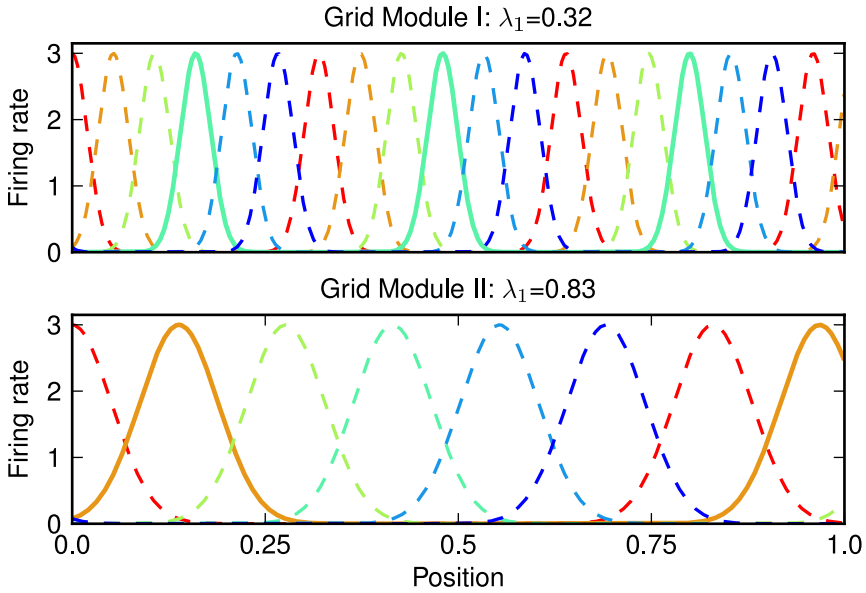

(b)

Figure 3: Families of tuning curves. (a) Family of place cell tuning curves: Different colors represent different cells. Tuning curves of 12 place cells with $\sigma = 0.1$ and maximum firing rate $f_{max} = 3$. (b) Family of grid cell tuning curves for two different spatial periods: Different colors represent different cells. Tuning curves of 12 grid cells with spatial periods $\lambda_1 = 0.32$ and $\lambda_2 = 0.83$, 6 phases per module and maximum firing rate $f_{max} = 3$. In this model, the tuning width of the grid cells scales with the spatial period, as suggested by experimental data (Brun et al., 2008).

width σ, whereas for the grid code the set of spatial periods $\{\lambda_1, \ldots, \lambda_L\}$ needs to be specified.

Both coding schemes should enable real-time readout of the rat's position *while* it is moving. During active exploration of the environment, $7 - 12$ Hz theta oscillations course through the parahippocampal loop, acting as a *Zeitgeber* (Buzsaki, 2006). Within this natural time-frame of roughly $T = 80 - 140$ ms, the maximal expected spike count of a grid or place cell is generally low. With measured peak firing rates of place and grid fields in the range of $10 - 30$ Hz (Hafting et al., 2005; Leutgeb et al., 2004), $f_{max} \cdot T \approx 1 - 4$ within one theta cycle. For our analysis, we choose $f_{max} \cdot T = 3$.

By observing the spike counts from a population of N neurons, one can build an estimator $\hat{x}$ of the position x. The average mean square error is (Salinas and Abbott, 1994; Bethge et al., 2002):

$$\chi^2 = \mathbb{E}\left((x-\hat{x})^2\right) = \sum_{K\in\mathbb{N}^N} \int_0^1 (x-\hat{x}(K))^2 \cdot P(K|x)p(x)dx, \tag{6}$$

The χ^2 error generally depends on the estimator $\hat{x}$. For instance, given a particular population response K, the most likely stimulus that gave rise to it is

$$\hat{x}_{\text{MLE}}(K) = \max_{x\in[0,1]} P(x|K), \tag{7}$$

which is known as the maximum likelihood estimate (MLE). The corresponding mean maximum likelihood estimate square error (MMLE) is defined as $\chi^2_{MLE} = \mathbb{E}\left((x-\hat{x}_{MLE})^2\right)$. We compute the MMLE as described in the appendix by Monte Carlo methods. As the MMLE is numerically expensive to compute for large population sizes, we compare it against a reference that can be computed analytically. The maximum likelihood estimate is both statistically efficient and consistent (Lehmann and Casella, 1998), which means that χ^2_{MLE} asymptotically approaches the mean asymptotic square error (AE) for an increasing number of independent, identically distributed (i.i.d.) observations:

$$\chi^2_{AE} = \mathbb{E}\left(1/J(x)\right), \tag{8}$$

as shown in (Bethge et al., 2002). Here $J(x)$ stands for the Fisher information

$$J(x) = \mathbb{E}\left(\left(\frac{\partial}{\partial x}\ln(P(K|x))\right)^2\right). \tag{9}$$

However, for low numbers of spikes and a single observation and low spike counts, the true χ^2 can exceed χ^2_{AE}, as reported by Bethge (Bethge et al., 2002) for the minimum mean square error. For this reason we will employ χ^2_{AE} as a practical benchmark that gives us scaling rules for grid and place codes and furthermore investigate how a population code can be cleverly constructed so that maximum likelihood decoding of the population response comes close to this benchmark, even for low, realistic spike counts.

The Fisher information (9) for a population model with independent, Poisson neurons has a simple structure (compare Paradiso, 1988; Seung and Sompolinsky, 1993, for instance):

$$J_{Population\ model}(x) = \sum_{i=1}^{N} \frac{T(\partial\alpha_i(x)/\partial x)^2}{\alpha_i(x)}, \tag{10}$$

so that the asymptotic error is

$$\chi^2_{AE} = \int_0^1 \left(\sum_{i\le N} \frac{T(\partial\alpha_i(x)/\partial x)^2}{\alpha_i(x)}\right)^{-1} dx. \tag{11}$$

This quantity only depends on the tuning curves and their first derivatives. Following the tradition of comparing neuronal codes on the basis of the Fisher information (Zhang

and Sejnowski, 1999; Eurich and Wilke, 2000; Wilke and Eurich, 2002; Brown and Bäcker, 2006), we will ask: based on the error measures χ^2_{MLE} and χ^2_{AE}, can a grid code outperform a place code? In particular, which spatial periods should be present in the grid code? What should the width of the firing field be relative to the spatial period?

3.1 Average Fisher Information and Asymptotic Resolution

For the families of place code (PC) and grid code (GC) tuning curves defined by equations (4) and (5), the Fisher information (9) of a single cell is given by

$$J_{PC,i}(x) = Tf_{max} \cdot \frac{(x - \frac{i}{N-1})^2}{\sigma^4} \cdot \exp\left(-\frac{(x - \frac{i}{N-1})^2}{2\sigma^2}\right) \tag{12}$$

and

$$J_{GC,ij}(x, \varphi_j) = Tf_{max} \cdot \frac{(-\frac{\lambda_i}{2} + \mod(\frac{\lambda_i}{2} + x - \varphi_j, \lambda_i))^2}{\sigma_i^4} \cdot \exp\left(-\frac{(-\frac{\lambda_i}{2} + \mod(\frac{\lambda_i}{2} + x - \varphi_j, \lambda_i))^2}{2\sigma_i^2}\right). \tag{13}$$

For the Fisher information of a population of cells, with $J(x) = \sum_{ij} J_{ij}(x)$, Jensen's inequality implies:

$$\chi^2_{AE} = \int_0^1 \frac{1}{J(x)} dx \geq \frac{1}{\int_0^1 J(x) dx}. \tag{14}$$

The closer $J(x)$ comes to being a constant, so that it is independent of the position x, the tighter the inequality. Therefore, the asymptotic error is easy to calculate in the following limits: For place codes, when the equidistant tuning curves tile the full range densely; or, for grid codes, when the phase-shifted tuning curves tile each spatial period densely.

In these limits, the Fisher information for the population approaches N times the average Fisher information per cell. The asymptotic error is simply the inverse of the Fisher information conveyed by the population. For the place code, we first compute the average Fisher information for a tuning curve centered at $c \in [0, 1]$ and then average over all possible centers c:

$$\overline{J_{PC}} = \int_0^1 \int_0^1 f_{max} T \cdot \frac{(x-c)^2}{\sigma^4} \exp\left(-\frac{(x-c)^2}{2\sigma^2}\right) dx dc. \tag{15}$$

$$= f_{max} T \cdot \left(\frac{\sqrt{2\pi}}{\sigma} \text{erf}\left(\frac{1}{\sqrt{2}\sigma}\right) + 4 \cdot \exp\left(-\frac{1}{2\sigma^2}\right) - 4\right)$$

$$\propto \frac{\sqrt{2\pi} f_{max} T}{\sigma} \qquad \text{for } \sigma \ll 1 \tag{16}$$

This result (Brown and Bäcker, 2006) shows that the average Fisher information of one place cell is inversely proportional to the tuning width σ —the narrower the tuning

curve, the better (Fig. 4a); this finding coincides with the result for stimuli that are not restricted to a compact subset of $\mathbb{R}$ (Zhang and Sejnowski, 1999). If the tuning curves for place cells cover the span $[0, 1]$ sufficiently densely and uniformly, then the resolution of the place code, as measured by the MLE, will approach the Cramér-Rao bound $\left(N \cdot \overline{J_{PC}}\right)^{-1}$. For fixed N, the tuning width cannot be reduced indefinitely while maintaining uniform coverage of the unit interval. Indeed, for fixed N and for any $\epsilon > 0$, there will be a $\sigma(\epsilon) > 0$ and subintervals $K \subset [0, 1]$ of fixed length l, such that for all $\sigma < \sigma(\epsilon)$ and $x \in K$: $J_{PC,N}(x) < \epsilon$. By Jensen's inequality (14), $\chi^2_{AE} =\geq \frac{l}{\epsilon}$, and hence $\chi^2_{AE}(PC, N) \to \infty$ for $\sigma \to 0$. This means that there is an optimal σ for finite ensembles. For instance, for $N = 100$, the smallest asymptotic error is attained for $\sigma \approx 4.1 \cdot 10^{-3}$, leading to a resolution of $\chi^2_{AE} \approx 6 \cdot 10^{-6}$. This value is used as a benchmark for comparison with grid codes.

In general, a population of place cells will have

$$\overline{J_{PC,N}} \propto f_{max} T \cdot \sum_{i=1}^{N} \frac{1}{\sigma_i} \approx f_{max} T \cdot N \left\langle \frac{1}{\sigma_i} \right\rangle, \tag{17}$$

if we do not assume that all tuning curves have equal width. In some cases, place cells have multiple peaks, although the average number peaks is close to one (Leutgeb et al., 2007; Fenton et al., 2009). If there are γ peaks per place cell, and the tuning widths are optimized, then the Fisher information at best scales as (γN^2) in the number of neurons. If the tuning widths are not simultaneously scaled, in contrast, the Fisher information scales linearly in N.

By comparison, the spatial map of a grid cell has multiple *bumps*, by definition. If the Fisher information for each bump scales as σ^{-1}, just as in a place cell, and there are λ^{-1} bumps in the unit interval, then the mean Fisher information in a grid cell scales as $(\lambda\sigma)^{-1}$. This is indeed correct, as the following more formal argument shows. For the mean Fisher information of a grid cell, we have to average the Fisher information (13) over all possible spatial phases φ. Due to periodicity, it suffices to average over phases from 0 to the spatial period λ.

$$\overline{J_{GC}} = \frac{1}{\lambda} \cdot \int_0^{\lambda} \int_0^1 J_{GC}(x, \varphi) dx d\varphi. \tag{18}$$

For $\lambda \ll 1$, $\int_0^1 J_{GC}(x, \varphi) dx \approx \frac{2}{\lambda} \cdot \int_0^{\frac{\lambda}{2}} J_{GC}(x, 0) dx$, because of the periodicity of $J_{GC}(x, \varphi)$ in x. Hence,

$$\begin{aligned} \overline{J_{GC}} &\approx \frac{2 f_{max} T}{\lambda} \int_0^{\lambda/2} \frac{x^2}{\sigma^4} \exp\left(-\frac{x^2}{2\sigma^2}\right) dx \\ &\sim \sqrt{2\pi}\, \frac{f_{max} T}{\lambda\, \sigma}, \end{aligned} \tag{19}$$

for $\sigma \ll \lambda$. The derivation of the exact formula is given in the appendix. The tuning width σ can be expressed as a product of the spatial period λ and the relative tuning width per spatial period, which we call the area ratio r_A. We define the tuning curve's

width by the firing rate relative to the maximum firing rate. If $f \geq \beta f_{max}$ delineates a firing field, then the following relationship holds:

$$\sigma = \frac{r_A \cdot \lambda}{2\sqrt{\log(1/\beta^2)}}. \tag{20}$$

Consequently, we have $\overline{J_{GC}} \sim \frac{f_{max}T}{\lambda^2 r_A}$. In Figure 4a, the average Fisher information of a grid and a place cell are compared. Both parameters, the spatial period and the tuning width, are expressed in terms of the normalized stimulus range and are varied between 0 and 1. Whereas the average Fisher information of a place cell is inversely proportional to the tuning width σ, the average Fisher information of a grid cell is inversely proportional to the square of the spatial period λ. As the tuning curve width σ narrows, the mean firing rate in a place code decreases, whereas a grid cell maintains a constant mean firing rate as λ changes, by construction. On a per spike basis, the scaling of the average Fisher information with σ is identical for place cells and grid cells.

By rescaling the lattice length scale λ, the local resolution of a grid cell population can improve. Yet periodicity also introduces ambiguity, such that a typical neuronal response for a single grid cell maps onto $\lfloor 2/\lambda \rfloor$ possible values of x. Adding neurons with shifted tuning curves of the same spatial period and considering the population response still leads to ambiguity. So the error made in decoding can be large, even though the Fisher information indicates otherwise. Indeed, for $\lambda \ll 1$, the expected error approaches the variance of x over the uniform distribution on the interval $[0, 1]$:

$$\chi^2_{AE} = 1/\overline{J_{GC}} \sim 1/\lambda^2 \qquad \underset{\lambda \to 0}{\ll} \qquad \mathbb{E}\left((x - \hat{x})^2\right) = 1/12. \tag{21}$$

Hence, χ^2_{AE} can be much less than χ^2_{MLE}, for instance; the asymptotic estimate falls far short of what can realistically be achieved using any decoder. The solution lies in using different length scales in parallel, which allows one to exploit the higher resolution at short length scales. This observation also emphasizes that the MASE analysis has to be supplemented by numerical studies of the MMLE for grid codes.

3.2 Modular Codes, Self-Similarity, and Power-Law Scaling

As pointed out above, the asymptotic error (AE) may never be achieved by maximum likelihood estimation (MLE) or any other estimator, as a grid code's periodicity causes ambiguity, even in the absence of noise: if we consider the population response as a code word, there will be distinct stimuli that give rise to the same code word. Therefore, we will now construct a class of grid codes, called nested grid codes, that will contain no recurring codewords for stimuli on the interval $[0, 1]$. For such codes, MLE can attain the asymptotic error, as we show later.

A nested modular code consists of dividing the population of N neurons into L subgroups of M_i neurons, whose tuning curves are periodic on the same length scale λ_i. Each subgroup is called a *module*. The range of stimuli that such a nested grid code represents is at least as long as the longest lattice length scale $max(\lambda_i)$, and possibly

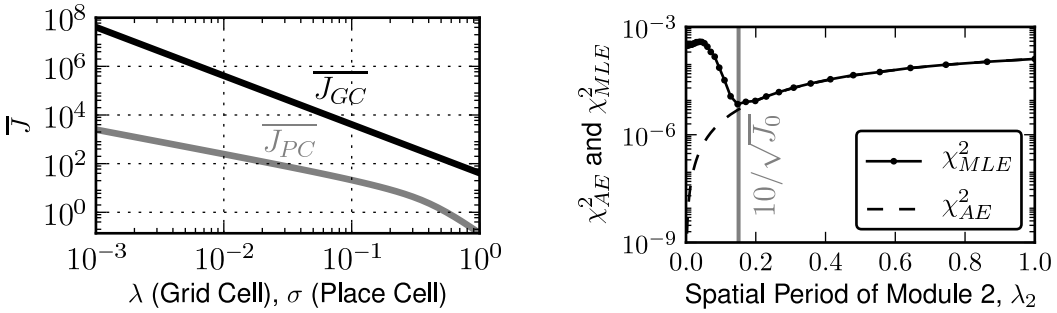

(a) (b)

Figure 4: (a) Average Fisher Information versus spatial period λ and tuning width σ, both normalized to the unit span $[0, 1]$. The average Fisher information of a grid cell $\overline{J_{GC}}$ scales as λ^{-2}, whereas the average Fisher information of a place cell $\overline{J_{PC}}$ scales as σ^{-1}. For $\sigma \approx 1$, the tuning curve becomes wider than the stimulus space, leading to a more rapid fall-off in the average Fisher information of the place cell than σ^{-1}. (b) Mean maximum likelihood estimate square error χ^2_{MLE} and mean asymptotic square error χ^2_{AE} for a grid code on an one dimensional unit interval with two modules of $M = 25$ neurons each. We use Monte Carlo methods to compute χ^2_{MLE}, whereas the analytical Fisher information is used for the asymptotic estimate. The first module is non-periodic and comprises 25 equidistantly arranged Gaussian tuning curves with tuning width $\sigma = 1/\left(5\sqrt{2}\right)$ and a 10 Hz peak firing rate, integrated over $T = 1$ second. This corresponds to a peak spike count of 10, much larger than $f_{max} \cdot T \approx 1$ in Bethge et al. (2002). The second module also comprises 25 equidistantly arranged cells with tuning curves that are periodically extended versions of the tuning curves of the first module with spatial period λ_2. The numerically determined χ^2_{MLE} closely follows the asymptotic error given by the inverse Fisher information χ^2_{AE} for spatial periods of $\lambda_2 > 0.18$. This is roughly $10 \cdot 1/\sqrt{J_0}$, that is, 10 times the square root of the inverse Fisher information of module 1. If the periodicity of the next module falls below the typical range of errors made by the first module, the Fisher information ceases to capture the MLE error.

much longer. But for simplicity take $max(\lambda_i) > 1$, as some of the ideal, modular grid codes with optimal resolution derived below will have a range that is exactly $max(\lambda_i)$. Furthermore, we make the *a priori* assumption that each module can be read out individually, *i.e.* that a spatial phase relative to the length scale λ_i can be determined from the population response of this module. According to Eq. (19), the Fisher information of a given module scales as

$$\bar{J}_i \sim \frac{M_i}{\lambda_i \langle \sigma_i \rangle}, \tag{22}$$

in which $\langle \sigma_i \rangle$ is the average width parameter for the tuning curves in the module (cf. appendix for the precise equalities). Within one spatial period, the grid cells code position the same way place cells do. Hence, as is the case for place cells, the optimal

tuning width scales as

$$\langle \sigma_i \rangle \sim \frac{\lambda_i}{M_i}. \tag{23}$$

So the Fisher information for the module scales as

$$\bar{J}_i = \frac{C_1^2 M_i^2}{\lambda_i^2}, \tag{24}$$

when the tuning curve widths are optimized. Here C_1^2 is a constant, which we write using a power of two for later convenience. Summing over all modules, the Fisher information of the grid code can be written as:

$$\overline{J_{GC,N}} = C_1^2 \sum_{0 \le i \le L-1} \frac{M_i^2}{\lambda_i^2}. \tag{25}$$

Within any grid code, the spatial periods can always be ordered so that $\lambda_0 > \lambda_1 > \cdots > \lambda_{L-1}$. In a nested grid scheme, two types of error can occur during decoding. Imagine a grid code with two modules and periods $\lambda_0 > \lambda_1$. The module with the shorter spatial scale λ_1 refines the representation at the coarser scale λ_0, such that the period λ_1 "discretizes" the period λ_0 —note that we do not assume that λ_0 is an integer multiple of λ_1. If $\hat{x}$ is an estimate of the position x based on module λ_0, then there is a finite probability that $|\hat{x} - x| > \lambda_1$. In such an event, which we call a discretization error, the module with period λ_1 cannot improve the estimate of x. The second type of error is the local error, which is less catastrophic and is bounded by the inverse of the Fisher information.

To limit the probability of a discretization error per module to less than ϵ, we will insist that

$$D(\epsilon) \Big/ \sqrt{\overline{J_i}} \le \lambda_{i+1} \le \lambda_i, \tag{26}$$

where $D(\epsilon)$ is a safety factor. This safety factor can be computed from the probability distribution of the deviation between the (efficient) estimate $\hat{x}$ and the true value x, based on the population spike count from a single module. In the asymptotic limit ($M_i \gg 1$ and $f_{max} T \gg 1$), this probability distribution can be modeled by the Laplace approximation $p(x - \hat{x}) \propto \exp\left[-(x-\hat{x})^2 \overline{J_i}/2\right]$; hence,

$$D(\epsilon) = \sqrt{2}\, \mathrm{erfc}^{-1}(\epsilon). \tag{27}$$

For instance, a safety factor $D(\epsilon) = 4$ guarantees that the discretization error probability is less than 10^{-4}. Given such a constraint, the Fisher information (25) is maximized when the lower bound in (26) is attained. This implies that

$$\lambda_i = \lambda_0 \cdot \left(\prod_{j<i} \frac{C_1}{D(\epsilon)} M_j \right)^{-1}. \tag{28}$$

Defining $\widetilde{M}_j = \sqrt{C_1/D(\epsilon)} M_j$, the population Fisher information (25) becomes

$$\overline{J_{GC,N}} = \frac{C_1 D(\epsilon)}{\lambda_0^2} \sum_{0 \le i \le L-1} \prod_{j \le i} \widetilde{M}_j^2. \tag{29}$$

Maximizing the Fisher information in Eq. (29) for integer M_i subject to the constraint $\sum_{i=0}^{L-1} M_i = N$ leads to

$$M_i \approx N/L, \tag{30}$$

as long as $L \ll \sqrt{C_1/D(\epsilon)}N$. For instance, if $\sqrt{C_1/D(\epsilon)} \sim \mathcal{O}(1)$, then the condition for $M_i \approx N/L$ reads $N/L \geq 3$. Otherwise, $M_i = 3$ for $i \leq \lfloor N/3 \rfloor$ and $M_i = 0$ for $i > \lceil N/3 \rceil$ leads to the maximal Fisher information. Therefore, we should assign an equal number M of grid cells to each grid module, so that all modules are *self-similar*. As a corollary, the area ratio r_A between mean field width and the spatial period should be constant across modules. This prediction is consistent with experimental data from Brun et al. (Brun et al., 2008). The experimentally determined ratio[2] of field width to period is $r_A \approx 0.3$. This ratio remains approximately constant along the dorso-ventral axis of mEC, even as the spatial period λ varies.

For constant M, eq. (26) indicates that the sequence of length scales λ_i should form a geometric progression. In this case, the population's Fisher information becomes:

$$\begin{aligned}\overline{J_{GC,N}} =& \frac{M^2 C_1^2}{\lambda_0^2} \cdot \sum_{i=0}^{L-1} \widetilde{M}^i = \frac{M^2 C_1^2}{\lambda_0^2} \frac{\widetilde{M}^{2L} - 1}{\widetilde{M}^2 - 1} \\ &\geq \frac{C_1 D(\epsilon)}{\lambda_0^2} \left(\widetilde{M}^2\right)^{N/M}\end{aligned} \tag{31}$$

Hence, the Fisher information for a nested grid code obeys a power law in the number of neurons N for fixed module size M. Such a coding scheme, therefore, outperforms a place code that scales at best as N^2, which happens when the tuning width scales as N^{-1}.

We need to resort to numerical simulations to test whether $\overline{J_{GC,N}}$, as given by Eq. (31), reliably predicts the true error in decoding x from the neuronal response measured over short time windows. Figure 4b reveals that the error in the maximum likelihood estimate is close to the asymptotic error, as long as the safety factor $D(\epsilon)$ is sufficiently large.

In summary, for a modular grid code to achieve high spatial resolution, the grid lattices should form a geometric progression in the spatial periods, and each module should be self-similar. Only relatively few distinct spatial phases are needed at each length scale, but they should generally number at least three. If the number of encoded phases is low, the spatial tuning width should be broad to ensure that the animal's position is uniformly and isotropically represented, even when observing only a finite subset of neurons.

[2]Experimentally defined as the median of the set of pairwise grid field to grid field spacings.

4 The Spatial Resolution of Maximum Likelihood Decoding

Within a fixed time window T, neurons will fire a finite number of spikes, yielding a population vector K of spike counts. As the animal moves, this time window needs to be short to create a running estimate x, which will rely only on a few spikes. Maximum likelihood (ML) decoding requires performing numerical calculations (cf. appendix) and returns the most likely position x given K. Such estimates will be subject to both local and global errors; the Fisher information only predicts the local error in the limit as $f_{max}T \to \infty$. Therefore, the ML error χ^2_{MLE} may diverge from the asymptotic error χ^2_{AE}, and the optimal parameter settings will change. We will use ML to study both grid codes for which the spatial periods are asymptotically optimal and grid codes drawn from random ensembles. Randomly selecting the spatial periods will reveal how generic the properties of good grid codes are.

4.1 Maximum Likelihood Decoding—Simulation Results

We calculated the spatial resolution by maximum likelihood methods, again for a population of 100 grid and place cells, respectively, and $f_{max}T = 3$. To examine the error made in reading out the place code, we varied the width σ of the tuning curves.

The simulations show that the mean maximum likelihood error (χ^2_{MLE}) of a place cell diverges substantially from the mean asymptotic square error (χ^2_{AE}) for small tuning widths sigma, i.e. for narrow place fields (Fig. 5a). In particular, the spatial width that minimizes the asymptotic error is ten times smaller than the width that minimizes the MLE.

The grid codes do not differ in the relative tuning width of the spatial firing rate profiles, but in the number of spatial periods and the length scales that describe the grid lattice spacing. Asymptotic theory (section 3.2) predicts that these length scales should form a geometric sequence. By choosing the largest spatial period λ_1 to be unity and then creating grid codes characterized by different ratios for the successive periods, we investigate the concordance between the maximum likelihood error (MMLE) and the asymptotic error (Fig. 5). If the modules are nested so that the contraction factor $0.5 < s < 1$, the MLE approaches the asymptotic error. For factors $s < 0.5$, the MMLE exceeds the asymptotic error; the asymptotic error keeps decreasing forever, whereas the MMLE will eventually increase. The MMLE is not convex, however, in s. When the contraction factor s is close to an even divisor of unity, such as $s = 1/2, 1/3, \ldots$, the MMLE diverges more strongly from the asymptotic error. In such exceptional cases, all modules attain a maximum close to $x = 1$, which, by the periodicity of the tuning curves, can be wrapped around to join the maximum at $x = 0$. In these cases, positions close to the boundaries of the unit interval, i.e., either close to zero or close to one, elicit similar patterns of spikes. Mistaking a position $x = \epsilon$, where $\epsilon \ll 1$, for a position close to $1 - \epsilon$, however, corresponds to a huge error. Hence, the MMLE is higher. Moreover, as the contraction factor becomes smaller, fewer intermediate modules remain. These

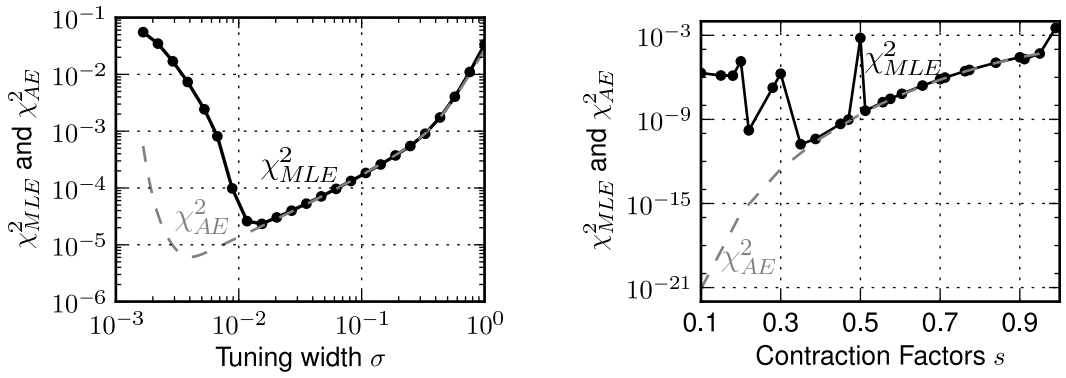

(a) (b)

Figure 5: Mean maximum likelihood estimate square error (χ^2_{MLE}) and mean asymptotic square error (χ^2_{AE}) of place code and histogram of MMLE of grid codes with 100 neurons, $f_{max}T$=3. (a) Double logarithmic plot of the mean maximum likelihood estimator square error χ^2_{MLE} as a function of the spatial width σ compared with the mean asymptotic square error χ^2_{AE} for place code comprising 100 cells and $f_{max}T = 3$. (b) The mean maximum likelihood estimate square error χ^2_{MLE} for geometric progressions of grid lattice spacings with contraction factor s, compared to the mean asymptotic square error χ^2_{AE} . The factor s determines the spatial periods as $\lambda_i = s^{i-1}$ for $1 \leq i \leq 10$. Each module comprises 10 equidistantly arranged spatial phases.

modules with intermediate lattice spacings allow maximum likelihood estimation to correct for errors in the spatial phase represented by coarser modules. For $s \ll 1/2$, the increasing lack of compensation for errors causes the MMLE to rise, whereas the asymptotic error becomes ever smaller. Additionally, as $s \to 0$, any contraction factor becomes close to $1/n$ for some n — these are the exceptional cases mentioned above that have high MMLE. Note that these exceptional cases can be avoided by taking λ_1 to be slightly larger than unity.

Hence, for grid codes whose modules are staggered in a geometric sequence, the resolution is much higher than in a place code (Fig. 5). Is this result, however, generic? In other words, if one were to randomly put together a grid code with different spatial periods, would the resolution still be higher? To answer this question, we created randomly sampled grid codes as described in section 2, for which we estimated the MMLE. The histogram in Figure 6 shows the distribution of MMLE's for the ensemble. The grid codes' MMLE can then be compared to the MMLE for the optimal place coding scheme with the same number of neurons, depicted as a dashed reference line in Figure 6. Some grid codes are worse than the optimal place code: choosing a narrow span of spatial periods leads to poor spatial resolution (cf. the second highlighted example in Figure 6).

Closely spaced spatial periods should confer upon the grid code the ability to uniquely represent an extended range of positions, going far beyond the unit interval (Fiete et al., 2008). Nonetheless, here we compare not the ranges of different grid codes, but the ability of the codes to resolve positions within the fixed unit interval. For some grid

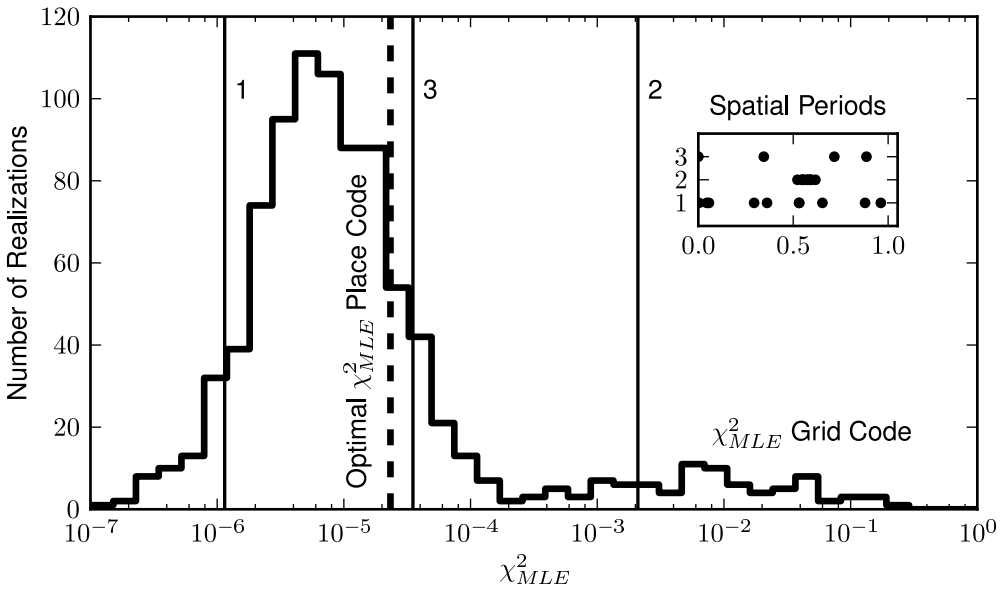

Figure 6: Histogram of mean maximum likelihood estimate square error (χ^2_{MLE}) for grid codes with 100 neurons, $f_{max}T$=3. Histogram of MMLE for 885 simulated grid codes, which were randomly drawn according to the method described in section 2, and contrasted with the optimal place-code MMLE depicted as a dashed line. The inset shows the spatial periods of the three example grid codes; the corresponding MMLE for these examples is marked on the histogram by a vertical line. Note that closely spaced spatial periods, such as in example 2, lead to poor spatial resolution.

codes, the unit interval corresponds only to a fraction of the full theoretical range.

Around three-quarters of the randomly drawn grid codes have better MMLE than the best place code; hence, it is likely that a generic grid code, one with unrestricted range, will lead to a higher spatial resolution than the best place code.

What common properties do the better grid codes have? One key feature is that their spatial periods span a large range. For Figure 7, we binned the smallest and largest period of each grid code in the ensemble, and depict the highest resolution for each binned pair of $\min_i \lambda_i$, $\max_i \lambda_i$. The resolution increases both in the direction of smaller $\min_i \lambda_i$ and, to a lesser degree, in the direction of larger $\max_i \lambda_i$. Each grid code is determined by the spatial periods of its modules. Figure 8a depicts the set of spatial periods for the ten best grid codes in the random ensemble. As suggested by the asymptotic analysis, the grid codes with the lowest MMLE have in common that the smallest spatial period $\min_i \lambda_i$ is close to zero. In many cases, the largest spatial period, $\max_i \lambda_i$, nearly covers the entire unit interval represented by the code. The random sampling of spatial periods was unbiased: the *a priori* distribution of spatial periods is almost uniform (Fig. 8b). In the best grid codes, the smaller spatial periods are overrepresented. Selecting the hundred spatial periods from the best grid codes in the sample strongly shifts the distribution of spatial periods to the lower range (Fig. 8b).

Unlike the asymptotic error, which monotonically decreases with the smallest spa-

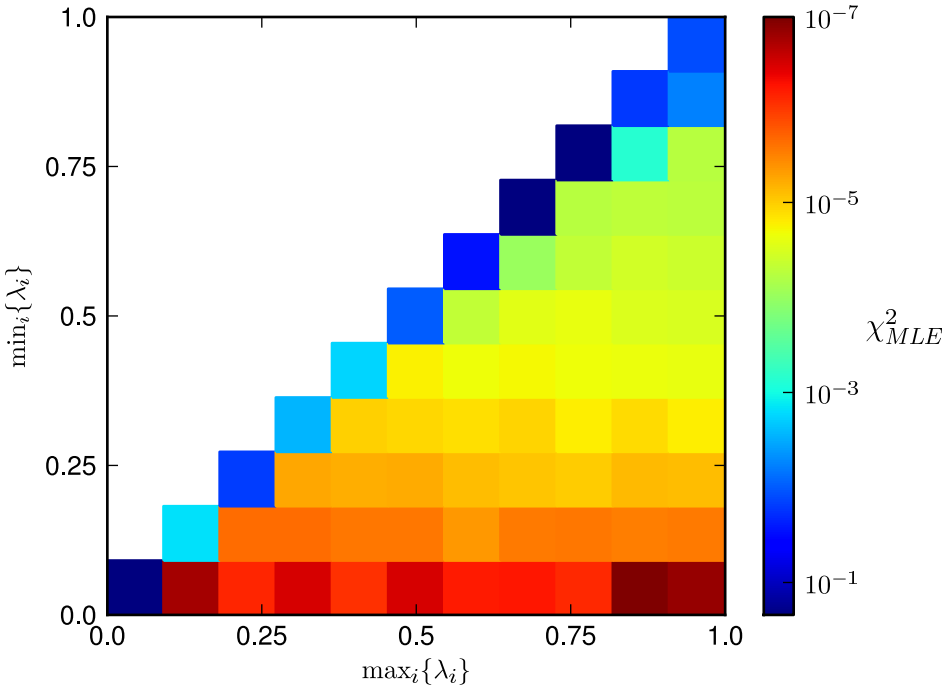

Figure 7: Mean maximum likelihood estimate square error (χ^2_{MLE}) as a function of the minimal and maximal spatial period. After dividing the spatial periods into bins, the smallest MMLE present in the random ensemble of grid codes is color-coded for each combination of smallest and largest spatial period. The results show that grid codes with similar smallest and largest spatial periods result in a large MMLE. Decreasing the smallest period, while keeping the largest period fixed, strongly improves the resolution; in contrast, keeping the smallest period fixed and increasing the largest period leads to a smaller improvement. The highest resolution is obtained when the smallest and largest period are far apart.

tial period, the MMLE reaches an optimum. In the randomly sampled ensemble, going below $\min_i \lambda_i \approx 10^{-2}$ typically confers no advantage. A direct comparison between MMLE and the asymptotic error is shown in Figure 9. In some cases, the MMLE is much higher than the asymptotic error; throughout all cases, the MMLE never drops below 10^{-7} relative to the unit interval, whereas the asymptotic error can be orders of magnitude lower. One should note, also, that deterministically generating sequences of grid modules using Eq. (26) yields a considerably lower MMLE than even the lowest MMLE's in the random ensemble that we tested.

5 Discussion

The neural representation of position in world coordinates is always subject to distortion due to the noisy, spiking nature of neurons. Just as photographing an athlete in motion

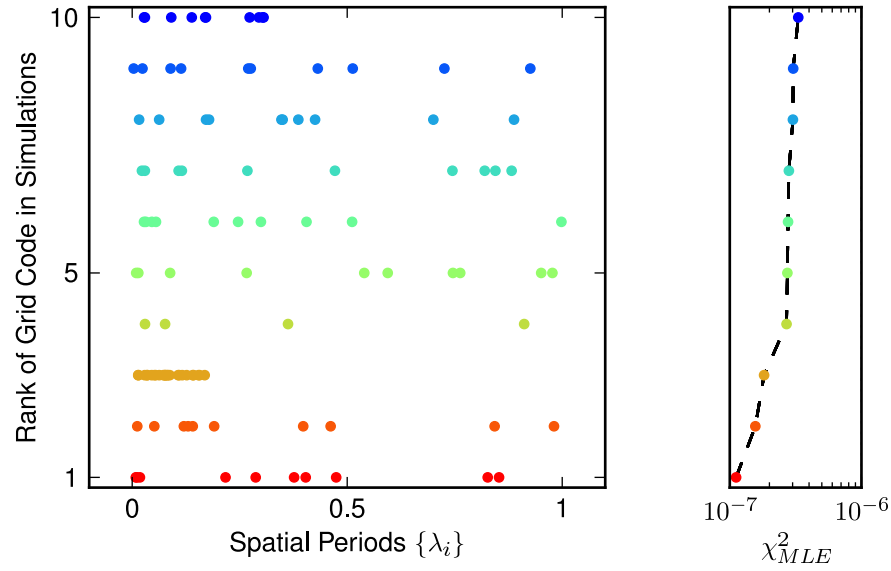

(a)

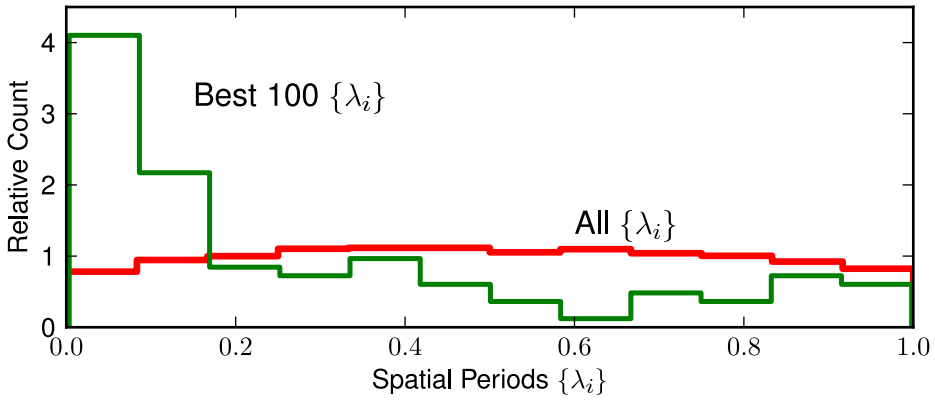

(b)

Figure 8: (a) Spatial periods of samples with highest mean maximum likelihood estimate square error (χ^2_{MLE}). Scatter plot of spatial periods of 10 best grid codes in simulations and their corresponding MMLE, arranged from small to large MMLE. (b) Distribution of spatial periods with highest mean maximum likelihood estimate square error (χ^2_{MLE}). Histogram of the spatial periods in all simulated grid codes and of the 100 samples with the lowest MMLE. The overall distribution has no substantial preference, whereas the distribution of the 100 spatial periods from the best grid codes is strongly skewed.

rules out a long shutter time, capturing the instantaneous position as an animal explores its environment precludes averaging over long times–no matter whether single neurons fire at labeled positions (place cells) or at triangular lattice points in space (grid cells), noise will limit the resolution an animal needs to orient itself and navigate.

By considering stochastic models for neuronal populations, we have shown that grid

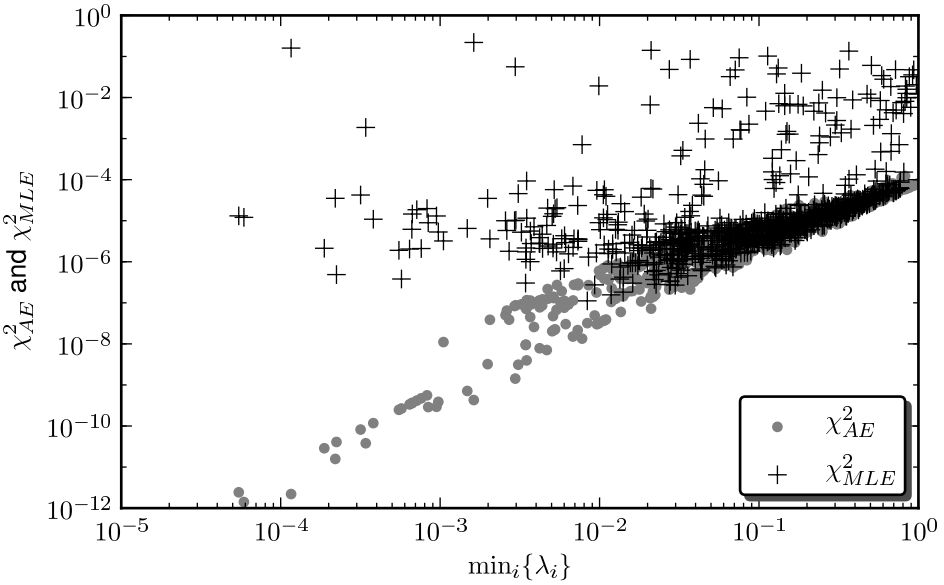

Figure 9: Comparison of mean maximum likelihood estimate square error (χ^2_{MLE}) and mean asymptotic square error (χ^2_{AE}) for grid codes. Double logarithmic plot of MMLE vs. asymptotic error for grid code plotted against the smallest spatial period. Smaller periods refine the unit interval more, yielding better spatial resolution. The asymptotic error decreases, on average, quadratically as the minimum spatial period becomes smaller, serving as a lower bound for the MMLE. Grid modules that are not properly nested lead to a much higher error than predicted asymptotically. Furthermore, the lower bound is no longer tight for $\min_i \lambda_i < 10^{-2}$. No generic grid code from the random ensemble achieved an MMLE lower than 10^{-8}, even though the asymptotic error values drop to 10^{-12}.

cells can achieve higher spatial resolution than any possible arrangement of the same number of place cells. We computed the resolution for both coding schemes by decoding the most likely position in space from the number of spikes across the population within a short time window. The average divergence between the true and estimated position is bounded from below by the inverse of the average Fisher information, an analytically calculable measure of the asymptotic local coding precision: whereas the average Fisher information scales inversely with the tuning width for place cells, it scales inversely with the *square* of the tuning width for grid cells. Grid cells gain this advantage by firing at multiple locations in space; place cells, in contrast, inherently exhibit 'sparser' neuronal discharge. But for a grid code to show improved spatial resolution over a place code, the grid lattices must be strategically arranged; many randomly constructed grid codes are actually worse than the best place codes.

Distortion theory predicts how good grid codes should be constructed. First, grid lattices should exist at different spatial scales, yet short length scales should predominate. Each scale constitutes an independent module, comprising grid cells with a common spatial period λ_i but different spatial phase offsets (Hafting et al., 2005, for instance).

After constructing an ensemble of grid codes by randomly sampling λ_i, we found that good grid codes strongly skewed the distribution of λ_i's to small values, such that larger spatial periods are fewer, yet still present: the full spatial range and the largest spatial period were typically of the same length scale and not an order of magnitude apart. Brun *et al.* recorded the spatial periods of different grid cells along the dorsoventral axis of the mEC; the histogram of spatial periods is similar in its skew (Brun et al., 2008). Some grid cells had spatial periods of more than 8 meters on a 18 meter linear track. The typical lattice spacing of grid cells grows along the dorsoventral axis, yet reported grid cells were recorded along the first 75% of this axis (Brun et al., 2008), implying that longer length scales may yet be found, particularly if it becomes feasible to record from rodents foraging on a football field. Our theoretical results also predict that the spatial periods should be plastic and adapt to the largest length scale in the local environment to achieve high spatial resolution. Indeed, grid lattices in mEC rescale when a familiar enclosure is artificially expanded or shrunk by a moderate factor, such that the relative positions of landmarks is maintained (Barry et al., 2007).

Secondly, achieving high spatial resolution with a fixed number of grid cells favors scaling the size of the firing fields with the spatial period of the grid module; furthermore, we can predict the ratio of firing field width to the spatial period. A grid module with spatial period λ_i consists of several grid cells, whose spatial lattices are shifted relative to each other. Hence, a grid code represents the spatial phase in firing field-sized bins, yielding a discretized phase.

If one only distinguishes whether a cell is active or not, one observes the following: Given M grid cells that tile the range $[0, 1)$ in a non-overlapping manner, the phase resolution is at least $\Delta\varphi = 1/M$. If the next module recursively tiles each phase of the preceding module into M bins, such a scheme would have a resolution of $\left(\frac{1}{M}\right)^{N/M}$, where N is the number of cells. The highest spatial resolution is reached by trading off the number of spatial periods per module with the number of grid modules.

For discrete encoding, three grid cells per module are ideal, with the firing field of each grid cell covering one-third the spatial period. Each module associated with one spatial period will be perfectly nested inside another module. Nesting naturally gives rise to a strongly skewed distribution of spatial periods on a linear scale.

Some of the conclusions from the binary coding case considered above carry over to the continuous coding case, in which one discerns between different firing rates. Maximizing the Fisher information of the population code reveals that the grid code should still stagger the modules' spatial periods in a geometric progression, $\lambda_{n+1} = s\lambda_n$. The contraction factor in the geometric series $s = \lambda_{i+1}/\lambda_i$ depends on the relative resolution of each module and hence crucially on the number of neurons per module and the peak firing rate. As having more modules at the expense of phases per module is advantageous, the ratio of field width to spatial period should be comparatively large; in fact, the optimal ratio will approach the minimum allowed by the number M of distinct phases. The ideal number M is no longer necessarily three, but rather depends on the tolerable level of risk for catastrophic error during decoding. The greater M, the lesser this risk.

The design principles for grid codes were derived from asymptotic theory, which assumes that the time window for observing the neuronal population's response is sufficiently long. While the (asymptotic) Fisher information reveals how the error scales with tuning curve parameters (Zhang and Sejnowski, 1999; Brown and Bäcker, 2006), it could severely underestimate the true error (Bethge et al., 2002). We, therefore, pursued a systematic comparison between the asymptotic theory and the true maximum likelihood error, which was evaluated numerically by simulating the neuronal response over short time windows. For instance, one can construct a grid code with two modules for which the asymptotic error goes to zero, as one lets the smallest spatial period become infinitely small. An analysis of the mean maximum likelihood error (MMLE), however, revealed that the minimal spatial period is, in fact, bounded. Likewise, the asymptotic error systematically underestimates the optimal tuning width for a place code. Yet the MMLE also confirmed some of the scaling properties of grid codes predicted by the Fisher information. For instance, the resolution of grid codes still scales exponentially in the number of neurons, implying that grid codes are superior to place codes, even under realistic conditions.

Our analysis suggests that even with noisy, spiking grid cells, the roughly 10^5 neurons in the mEC (Mulders et al., 1997) should be able to encode the animal's position in space with exquisite precision. Four factors limit the effective resolution:

- The smallest spatial period cannot be arbitrarily small.
- Not all neurons in mEC contribute to encoding the position.
- A realistic decoding mechanism will not achieve the resolution of an ideal observer.
- A putative decoder network may not have access to the whole ensemble of grid cells.

If we read out the spikes within one cycle T of the ongoing theta oscillation while a rodent is running near its peak speed of about 150 cm/s on a linear track, the minimal spatial period has to be bounded by $\lambda_{min} > T/v_{max} \approx 20$ cm. Otherwise, the animal will traverse multiple grid lattice points within a single theta cycle. The spatial resolution for an ideal grid code scales with the square of the smallest period. Moreover, the spatial resolution will increase with the square root of the number of neurons that share this spatial period, but the effective number might be less than gross anatomy suggests. While place cells in the dentate gyrus and area CA3 of hippocampus are targets of layer II of mEC, such neurons will presumably not be strongly connected to all neurons in mEC, but just to a few. In general, a downstream neuron that "decodes" the animal's position might only have access to a restricted number of grid cell inputs; predicting the size of grid fields also required us to assume that the number of grid cells is finite. Several theoretical models propose that the ensemble firing of grid cells gives rise to single, isolated place fields in hippocampus by superposition (Fuhs and Touretzky, 2006; Solstad et al., 2006; Rolls et al., 2006; Franzius et al., 2007; Si and Treves, 2009; Cheng and Loren, 2010); arbitrary or all-to-all connections between grid and place cell

layers, however, often give rise to multiple firing fields (Solstad et al., 2006). The average of measured firing field to period ratios lies around 0.3 (Brun et al., 2008), which is consistent both with the theoretical prediction and the hypothesis that each place cell in DG and CA3 is strongly innervated only by a small subsample of grid cells from each grid module along the dorsoventral band (Solstad et al., 2006).

A key assumption in this analysis was that the spike counts obey a Poisson distribution. The fine temporal pattern of spike trains in both place and grid cells is anything but Poisson, as ongoing hippocampal-entorhinal-cortical rhythms imprint their structure on the timing of spikes (Deshmukh et al., 2010; Quilichini et al., 2010; Bragin et al., 1995). These rhythms might, indeed, be essential for generating the spatially localized firing fields in these cells (Burgess et al., 2007; Hasselmo et al., 2007; Burgess, 2008; Remme et al., 2010; Geisler et al., 2010). For instance, Geisler *et al.* correlate the frequency shift between intrinsic firing and the 7-12 Hz theta oscillation in the local field potential with the size of the firing field in CA1 of hippocampus. Likewise, the spatial period and neural resonance properties correlate along the dorsoventral axis of the mEC (Garden et al., 2008; Giocomo et al., 2007). We used the time scale of the theta oscillation to define the time window in which to count spikes, but discount the fine structure of spike timing within this time window. Rapid oscillations largely average out in the sum that represents the probability of the spike count. The detailed temporal structure of hippocampal place cell firing can be captured by multiplying or linearly convolving the oscillations with the spatial tuning curve (Itskov et al., 2008); repeated traversals of the firing field are accompanied by different phases of the oscillations, which adds to the variance of the spike count. Preliminary analysis of linear track data (Hafting et al., 2005) for grid cells indicate that the spike counts generally are close to Poisson (Kluger et al., 2010), notwithstanding the fact that the fine temporal structure is not Poisson. For place cells, Fenton and colleagues (Fenton and Muller, 1998) find that place cells fire even more variably than would be predicted by a Poisson model; the excess variance is attributable to attention (Fenton et al., 2010) or nonspatial signals that modulate the firing rate, but not the location of place cell firing (Leutgeb et al., 2005; Jackson and Redish, 2007). The spatial resolution of a place code should suffer when the position signal is conflated with other signals, providing one more reason why the grid code in mEC might be better suited for integrating path information than the place code in CA1. Both place cells and grid cells encode position not only in the firing rate, but also in the timing of spikes relative to the ongoing theta oscillation (O'Keefe and Recce, 1993; Hafting et al., 2008). A temporal phase code at the single cell or population level is potentially more precise in resolving spatial location than counting spikes; decoding such a code, however, was beyond the scope of this study.

Estimating the most likely spatial location relies on having full knowledge of the place and grid field firing rate profiles at each location. For the grid code, the lattices need not be perfectly regular to achieve high spatial resolution. What is required is simply a disjunctive union of intervals at successively finer spatial scales; the periodicity of the intervals is irrelevant. For instance, applying different lateral shifts to different firing fields of within one module would disrupt the periodicity, but not change the

resolution. Moreover, the existence of modules, defined as subpopulations of neurons whose grid fields have the same spacing, is not truly required—each grid cell can possess its own lattice spacing, drawn from the entire continuum of possible length scales. As long as all length scales are densely represented, maximum likelihood decoding of the population response will be highly accurate and subject to low error.

On the other hand, both periodicity and modularity are crucial for the 'modular arithmetic scheme.' The spatial range, defined as the maximum distance that is uniquely represented by the set of all modules, is unbounded in the absence of noise, leading to the remarkable property that a huge spatial range, on the order of kilometers, could be supported by modules with λ_i's ranging from thirty to seventy centimeters (Fiete et al., 2008). To extend the spatial range beyond the maximum grid period, Fiete *et al.* proposed that the spatial periods should not be multiples of each other nor, more generally, have common divisors. Such a constraint can be satisfied aptly by a set of close spatial periods; indeed, the largest spatial range will be obtained when the periods cluster near the maximal period. In the presence of noise, though, narrow spatial periods make the grid code excruciatingly prone to error, leading to a dramatic loss of spatial resolution. In principle, these problems can be overcome by adding redundancy, using modules with very low errors and fine correction algorithms, yet this is a non-trivial challenge. In addition, the grid modules should be highly stable over time for such computations to be feasible. Experimental results indicate that the spatial periods rescale in response to changing the geometry of the environment (Derdikman et al., 2009) or the context (Fyhn et al., 2007), and in general exhibit a high variability between trials (Brun et al., 2008; Kluger et al., 2010; Reifenstein et al., 2010). While variability may greatly diminish the effective spatial range of a grid code, the local resolution can still be sufficiently high, as we have shown. In this interpretation, the entorhinal cortex's function is to *locally* represent the animal's position with high resolution, using grid-based coordinate maps that are continually reset and calibrated by landmarks or spatial memory via the hippocampus (McNaughton et al., 2006).

Grid coding maintains its advantage over place coding even in higher-dimensional stimulus spaces. For a grid cell encoding more than one stimulus dimension, the average Fisher information of the population scales as λ^{-2} in each dimension. Indeed, if the tuning curve is separable into its individual components (i.e., dimensions), then the Fisher information of grid cell is simply related to the Fisher information of a place cell with a comparable tuning curve width:

$$\overline{J_{GC}} \sim \begin{pmatrix} \frac{1}{\lambda_1} & & 0 \\ & \ddots & \\ 0 & & \frac{1}{\lambda_N} \end{pmatrix} \cdot \overline{J_{PC}},$$

In general, the Fisher information is a matrix, which is diagonal in simple cases. The more general case, for tuning curves that are periodic on arbitrary lattices in more than one dimension, is treated by Mathis et al. (2011a,b).

Given that the grid code can be orders of magnitude better than the place code, based on the mean maximum likelihood error (MMLE), why are both codes used? Hippocampus may have ten times as many neurons as medial entorhinal cortex (Mulders

et al., 1997), but achieves the same spatial resolution, based on these arguments. Yet grid codes and place codes may well serve different purposes. Entorhinal cortex draws on head-direction and velocity inputs (Sargolini et al., 2006), integrating over the path of motion. Grid lattice representations of the external world are well suited for dead reckoning during navigation. As the hippocampus is essential for forming new episodic memories (O'Keefe and Nadel, 1978), we speculate that place fields are needed for associating specific events with specific locations. Synaptic plasticity and long-term potentiation occurs between pairs of cells, so that if the firing of a single cell already represents a unique location, synapses can easily adapt to the conjunction of location and sensory information. A distributed representation of location, as in a grid code, is less suited for forming such associations.

Acknowledgments

We would like to thank Carleen Kluger for helpful comments on earlier drafts of the manuscript and Dinu Paterniche for his graphics support. This work was supported by the Federal Ministry for Education and Research (through the Bernstein Center for Computational Neuroscience Munich 01GQ0440).

Appendix: Annalytical derivation and numerical methods

Fisher information of grid and place cell

The average Fisher information of a place cell $\overline{J_{PC}}$, was defined in equation (15), which stated:

$$\overline{J_{PC}} = \int_0^1 \int_0^1 f_{max} T \cdot \frac{(x-c)^2}{\sigma^4} \exp\left(-\frac{(x-c)^2}{2\sigma^2}\right) dx dc. \tag{32}$$

Here the details of the computation are given. The inner integral from (32) can be simplified by applying integration by parts.

$$\begin{aligned}\int_0^1 \frac{(x-c)^2}{\sigma^4} \exp\left(-\frac{(x-c)^2}{2\sigma^2}\right) dx = &\left[-\frac{x}{\sigma^2}\exp\left(-\frac{x^2}{2\sigma^2}\right) + \frac{\sqrt{2\pi}}{\sigma}\cdot \text{erf}\left(\frac{x}{\sqrt{2}\sigma}\right)\right]_{-c}^{1-c} = \\ =&\frac{c-1}{\sigma^2}\exp\left(-\frac{(c-1)^2}{2\sigma^2}\right) - \frac{c}{\sigma^2}\exp\left(-\frac{c^2}{2\sigma^2}\right) \\ &- \frac{\sqrt{2\pi}}{2\sigma}\cdot\left(\text{erf}\left(\frac{c-1}{\sqrt{2}\sigma}\right) - \text{erf}\left(\frac{c}{\sqrt{2}\sigma}\right)\right).\end{aligned} \tag{33}$$

In order to obtain (32) one has to integrate the result over $c \in [0,1]$. For the first two terms of (33): Since $-\exp(-\frac{x^2}{2\sigma^2})$ is a primitive for $\frac{x}{2\sigma^2}\cdot\exp(-\frac{x^2}{2\sigma^2})$ we obtain:

$$\left[-\exp\left(-\frac{(c-1)^2}{2\sigma^2}\right) + \exp\left(-\frac{c^2}{2\sigma^2}\right)\right]_0^1 = 2\cdot\left(exp\left(-\frac{1}{2\sigma^2}\right) - 1\right) \tag{34}$$

and for the second part again by integration by parts:

$$
\begin{aligned}
&-\frac{\sqrt{2\pi}}{2\sigma}\cdot\int_0^1\left(\text{erf}\left(\frac{c-1}{\sqrt{2}\sigma}\right)-\text{erf}\left(\frac{c}{\sqrt{2}\sigma}\right)\right)dc\\
&=\frac{\sqrt{2\pi}}{2\sigma}\cdot\sqrt{2}\sigma\cdot\left(\int_{-\frac{1}{\sqrt{2}\sigma}}^0-\text{erf}(s)ds+\int_0^{\frac{1}{\sqrt{2}\sigma}}\text{erf}(s)ds\right)\\
&=\sqrt{\pi}\cdot 2\cdot\int_0^{\frac{1}{\sqrt{2}\sigma}}\text{erf}(s)ds\\
&=2\sqrt{\pi}\cdot\left[s\cdot\text{erf}(s)+\frac{1}{\sqrt{\pi}}\exp\left(-s^2\right)\right]_0^{\frac{1}{\sqrt{2}\sigma}}\\
&=2\sqrt{\pi}\left(\frac{1}{\sqrt{2}\sigma}\text{erf}\left(\frac{1}{\sqrt{2}\sigma}\right)+\frac{1}{\sqrt{\pi}}\exp\left(-\frac{1}{2\sigma^2}\right)-\frac{1}{\sqrt{\pi}}\cdot\exp\left(0\right)\right)\\
&=\frac{\sqrt{2\pi}}{\sigma}\text{erf}\left(\frac{1}{\sqrt{2}\sigma}\right)+2\cdot\exp\left(-\frac{1}{2\sigma^2}\right)-2
\end{aligned}
\tag{35}
$$

Summing (34) and (35) the average Fisher information of a place cell (32) is:

$$
\overline{J_{PC}}=f_{max}T\cdot\left(\frac{\sqrt{2\pi}}{\sigma}\text{erf}\left(\frac{1}{\sqrt{2}\sigma}\right)+4\cdot\exp\left(-\frac{1}{2\sigma^2}\right)-4\right). \tag{36}
$$

The second and third term together behave like a staircase function that is zero for large σ and quickly approaches -4 for small values. The first term is the leading term, where erf $\left(\frac{1}{\sqrt{2}\sigma}\right)\approx 1$ for $\sigma<1$. Hence, e the average Fisher information scales as $\propto\frac{1}{\sigma}$ for small σ. The other terms change the behavior slightly, contribute a bend to the curve for $\sigma>0.1$ in Fig. (4a). This result is reported in the main text (Eq. (16)).

The average firing rate of a place cell can be calculated as follows:

$$
\overline{f_{PC}}=\int_0^1\int_0^1 f_{max}\exp\left(-\frac{(x-c)^2}{2\sigma^2}\right)dxdc, \tag{37}
$$

Analogously to the average Fisher information this integral can be computed by:

$$
\begin{aligned}
\overline{f_{PC}}&=\sqrt{2}\sigma f_{max}\int_0^1\int_{-\frac{c}{\sqrt{2}\sigma}}^{\frac{1-c}{\sqrt{2}\sigma}}\exp\left(-t^2\right)dtdc\\
&=\sqrt{2}\sigma f_{max}\int_0^1\frac{\sqrt{\pi}}{2}\left(-\text{erf}\left(\frac{c-1}{\sqrt{2}\sigma}\right)+\text{erf}\left(\frac{c}{\sqrt{2}\sigma}\right)\right)dc\\
&=f_{max}\left(\sqrt{2\pi}\sigma\text{erf}\left(\frac{1}{\sqrt{2}\sigma}\right)+2\sigma^2\cdot\exp\left(-\frac{1}{2\sigma^2}\right)-2\sigma^2\right),
\end{aligned}
\tag{38}
$$

where the last equation followed from (35).

Next, we present the computation of the average Fisher information of a grid cells $\overline{J_{GC}}$, as defined in equation 18, which stated:

$$
\overline{J_{GC}}=\frac{1}{\lambda}\cdot\int_0^\lambda\int_0^1 J_{GC}(x,\varphi)dxd\varphi. \tag{39}
$$

Due to the periodicity of $J_{GC}(x,\varphi)$ in x, $\overline{J_{GC}}$ need only be integrated over one half of the periodic domain, followed by multiplication with $2/\lambda$. Furthermore, for small periods averaging over different phases is not necessary, again due to the periodicity. Hence, for small λ, the case we are actually interested in is:

$$\overline{J_{GC}} = \frac{1}{\lambda} \cdot \int_0^{\lambda} \int_0^1 J_{GC}(x,\varphi) dx d\varphi \approx \frac{2 f_{max} T}{\lambda} \int_0^{\lambda/2} \frac{x^2}{\sigma^4} \exp\left(-\frac{x^2}{2\sigma^2}\right) dx \tag{40}$$

The last integral can be computed by similar means as above:

$$\begin{aligned}
&\int_0^{\lambda/2} \frac{-x}{\sigma^2} \cdot \underbrace{\frac{-x}{\sigma^2} \exp\left(-\frac{x^2}{2\sigma^2}\right)}_{=\left(\exp\left(-\frac{x^2}{2\sigma^2}\right)\right)'} dx \\
&= \left[\frac{-x}{\sigma^2} \exp\left(-\frac{x^2}{2\sigma^2}\right)\right]_0^{\lambda/2} + \frac{1}{\sigma^2} \cdot \int_0^{\lambda/2} \exp\left(-\frac{x^2}{2\sigma^2}\right) dx \\
&= \frac{-\lambda}{2\sigma^2} \exp\left(-\frac{\lambda^2}{8\sigma^2}\right) + \frac{\sqrt{2}}{\sigma} \cdot \int_0^{\frac{\lambda}{2\sqrt{2}\sigma}} \exp\left(-t^2\right) dt \\
&= \frac{-\lambda}{2\sigma^2} \exp\left(-\frac{\lambda^2}{8\sigma^2}\right) + \frac{\sqrt{2\pi}}{2\sigma} \mathrm{erf}\left(\frac{\lambda}{2\sqrt{2}\sigma}\right)
\end{aligned} \tag{41}$$

Thus Eq. (39) becomes

$$\overline{J_{GC}} = f_{max} T \left(\frac{\sqrt{2\pi}}{\sigma\lambda} \mathrm{erf}\left(\frac{\lambda}{2\sqrt{2}\sigma}\right) - \frac{1}{\sigma^2} \exp\left(-\frac{\lambda^2}{8\sigma^2}\right) \right). \tag{42}$$

In terms of the area ratio r_A from Eq. (20), *i.e.* $\sigma = \frac{r_A \cdot \lambda}{2\sqrt{-2\log(\beta)}}$, we can write

$$\overline{J_{GC}} = \frac{f_{max} T}{r_A \cdot \lambda^2} \underbrace{\left(2\sqrt{-4\pi \log(\beta)} \mathrm{erf}\left(\frac{\sqrt{-\log(\beta)}}{r_A}\right) - \frac{8\log(\beta)}{r_A} \exp\left(\frac{\log(\beta)}{r_A^2}\right) \right)}_{=: f(r_A, \beta)}. \tag{43}$$

For the parameters we are interested in, *i.e.* $\beta = 0.05$ and $r_A < 0.5$ the right term is negligible, and the first term is effectively constant in for $r_A < 0.5$. Therefore, $\overline{J_{GC}} \propto \frac{f_{max}}{r_A \cdot \lambda^2}$ (Eq. (19)).

Here we derived an approximation for small spatial periods. For larger spatial periods, there will be boundary effects when averaging over the spatial periods. However, numerical comparison actually showed that the derived formula for $\overline{J_{GC}}$ gives a good approximation, even for spatial periods close to one.

For the grid cell, the average rate is defined by:

$$\overline{f_{GC}} = \frac{1}{\lambda} \int_0^{\lambda} \int_0^1 \alpha(x,\varphi) dx d\varphi, \tag{44}$$

with α being the firing rate as defined in equation (5), but with spatial phase φ. Analogously to the average Fisher information this value can be approximately computed by:

$$\begin{aligned}\overline{f_{GC}} &\approx \frac{2}{\lambda}\int_0^{\frac{\lambda}{2}} f_{max}\cdot exp\left(-\frac{x^2}{2\sigma^2}\right)dx = \frac{2\sqrt{2}f_{max}\sigma}{\lambda}\int_0^{\frac{\lambda}{2\sqrt{2}\sigma}}\cdot exp\left(-t^2\right)dt \\ &= \frac{\sqrt{2\pi}f_{max}\sigma}{\lambda}\text{erf}\left(\frac{\lambda}{2\sqrt{2}\sigma}\right) = f_{max}\cdot\frac{\sqrt{2\pi}r_A}{2\sqrt{-2\log(\beta)}}\text{erf}\left(\frac{\sqrt{-\log(\beta)}}{r_A}\right). \quad (45)\end{aligned}$$

Whereas,the average firing rate for a place cell is characterized by linear growth in σ, the average firing rate of a grid cell remains constant for changing spatial periods, because the firing field size is determined by the spatial period. This manifests itself in that the average Fisher information per average firing rate falls with the inverse square of λ and σ for grid and place cells, respectively.

Monte Carlo Integration and MMLE

The mean maximum likelihood error (MMLE) is best computed by Monte Carlo integration. Each set of parameters governing a grid or place code determines a joint probability distribution $P(K,x)$, from which we realized samples $(x_l,K_l)_{1\leq l\leq R}$ with $R\geq 10^5$. From these realizations, we compute:

$$\chi^2_{MLE}\approx\frac{1}{R}\sum_{l=1}^{R}(x_l-\hat{x}_{MLE}(K_l))^2 =: \widehat{\chi}^2_{MLE}(R). \quad (46)$$

The right hand side converges with $\frac{1}{\sqrt{R}}$ towards the MMLE. The Monte Carlo integration is stopped if:

$$|\widehat{\chi}^2_{MLE}(R)-\widehat{\chi}^2_{MLE}(R+10^4)|<1.001\cdot\widehat{\chi}^2_{MLE}(R+10^4). \quad (47)$$

In other words, convergence is said to be reached reached when the $\widehat{\chi}^2_{MLE}$ changes by less than 10^{-3} over the last $10,000$ iterations. A similar convergence criteria was used in (Bethge et al., 2002). As an additional test, we corroborate the error estimates by bootstrapping methods.

References

Attneave, F. (1954). Some informational aspects of visual perception. *Psychological Review*, 61(3):183–193.

Barlow, H. (1959). Sensory mechanisms, the reduction of redundancy, and intelligence. In *The mechanisation of thought processes*, 10: 535–539, London. Her majesty's Stationary Office.

Barry, C., Hayman, R., Burgess, N., and Jeffery, K. (2007). Experience-dependent rescaling of entorhinal grids. *Nature Neuroscience*, 10(6):682–4.

Bethge, M., Rotermund, D., and Pawelzik, K. (2002). Optimal short-term population coding: when Fisher information fails. *Neural Comput.*, 14:2317– 2351.

Bobrowski, O., Meir, R., and Eldar, Y. (2009). Bayesian filtering in spiking neural networks: noise, adaptation, and multisensory integration. *Neural comput.*, 21(5):1277–320.

Boccara, C., Sargolini, F., Thoresen, V., Solstad, T., Witter, M., Moser, E., and Moser, M.-B. (2010). Grid cells in pre- and parasubiculum. *Nature Neuroscience*, 13(8):987–994.

Bragin, A., Jando, G., Nadasdy, Z., Hetke, J., Wise, K., and Buzsaki, G. (1995). Gamma (40-100 Hz) oscillation in the hippocampus of the behaving rat. *J. Neuroscience*, 15(1):47-60.

Brown, W. and Bäcker, A. (2006). Optimal Neuronal Tuning for Finite Stimulus Spaces. *Neural Comput.*, 18:1511–1526.

Brun, V., Solstad, T., Kjelstrup, K., Fyhn, M., Witter, M., Moser, E., and Moser, M.-B. (2008). Progressive Increase in Grid Scale From Dorsal to Ventral Medial Entorhinal Cortex. *Hippocampus*, 18:1200–1212.

Brunel, N. and Nadal, J.-P. (1998). Mutual Information, Fisher Information, and Population Coding. *Neural Comput.*, 10:1731–1757.

Burak, Y., Brookings, T., and Fiete, I. (2006). Triangular lattice neurons may implement an advanced numeral system to precisely encode rat position over large ranges. *arXiv:q-bio/0606005v1*, 93106:4.

Burak, Y. and Fiete, I. (2009). Accurate Path Integration in Continuous Attractor Network Models of Grid Cells. *PLoS Computational Biology*, 5(2):1–16.

Burgess, N. (2008). Grid Cells and Theta as Oscillatory Interference : Theory and Predictions. *Hippocampus*, 1174:1157–1174.

Burgess, N., Barry, C., and O'Keefe, J. (2007). An Oscillatory Interference Model of Grid Cell Firing. *Hippocampus*, 17:801–812.

Buzsaki, G. (2006). *Rhythms of the Brain*. Oxford University Press, USA.

Cheng, S. and Loren, F. (2010). From grid cells to place cells: a generic and robust principle accounts for multiple spatial Maps. *Frontiers in Computational Neuroscience. Conference Abstract: Bernstein Conference on Computational Neuroscience*, 4.

Derdikman, D., Whitlock, J., Tsao, A., Fyhn, M., Hafting, T., Moser, M.-B., and Moser, E. (2009). Fragmentation of grid cell maps in a multicompartment environment. *Nature Neuroscience*, 12(10):1325–32.

Deshmukh, S., Yoganarasimha, D., Voicu, H., and Knierim, J. (2010). Theta modulation in the medial and the lateral entorhinal cortex. *J. Neurophysiology*, 104:994–1006.

Doeller, C., Barry, C., and Burgess, N. (2010). Evidence for grid cells in a human memory network. *Nature*, 463(7281):657–61.

Eurich, C. and Wilke, S. (2000). Multidimensional encoding strategy of spiking neurons. *Neural comput.*, 12(7):1519–29.

Fenton, A., Kao, H.-Y., Neymotin, S., Olypher, A., Vayntrub, Y., Lytton, W., and Ludvig, N. (2009). Unmasking the CA1 ensemble code by exposures to small and large environments: more place cells and multiple, irregularly arranged and expanded place fields in the larger space. *J. Neuroscience*, 28(44):11250–11262.

Fenton, A., Lytton, W., Barry, J., Lenck-Santini, P.-P., Zinyuk, L., Kubík, S., Bures, J., Poucet, B., Muller, R., and Olypher, A. (2010). Attention-like modulation of hippocampus place cell discharge. *J. Neuroscience*, 30(13):4613–25.

Fenton, A. and Muller, R. (1998). Place cell discharge is extremely variable during individual passes of the rat through the firing field. *Proceedings of the National Academy of Sciences USA*, 95:3182–3187.

Fiete, I., Burak, Y., and Brookings, T. (2008). What Grid Cells Convey about Rat Location. *J. Neuroscience*, 28(27):6858 – 6871.

Franzius, M., Vollgraf, R., and Wiskott, L. (2007). From grids to places. *J. Computational Neuroscience*, 22:297–299.

Fuhs, M. and Touretzky, D. (2006). A Spin Glass Model of Path Integration in Rat Medial Entorhinal Cortex. *J. Neuroscience*, 26(16):4266 – 4276.

Fyhn, M., Hafting, T., Treves, A., Moser, M.-B., and Moser, E. (2007). Hippocampal remapping and grid realignment in entorhinal cortex. *Nature*, 446(7132):190–4.

Fyhn, M., Molden, S., Witter, M., Moser, E., and Moser, M.-B. (2004). Spatial representation in the entorhinal cortex. *Science*, 305(5688):1258–64.

Garden, D., Dodson, P., O'Donnell, C., White, M., and Nolan, M. (2008). Tuning of synaptic integration in the medial entorhinal cortex to the organization of grid cell firing fields. *Neuron*, 60(5):875–89.

Geisler, C., Diba, K., Pastalkova, E., Mizuseki, K., Royer, S., and Buzsáki, G. (2010). Temporal delays among place cells determine the frequency of population theta oscillations in the hippocampus. *Proceedings of the National Academy of Sciences USA*, 107(17):7957–7962.

Giocomo, L., Zilli, E., Fransén, E., and Hasselmo, M. (2007). Temporal frequency of subthreshold oscillations scales with entorhinal grid cell field spacing. *Science*, 315(5819):1719–22.

Hafting, T., Fyhn, M., Bonnevie, T., Moser, M.-B., and Moser, E. (2008). Hippocampus-independent phase precession in entorhinal grid cells. *Nature*, 453(7199):1248–52.

Hafting, T., Fyhn, M., Molden, S., Moser, M.-B., and Moser, E. (2005). Microstructure of a spatial map in the entorhinal cortex. *Nature*, 436(7052):801–6.

Hasselmo, M., Giocomo, L., and Zili, E. (2007). Grid cell firing may arise from interference of theta frequency membrane potential oscillations in single neurons. *Hippocampus*, 17(12):1252–1271.

Huys, Q., Zemel, R., Natarajan, R., and Dayan, P. (2007). Fast population coding. *Neural Comput.*, 19(2):404–441.

Itskov, V., Pastalkova, E., Mizuseki, K., Buzsaki, G., and Harris, K. (2008). Theta-mediated dynamics of spatial information in hippocampus. *J. Neuroscience*, 28(23):5959–64.

Jackson, J. and Redish, D. (2007). Network Dynamics of Hippocampal Cell-Assemblies Resemble Multiple Spatial Maps Within Single Tasks. *Hippocampus*, 1229:1209–1229.

Jeffery, K. (2008). Self-localization and the entorhinal-hippocampal system. *Current Opinion in Neurobiology*, 17:1–8.

Kjelstrup, K., Solstad, T., Brun, V., Hafting, T., Leutgeb, S., Witter, M., Moser, E., and Moser, M.-B. (2008). Finite scale of spatial representation in the hippocampus. *Science*, 321(5885):140–3.

Kluger, C., Mathis, A., Stemmler, M., and Herz, A. (2010). Movement Related Statistics of Grid Cell Firing. *Frontiers in Computational Neuroscience. Conference Abstract: Bernstein Conference on Computational Neuroscience*, 4.

Kropff, E. and Treves, A. (2008). The Emergence of Grid Cells: Intelligent Design or Just Adaptation ? *Hippocampus*, 18:1256–1269.

Lehmann, E. and Casella, G. (1998). *Theory of Point Estimation*. Springer-Verlag, New York, 2nd edition.

Leutgeb, J. K., Leutgeb, S., Moser, M.-B., and Moser, E. I. (2007). Pattern separation in the dentate gyrus and CA3 of the hippocampus. *Science*, 315(5814):961–6.

Leutgeb, S., Leutgeb, J., Moser, M.-B., and Moser, E. (2005). Place cells, spatial maps and the population code for memory. *Current Opinion in Neurobiology*, 15(6):738–46.

Leutgeb, S., Leutgeb, J., Treves, A., Moser, M.-B., and Moser, E. (2004). Distinct ensemble codes in hippocampal areas CA3 and CA1. *Science*, 305(5688):1295–8.

Mathis, A., Stemmler, M., and Herz, A. (2010). How good is grid coding versus place coding for navigation using noisy, spiking neurons? *BMC Neuroscience*, 11(Suppl 1):O20.

Mathis, A., Herz, AVM. and Stemmler, M. (2011). The Resolution of Nested Neuronal Representations can be Exponential in the Number of Neurons. *Submitted*, September 2011

Mathis, A., Stemmler, M., and Herz, A. (2011). Exponential Scaling of Nested Neuronal Representations. *Front. Comput. Neurosci. Conference Abstract: BC11: Computational Neuroscience & Neurotechnology Bernstein Conference & Neurex Annual Meeting 2011*.

McNaughton, B., Battaglia, F., Jensen, O., Moser, E., and Moser, M.-B. (2006). Path integration and the neural basis of the 'cognitive map'. *Nature Reviews. Neuroscience*, 7(8):663–78.

Mhatre, H., Gorchetchnikov, A., and Grossberg, S. (2010). Grid cell hexagonal patterns formed by fast self-organized learning within entorhinal cortex. *Hippocampus*, 22(2):320-34

Mulders, W., West, M., and Slomianka, L. (1997). Neuron numbers in the presubiculum, parasubiculum, and entorhinal area of the rat. *J. Comparative Neurology*, 385(1):83–94.

O'Keefe, J. (1976). Units in the Hippocampus Moving Rat. *Experimental Neurology*, 51:78–109.

O'Keefe, J. and Dostrovsky, J. (1971). The hippocampus as a spatial map: Preliminary evidence from unit activity in the freely-moving rat. *Brain Research*, 34:171–175.

O'Keefe, J. and Nadel, L. (1978). *The Hippocampus as a cognitive map*. Oxford University Press.

O'Keefe, J. and Recce, M. (1993). Phase relationship between hippocampal place units and the EEG theta rhythm. *Hippocampus*, 3(3):317–30.

Paradiso, M. (1988). A Theory for the Use of Visual Orientation Information which Exploits the Columnar Structure of Striate Cortex. *Biological Cybernetics*, 58:35–49.

Pouget, A., Dayan, P., and Zemel, R. (2003). Inference and Coding with Population Codes. *Annu. Rev. Neurosci.*, 26:381–410.

Pouget, A., Deneve, S., Ducom, J., and Latham, P. (1999). Narrow versus wide tuning curves: What's best for a population code? *Neural comput.*, 11:85–90.

Quilichini, P., Sirota, A., and Buzsaki, G. (2010). Intrinsic Circuit Organization and Theta-Gamma Oscillation Dynamics in the Entorhinal Cortex of the Rat. *J. Neuroscience*, 30(33):11128–11142.

Reifenstein, E., Stemmler, M., and Herz, A. (2010). Single-run phase precession in entorhinal grid cells. *Frontiers in Computational Neuroscience. Conference Abstract: Bernstein Conference on Computational Neuroscience*, 4.

Remme, M., Lengyel, M., and Gutkin, B. (2010). Democracy-Independence Trade-Off in Oscillating Dendrites and Its Implications for Grid Cells. *Neuron*, 66(3):429–437.

Rolls, E., Stringer, S., and Elliot, T. (2006). Entorhinal cortex grid cells can map to hippocampal place cells by competitive learning. *Network: Computation in Neural Systems*, 447:447–465.

Salinas, E. and Abbott, L. (1994). Vector reconstruction from firing rates. *J. Computational Neuroscience*, 1:89–107.

Sargolini, F., Fyhn, M., Hafting, T., McNaughton, B., Witter, M., Moser, M.-B., and Moser, E. (2006). Conjunctive representation of position, direction, and velocity in entorhinal cortex. *Science*, 312(5774):758–62.

Seung, H. and Sompolinsky, H. (1993). Simple models for reading neuronal population codes. *Proceedings of the National Academy of Sciences USA*, 90(22):10749–53.

Shadlen, M. and Newsome, W. (1998). The variable discharge of cortical neurons: implications for connectivity, computation, and information coding. *J. Neuroscience*, 18(10):3870–96.

Si, B. and Treves, A. (2009). The role of competitive learning in the generation of DG fields from EC inputs. *Cogn Neurodyn*, 3:177–187.

Softky, W. and Koch, C. (1993). The highly irregular firing of cortical cells is inconsistent with temporal integration of random EPSPs. *J. Neuroscience*, 13(1):334–50.

Solstad, T., Moser, E., and Einevoll, G. (2006). From Grid Cells to Place Cells : A Mathematical Model. *Hippocampus*, 16:1026–1031.

Taube, J., Muller, R., and Ranck, J. (1990a). Head-direction cells recorded from the postsubiculum in freely moving rats. I. Description and quantitative analysis. *J. Neuroscience*, 10(2):420–35.

Taube, J., Muller, R., and Ranck, J. (1990b). Head-direction cells recorded from the postsubiculum in freely moving rats. II. Effects of environmental manipulations. *J. Neuroscience*, 10(2):436–47.

Wilke, S. and Eurich, C. (2002). Representational Accuracy of Stochastic Neural Populations. *Neural comput.*, 14:155–189.

Wilson, M. and McNaughton, B. (1993). Dynamics of the hippocampal ensemble code for space. *Science*, 261(5124):1055–8.

Zhang, K. and Sejnowski, T. (1999). Neuronal tuning: to sharpen or broaden. *Neural Comput.*, 11(1):75–84.

Zilli, E. and Hasselmo, M. (2010). Coupled noisy spiking neurons as velocity-controlled oscillators in a model of grid cell spatial firing. *J. Neuroscience*, 30(41):13850–60.

3 NESTED CODES REPRESENT CONTINUOUS VARIABLES WITH EXPONENTIAL ACCURACY

3.1 SUMMARY

Population codes that are based on neurons with unimodal tuning curves are abundant in the mammalian brain. The most prominent locations are the hippocampus, the visual, auditory, somatosensory and the motor system [48, 59, 60, 66, 77, 102]. These codes have been studied extensively [8, 9, 11, 14, 17, 93, 106, 109, 120, 153], often with special emphasis on how the accuracy of the population code depends on the tuning width. In a seminal paper Zhang and Sejnowski (1999) showed that for radial symmetric tuning curves the optimal tuning width is solely related to the number of dimensions of the signal [153]. However, common to all these coding schemes is that the Fisher information scales linearly with the number of neurons.[1]

In chapter 2 we point out that a nested grid code can give rise to a qualitatively different scaling for encoding a one dimensional variable like space. Building on this work we generalize the design of a nested grid code to stimulus spaces of arbitrary dimension and prove that such a code can offer a Fisher information that scales exponentially in the number of neurons. In particular, we give a general construction of how to periodify any unimodal tuning curve to an arbitrary affine lattice. We show how the Fisher information of this constructed periodic population code is related to the population of unimodal tuning curves. This connection is then used to provide an argument for the scaling that is independent of the specific tuning curve shape.

In chapter 2 we show that for certain parameter regimes the Cramér-Rao bound, given by the Fisher information, cannot be attainable by an ideal observer. Here a formula is presented for how the nesting should be devised, based on the explicit noise level of the first module, in order to be attainable by an estimator. This formula is corroborated by numerical simulations.

1 This linear scaling can be improved to quadratic scaling in the case of a one dimensional stimulus as pointed out in the paper presented here.

3.2 REFERENCE

This work was done under the supervision of Andreas Herz and Martin Stemmler; AM, AH and MS conceived and designed the research. AM performed research, MS did numerical simulation of estimator errors in Fig. 2c/d. AM, AH and MS discussed the results and wrote the paper. Parts of it were presented as a poster at the 2011 Bernstein Conference on Computational Neuroscience [84].

The paper has been accepted in *Physical Review Letters* under the following reference:

A Mathis, AVM Herz, and M Stemmler: "The Resolution of Nested Neuronal Representations can be Exponential in the Number of Neurons". *Physical Review Letters*, accepted April 18, 2012.

Resolution of Nested Neuronal Representations Can Be Exponential in the Number of Neurons

Alexander Mathis, Andreas V. M. Herz, and Martin B. Stemmler
Bernstein Center for Computational Neuroscience, Graduate School of Systemic Neurosciences, Ludwig-Maximilians-Universität München, Grosshadernerstrasse 2, D-82152 Martinsried, Germany
(Received 20 September 2011; published 6 July 2012)

Collective computation is typically polynomial in the number of computational elements, such as transistors or neurons, whether one considers the storage capacity of a memory device or the number of floating-point operations per second of a CPU. However, we show here that the capacity of a computational network to resolve real-valued signals of arbitrary dimensions can be exponential in N, even if the individual elements are noisy and unreliable. Nested, modular codes that achieve such high resolutions mirror the properties of grid cells in vertebrates, which underlie spatial navigation.

DOI: 10.1103/PhysRevLett.109.018103 PACS numbers: 87.19.ls, 87.10.Ca, 87.10.Vg

The brain encodes many stimulus variables, such as the position of an object, the orientation of an edge, or the frequency of a sound, with high precision. Multidimensional stimulus spaces are represented by joint activity across neurons, each of which fires noisy, unreliable spikes. Yet, despite the stochastic nature of neuronal discharge, the nervous system achieves a highly efficient representation of the outside world [1].

The simplest representation of a continuous stimulus variable is a one-to-one map onto a neuronal firing rate. Given unreliable spikes, however, a labeled line code across different neurons is more robust and efficient [2]. The place code for spatial position in the hippocampus is an instance of such a labeled line code. One drawback of such a code is that the resolution only scales linearly in the number of neurons [2–4].

A place code can be improved upon by using a cascade of self-similar, periodic representations at different scales, as depicted in Fig. 1. Each successive level refines the representation at the previous coarser scale, such that the overall resolution scales exponentially in the number of neurons, as we show in this Letter.

Neuronal coding of sensory information at multiple scales occurs in many brain areas [5] and arises naturally in the theory of sparse coding [6]; we show here how the dense coding at multiple scales found in the entorhinal cortex and related areas, where each neuron has multiple firing fields, can be highly efficient, even though the firing rate of a single neuron no longer maps onto a single stimulus, but to many possible stimuli.

We consider N statistically independent neurons encoding a compact but possibly high-dimensional stimulus space, normalized to $[0, 1]^D$. For simplicity, each stimulus is assumed to be equally likely. Each neuron's response is characterized by the number of spikes k_i emitted within a time τ after stimulus onset. The neuron's mean firing rate depends on the stimulus x through its tuning curve $\Omega_i(x)$. The number of spikes is stochastic, so that observing a response $K = (k_1, \ldots, k_N)$ across the population of neurons has a probability

$$P(K|x) = \prod_{i=1}^{N} P_i(k_i|\tau\Omega_i(x)). \quad (1)$$

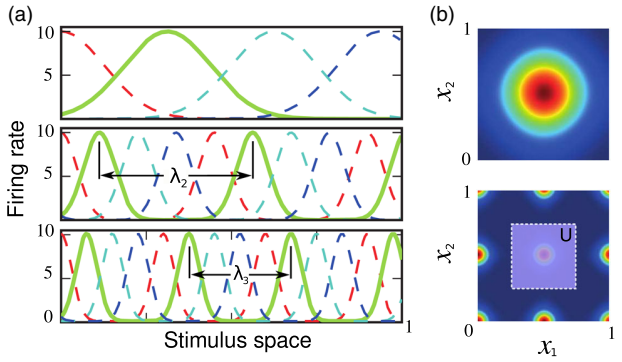

FIG. 1 (color online). Example of nested modules. (a) All modules, except for the coarsest one, have periodic tuning curves $\Omega_i(x - c_i)$. A module consists of a set of tuning curves with the same period but different phases c_i. The spatial period for modules 2 and 3 are $\lambda_2 = 0.45$ and $\lambda_3 = 0.3$, respectively. In each module, we highlight a single tuning curve by a solid line to show the period. Shifted but otherwise identical tuning curves are dashed. Nested modules successively refine the representation of the stimulus. Periodicity implies that the map from stimulus to population response is not one-to-one within a single module. Only the ensemble response provides a unique representation of x. (b) A unimodal tuning curve Ω in two dimensions, shown at the top, can be rescaled and periodically extended using Eqs. (5) and (6). The periodic tuning curves Ω_Γ in the lower panel is based on a rectangular lattice Γ spanned by $v_1 = \lambda(1, 0)'$ and $v_2 = \lambda(0, 1)'$, with $\lambda = 1/2$. For this lattice, a fundamental domain U is depicted.

We ask how accurately an ideal observer can deduce the stimulus x from K. For this purpose, we use the Fisher information matrix $\boldsymbol{J}$ with components

$$\boldsymbol{J}_{\alpha\beta}(x) = \int \frac{\partial \ln P(K,x)}{\partial x_\alpha} \frac{\partial \ln P(K,x)}{\partial x_\beta} P(K,x) dK, \quad (2)$$

where $\alpha, \beta \in \{1, \cdots, D\}$. The Cramér-Rao inequality [7] relates the inverse of $\boldsymbol{J}$ to the covariance matrix Σ of any unbiased estimator $\hat{x}$ of the encoded stimulus x,

$$\Sigma(\hat{x}|x) \geq \boldsymbol{J}(x)^{-1}. \quad (3)$$

Let us first consider a population of neurons with tuning curves $\Omega_i(x)$ such that each has a single peak of width σ. Suppose the tuning curves differ only in the center c_i of the peak, so that $\Omega_i(x) = \Omega(x - c_i)$. A single tuning curve has Fisher information $\boldsymbol{J}_{\Omega_i}(x)$. For the stochastic population model in Eq. (1), the Fisher information $\overline{\boldsymbol{J}_\Omega(x)}$ for the population is simply the sum

$$\overline{\boldsymbol{J}_\Omega(x)} \stackrel{\text{def}}{=} \sum_{i=1}^{N} \boldsymbol{J}_{\Omega_i}(x) = \int_{[0,1]^D} \boldsymbol{J}_\Omega(x - \varphi)\rho(\varphi) d\varphi,$$

where $\rho(\varphi) = \sum_{i=1}^{N} \delta(\varphi - c_i)$ is the density of the centers.

Assume that the centers c_i are uniformly distributed in $[0, 1]^D$, so that the tuning curves cover the entire stimulus space. As the centers become increasingly dense with increasing N, the Fisher information $\overline{\boldsymbol{J}_\Omega(x)}$ becomes independent of the specific stimulus x and scales linearly in the number of neurons

$$\overline{\boldsymbol{J}_\Omega} = N K_\Omega(\sigma, \tau, D) \quad (4)$$

for some function K_Ω [3,8,9]. If the stimulus space were not compact, but instead encompassed all of $\mathbb{R}^D$, then $K_\Omega \sim \sigma^{D-2}$ [3].

The linear scaling of Eq. (4) in N can be dramatically improved by switching to a nested modular code, in which each module consists of a subpopulation of M periodic tuning curves, as in Fig. 1. Each module is associated with a unique spatial period.

We first compute the Fisher information for a single module that has periodic tuning curves, such that $M = N$. Any unimodal tuning curve $\Omega(x)$ on $[0, 1]^D$ can be periodically extended. Let $\Gamma \subset \mathbb{R}^D$ be a nondegenerate, affine point lattice [10]

$$\Gamma = u + \sum_{\alpha=1}^{D} k_\alpha v_\alpha \quad \text{for } k_\alpha \in \mathbb{Z}, \quad u, \quad v_\alpha \in \mathbb{R}^D, \quad (5)$$

such that $(v_\alpha)_{1\leq\alpha\leq D}$ is a basis for $\mathbb{R}^D$ and u a center. Let $U \subset \mathbb{R}^D$ be a fundamental domain of this lattice. Then there is a canonical coordinate transformation Φ: $U \to [0, 1)^D$ in terms of an invertible matrix $\boldsymbol{T}$ and a vector w, such that $\Phi = -w + \boldsymbol{T}$. One defines the periodic extension of Ω as

$$\Omega_\Gamma: \mathbb{R}^D \to \mathbb{R}^+, \qquad x \mapsto \Omega \circ \Phi(x \bmod \Gamma). \quad (6)$$

This definition is illustrated in Fig. 1(b) and is independent of the particular representation (or translational shift) for U.

A family of shifted, periodic tuning curves on the lattice Γ constitutes a module and is associated with Fisher information $\overline{\boldsymbol{J}_{\Omega,\Gamma}}$. We now relate $\overline{\boldsymbol{J}_{\Omega,\Gamma}}$ to the original $\overline{\boldsymbol{J}_\Omega}$. Under the inverse map Φ^{-1}, the transformed tuning curves have centers $c_i' = \Phi^{-1}(c_i) \in U$. Therefore,

$$\overline{\boldsymbol{J}_{\Omega,\Gamma}(x)} \stackrel{\text{def}}{=} \sum_{i=1}^{N} \boldsymbol{J}_{\Omega_\Gamma}(x + c_i') = \int_U \boldsymbol{J}_{\Omega_\Gamma}(x + \varphi)\rho'(\varphi) d\varphi,$$

where $\rho'(\varphi) = \sum_{i=1}^{N} \delta(\varphi - c_i')$. By changing the variables in the Fisher information [7] and using the periodicity of $\Phi((x + \varphi) \bmod \Gamma)$ on U, we get

$$\begin{aligned}\overline{\boldsymbol{J}_{\Omega,\Gamma}(x)} &= \int_U \boldsymbol{T}\boldsymbol{J}_\Omega(\Phi(x + \varphi))\boldsymbol{T}'\rho'(\varphi) d\varphi \\ &= \boldsymbol{T} \int_U \boldsymbol{J}_\Omega(\Phi(x + \varphi))\rho'(\varphi) d\varphi \boldsymbol{T}'.\end{aligned}$$

In the last step, we interchanged the multidimensional integration and matrix multiplication, as T and its transpose T' are independent of φ. Under the map Φ, we obtain

$$\begin{aligned}\overline{\boldsymbol{J}_{\Omega,\Gamma}(x)} &= \boldsymbol{T} \int_{[0,1]^D} \boldsymbol{J}_\Omega(x + y) \cdot \rho(y) dy \boldsymbol{T}' \\ &= \boldsymbol{T}\Big(\sum_{i=1}^{N} \boldsymbol{J}_\Omega(x + c_i)\Big)\boldsymbol{T}' = \boldsymbol{T}\overline{\boldsymbol{J}_\Omega(x)}\boldsymbol{T}'. \quad (7)\end{aligned}$$

Thus, we have derived the following rule: $\overline{\boldsymbol{J}_{\Omega,\Gamma}(x)} = \boldsymbol{T}\overline{\boldsymbol{J}_\Omega(x)}\boldsymbol{T}'$. For an orthogonal lattice Γ defined by $v_\alpha = \lambda_\alpha e_\alpha$ on the canonical basis $(e_\alpha)_{1\leq\alpha\leq D}$ of $\mathbb{R}^D$, each entry in the Fisher information matrix is rescaled by $(\lambda_\alpha\lambda_\beta)^{-1}$ under this transformation. If the original Fisher information matrix is diagonal, then so is $\overline{\boldsymbol{J}_{\Omega,\Gamma}(x)}$. Therefore, rescaling the periodic tuning curves by a factor of 2 quadruples the Fisher information, but at the cost of introducing ambiguity—the value of x can only be recovered modulo the lattice Γ. Resolving this ambiguity requires a multiscale representation consisting of multiple modules spanning different spatial periods.

How should these different spatial periods be chosen? Suppose there are L modules with spatial periods $\{\lambda_1, \ldots, \lambda_L\}$, arranged in decreasing order from the longest period to the shortest, as in Fig. 1. Each module has $M = N/L$ tuning curves, and each tuning curve within a module is associated with a different phase shift.

The easiest case to analyze is the one in which the lattices Γ_k are orthogonal [11], the rescaling is uniform in each dimension, and the tuning curve Ω is radially symmetric. In such a case, a module on lattice Γ_k has a Fisher information matrix $\overline{\boldsymbol{J}_{\Omega,\Gamma_k}(x)} = \lambda_k^{-2}\overline{\boldsymbol{J}_\Omega}$, and radial symmetry implies that $\overline{\boldsymbol{J}_\Omega} = J\mathbf{I}$ is diagonal and proportional to the identity matrix $\mathbf{I}$ [3]. To ensure that the first module represents $x \in [0, 1]^D$ unambiguously, we treat this module as a special case and make it aperiodic;

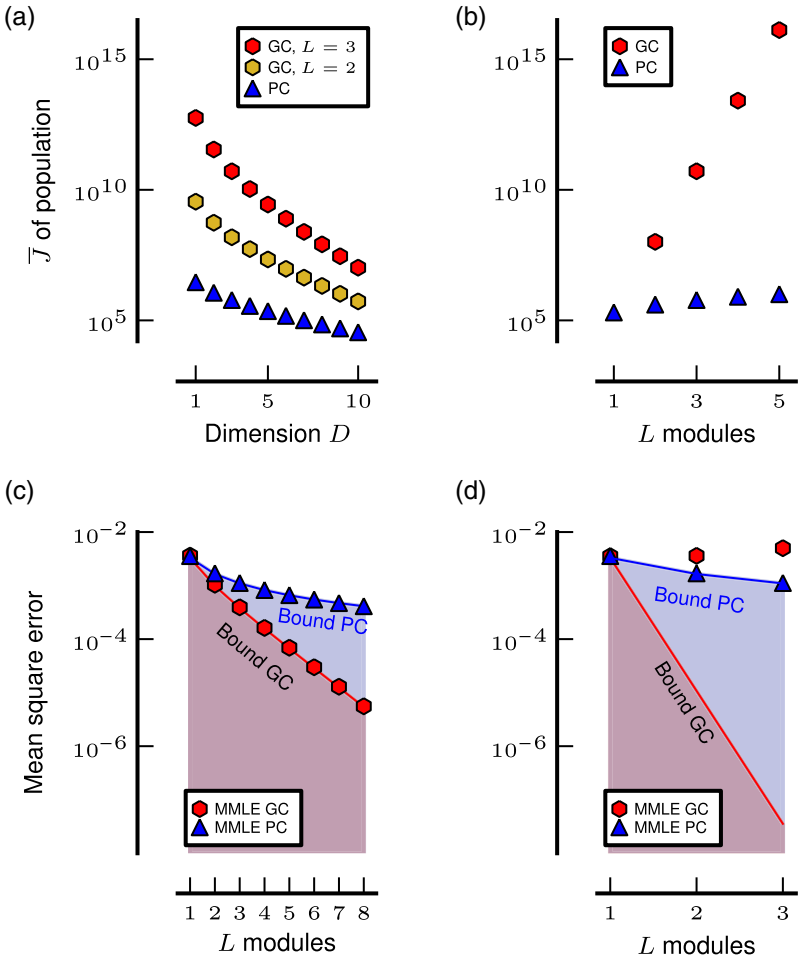

FIG. 2 (color online). (a) Grid codes (GC) outperform place codes (PC), regardless of the number of stimulus dimensions. A population of $N = 3 \times 10^5$ neurons is divided into one, two, or three modules, according to Eq. (8). The neurons' tuning width is fixed as $\sigma = 2$. (b) The Fisher information for a neuronal population with $M = 10^5$ neurons per module and $D = 3$. For a nested modular code with L modules, the Fisher information grows exponentially in $N = L \cdot M$, whereas it is linear in N for a place code. (c) The error of the estimator that minimizes $(x - \hat{x})^2$ for place and grid codes in $D = 3$ dimensions, based on sampling the stochastic response 1200 times. Each module comprises $M = 8^3$ equidistantly spaced cells. The lattice lengths for different modules are scaled according to Eq. (8), with a safety factor $C = 20$. The Cramér-Rao bound of Eq. (10) is tight for both the grid and place codes. (d) When the lattice lengths contract more strongly than allowed by Eq. (8), such that $C = 1$, the error fails to improve in a nested modular code. Although the Fisher information predicts an error even lower than in (c), the uncertainty derived from the first module's response is larger than the lattice length scale of the next finer-grained module, so that adding modules with finer spacing does not improve the resolution.

i.e., the first module is a place code with the same tuning width that a periodic module with $\lambda = 1$ would have.

Within the first module, the expected error in an unbiased estimate of x asymptotically approaches $1/\sqrt{J}$, according to Eq. (3). This error sets a lower bound on the period of the next module that refines the representation of x. Hence, each λ_k should obey

$$\lambda_{k+1} = \frac{C\lambda_k}{\sqrt{J}}, \tag{8}$$

where C is a safety factor, such that $1 \ll C < \sqrt{J}$. For a C larger than unity, the next module can correct for the error in the previous module. The Fisher information for the nested population is $\overline{\boldsymbol{J}_{\Omega,\Gamma_1\cdots\Gamma_L}} = \overline{J_{\Omega,\Gamma_1\cdots\Gamma_L}}\boldsymbol{I}$ with

$$\overline{J_{\Omega,\Gamma_1\cdots\Gamma_L}} = \sum_{k=1}^{L} \frac{J}{\lambda_k^2} = \sum_{k=1}^{L} \frac{J^k}{C^{2(k-1)}}.$$

If we take only the last term in the series and substitute $L = N/M$, we see that

$$\overline{J_{\Omega,\Gamma_1\cdots\Gamma_L}} > \frac{J^{N/M}}{C^{2(N/M-1)}}. \tag{9}$$

For fixed module size M, the Fisher information scales exponentially in the number of neurons N. Such a coding scheme, therefore, outperforms a single module that only

scales linearly in N. Note that this scaling is independent of the dimension D.

As a concrete example, we consider a set of tuning curves with Poisson noise, centers c_i, tuning width σ, and period λ, as given by $\Omega_i(x) = f_{\max} \exp(\frac{1}{\sigma^2}\sum_{\alpha=1}^{D}\{\cos[2\pi(x_\alpha - c_{i,\alpha})/\lambda] - 1\})$ [12]. If the number of neurons per period λ is $M \gg 1$ and the centers are uniformly distributed, the module's average Fisher information is given by

$$\overline{J} = \frac{M 4\pi^2 f_{\max} \tau}{\lambda^2 \sigma^2} K_1(\sigma^2) K_0^{D-1}(\sigma^2)\mathbf{I} \qquad (10)$$

where $K_n(x) = \exp(-1/x) I_n(-1/x)$ and $I_n(x)$ is the nth order modified Bessel function of the first kind. In Fig. 2(a), the Fisher information for a large population of $N = 300\,000$ (place) cells is plotted for stimulus dimensions $D = 1$ to 10. Dividing the population into separate grid modules according to Eq. (10) with $C = 20$ leads to a much higher Fisher information—orders of magnitude, irrespective of the dimension D of the stimulus space. Figure 2(b) underscores the key finding of this Letter: the Fisher information grows exponentially in the number N of encoding neurons. The place code, in contrast, is linear in N. To corroborate these analytical results, we sampled the response K and estimated the minimum mean square error based on the posterior probability distribution $p(x|K)$ [13], as shown in Figs. 2(c) and 2(d). These simulations show that the Cramér-Rao bound is tight as long as the grid codes obey the constraint in Eq. (8). For place codes, it is known that on short time scales [14], or for low numbers of neurons [9], the Cramér-Rao bound will not be tight, so that the Fisher information underestimates the error in decoding the signal. The same will hold true for grid codes. However, when $N > M \gg 1$ and the expected number of spikes at the center of each tuning curve is appreciable, a nested modular code leads to an error that scales as $M^{-N/M}$.

Note that we assume that the firing of neurons is uncorrelated. Whether this assumption holds in cortex is a matter of fierce debate [15]. The Fisher information deteriorates with increasing noise correlations, but its scaling in N does not, at least not for the correlation strengths measured by Ecker *et al.* in cortex.

Periodic tuning curves have been found in entorhinal cortex of rodents—coined grid cells ([16]; see Supplemental Material [17]). This unexpected discovery has inspired theorists to explore the combinatorial capacity of modular periodic codes and how they might be used in the brain [18]. In some cases, the stimulus space is intrinsically periodic—orientation and color hue are but two examples. But when the space of stimulus x is infinite instead of periodic, different spatial periods can be combined to encode a much larger range of x uniquely than would otherwise be possible [19]. Indeed, the exponential range that can result confers a relative precision that is also exponential [20]. This Letter, in contrast, shows that the *absolute* precision in x can be exponential in N. Precision is of paramount importance for path integration, for which the mammalian brain is thought to use grid cells [21]. Interestingly, the periodic lattices for neighboring grid cells share similar spatial periods and orientations, but are spatially translated relative to each other [16]. Moreover, along the dorso-ventral axis of the entorhinal cortex, the typical spatial period of the lattice grows from roughly 20 cm to several meters, while the ratio of grid field width to spatial period remains constant [22]. Our theoretical analysis indicates that these grid cell properties may endow the brain with a highly accurate representation of space; the same principles might be used for representing other continuous, high-dimensional stimuli.

[1] H. B. Barlow, *The Mechanisation of Thought Processes* (Her Majesty's Stationery Office, London, 1959), p. 535; J. J. Atick, Network **3**, 213 (1992).

[2] M. Bethge and K. Pawelzik, Neurocomputing **44-46**, 323 (2002).

[3] K. Zhang and T. Sejnowski, Neural Comput. **11**, 75 (1999).

[4] If the width of each neuron's tuning curve is simultaneously scaled as N^{-1}, the net resolution scales as N^2.

[5] D. H. Hubel and T. N. Wiesel, J. Physiol. **195**, 215 (1968); R. L. De Valois, D. G. Albrecht, and L. G. Thorell, Vision Res. **22**, 545 (1982); M. S. Lewicki, Nat. Neurosci. **5**, 356 (2002).

[6] E. P. Simoncelli, W. T. Freeman, E. H. Adelson, and D. J. Heeger, IEEE Trans. Inf. Theory **38**, 587 (1992); B. Olshausen and D. Field, Vision Res. **37**, 3311 (1997).

[7] E. L. Lehmann and G. Casella, *Theory of Point Estimation* (Springer, New York, 1998), 2nd ed.

[8] W. M. Brown and A. Bäcker, Neural Comput. **18**, 1511 (2006).

[9] C. W. Eurich and S. D. Wilke, Neural Comput. **12**, 1519 (2000).

[10] We use the more generalized concept of an affine point lattice, in which u is an arbitrary affine translation.

[11] The rescaling rule of Eq. (8) becomes a matrix equation in the general case. Let $\mathbf{\Lambda}_i$ be a diagonal matrix of scaling factors for the point lattice Γ. If the tuning curves form a complete cover for the unit hypercube $[0, 1]^D$, then the Fisher information is a positive-definite symmetric matrix with no zero eigenvalues. Therefore, there is an orthonormal matrix $\boldsymbol{O}$ and a positive definite diagonal matrix $\boldsymbol{D}$ such that $\boldsymbol{J} = \boldsymbol{O}\boldsymbol{D}\boldsymbol{O}'$. By the Cramér-Rao bound, $\Sigma \geq \boldsymbol{J}^{-1}$. Hence, we define the following refinement rule: $\mathbf{\Lambda}_{k+1} = C(\boldsymbol{O}\boldsymbol{D}^{-1/2}\boldsymbol{O}')\mathbf{\Lambda}_k$.

[12] Similar tuning curves were used by A. Montemurro and S. Panzeri, Neural Comput. **18**, 1555 (2006).

[13] S. Yaeli and R. Meir, Front. Comput. Neurosci. **4**, 130 (2010).

[14] M. Bethge, D. Rotermund, and K. Pawelzik, Neural Comput. **14**, 2317 (2002); P. Berens, A. S. Ecker, S. Gerwinn, A. S. Tolias, and M. Bethge, Proc. Natl. Acad. Sci. U.S.A. **108**, 4423 (2011).

[15] M. A. Smith and A. Kohn, J. Neurosci. **28**, 12591 (2008); A. S. Ecker, P. Berens, G. A. Keliris, M. Bethge, N. K. Logothetis, and A. S. Tolias, Science **327**, 584 (2010).

[16] T. Hafting, M. Fyhn, S. Molden, M-B Moser, and E. I. Moser, Nature (London) **436**, 801 (2005); F. Sargolini, M. Fyhn, T. Hafting, B. L. McNaughton, M. P. Witter, M-B Moser, and E. I. Moser, Science **312**, 758 (2006); C. N. Boccara, F. Sargolini, V. H. Thoresen, T. Solstad, M. P. Witter, E. I. Moser, and M-B Moser, Nat. Neurosci. **13**, 987 (2010).

[17] See Supplemental Material at http://link.aps.org/supplemental/10.1103/PhysRevLett.109.018103 for a more detailed discussion of grid cells.

[18] A. Guanella and P. Verschure, J. Integ. Neurosci. **6**, 433 (2007).

[19] I. R. Fiete, Y. Burak, and T. Brookings, J. Neurosci. **28**, 6858 (2008).

[20] S. Sreenivasan and I. Fiete, Nat. Neurosci. **14**, 1330 (2011).

[21] B. L. McNaughton, F. P. Battaglia, O. Jensen, E. I. Moser, and M-B Moser, Nat. Rev. Neurosci. **7**, 663 (2006).

[22] M. Fyhn, S. Molden, M. P. Witter, E. I. Moser, and M-B Moser, Science **305**, 1258 (2004); L. M. Giocomo, E. A. Zilli, E. Fransén, and M. E. Hasselmo, Science **315**, 1719 (2007); V. H. Brun, T. Solstad, K. B. Kjelstrup, M. Fyhn, M. P. Witter, E. I. Moser, and M-B Moser, Hippocampus **18**, 1200 (2008).

4 THE EFFECT OF CORRELATIONS ON GRID CODES

The material presented in this chapter is the core of an unfinished manuscript. Due to small gaps in the current version of the manuscript the material is presented abbreviated, yet cohesive.

4.1 INTRODUCTION

In chapter 3 the favorable scaling properties of nested grid codes have been demonstrated. There the individual noisy elements are assumed to be statistically independent. A type of statistical dependence among neurons that has been observed in the cortex are *correlated response fluctuations* (noise correlations). According to a widely believed hypothesis these correlations of a pair of neurons are caused by random fluctuations of neurons that are presynaptic to both [29, 121]. The strength of these noise correlations in cortical neurons has been reported to lie between 0 and 0.3 [22, 29, 47, 47, 113, 126, 154]. These measurements are from visual areas, and to our knowledge the noise correlations in the entorhinal cortex have not been determined so far.

Such correlations can have a strong effect on the coding precision of population codes – and nested grid codes are no exception. In the theoretical study of this chapter we investigate the effects by extending the framework from chapter 3. In particular, we determine the effect of noise correlations on the population's Fisher information. As the basic building block of nested grid codes is given by a module, we can start by studying place codes. This case has often been considered in the literature; for families of unimodal tuning curves it has been reported that reducing the correlations improves the resolution of the population code [1, 29, 30, 122, 123, 144]. As we will demonstrate, this tendency is correct for nested grid codes too.

4.2 METHODS: POPULATION CODING MODEL WITH NOISE CORRELATIONS

The model presented here, is an extension of the work by Ecker et al. on correlated unimodal tuning curve families [30, 123]. As this chapter generalizes the statistically independent model of chapter 3 the terminology is the same.

4.2.1 Population coding model

Assume that we have N neurons encoding a one-dimensional circular variable $x \in [-\pi, \pi)$. The response of neuron i is given by:

$$r_i(x) = \Omega_i(x) + \eta_i(x). \tag{4.1}$$

Here $\Omega_i(x)$ is the tuning curve of the i-th neuron and η_i is the trial-to-trial variability. For simplicity, assume that this variability follows a multivariate normal distribution with zero mean and covariance matrix $Q(x)$.

As in the example of chapter 3, let the tuning curves be given by *von Mises functions*:

$$\Omega_i(x) = f_{max} \cdot \exp\left(1/\sigma^2 \cdot (\cos(2\pi/\lambda_i \cdot (x - c_i)) - 1)\right). \tag{4.2}$$

Thereby f_{max} stands for the peak firing rate, σ the tuning width, λ_i for the spatial period, and c_i for the angular preference of the tuning curve.

We assume a modular structure of the population comprising L modules of M neurons each, so altogether that means $N = L \cdot M$. Within each module the period λ_i is identical, and the angular preferences are equally spaced, i.e.

$$c_i \in \{0, \frac{2\pi \cdot \lambda_i}{M}, \ldots, \frac{2\pi \cdot (M-1)\lambda_i}{M}\}. \tag{4.3}$$

In the example considered in chapter 3, the neurons are independent and Poisson statistics governs their firing, so that each $\eta_i(x)$ is normally distributed with mean zero and variance $\Omega_i(x)$. Here we treat the more general case with a non-trivial *correlation structure*. More specifically, we assume that the correlation factor between two neurons r_{ij} is independent of the stimulus. In this case, the covariance matrix can be written as a product [30]:

$$Q_{ij}(x) = \sqrt{\Omega_i(x)} \cdot r_{ij} \cdot \sqrt{\Omega_j(x)}. \tag{4.4}$$

For the correlation coefficients r_{ij} we will assume the following. Within each module, each cell's tuning curve has a spatial phase c_i. We let the correlation coefficient between two cells depend on the difference in spatial phase. This is motivated by the functional organization of the cortex ([30], also see discussion). Mathematically, for any two neurons with phases c_i and c_j, their correlation coefficient is given by the following function:

$$r_{ij} = c\left(-\pi + (c_i - c_j + \pi) \mod 2\pi\right) + \delta_{ij}(1 - c(0)). \quad (4.5)$$

Here δ_{ij} is the Kronecker delta, and c is a monotonously decreasing function. In particular, we will use $c(t) = c_0 \cdot \exp\left(-\frac{t}{\tau}\right)$, with $\tau = 1$. For the correlations across modules we will assume that they vanish. Hence, for grid codes, the correlation coefficient matrix and also the covariance matrix Q have a block-structure.[1] Figure 4 illustrates the block-structure of the correlation coefficient matrix (r_{ij}).

4.2.2 Fisher information

For the outlined model the Fisher information can be written as a sum [30, 69, 123]:

$$J(x) = J_{mean}(x) + J_{cov}(x) \quad (4.6)$$

with the following individual parts:

$$J_{mean}(x) = (\Omega'(x))^t Q(x)^{-1} \Omega'(x) \quad (4.7)$$

$$J_{cov}(x) = \tfrac{1}{2} \mathrm{Tr}\left(\left(Q'(x)Q(x)^{-1}\right)^2\right). \quad (4.8)$$

Thereby Ω' and Q' are the derivatives with respect to the stimulus variable x. The names of these quantities derive from the fact that J_{mean} depends on the changes of the mean firing rate Ω' and J_{cov} depends on changes of the covariance structure Q'.

In the following we study how the Fisher information changes with the defined noise correlation structure. Thereby, the effect of the scaling parameter Q' on the Fisher information of the population is of chief interest.

1 If the indices are canonically arranged, which we assume from now on. By canonically we mean that the first M indices belong to the first module, the next M indices to the second module, etc. And within each module we assign the index according to growing phase-preference starting with phase 0.

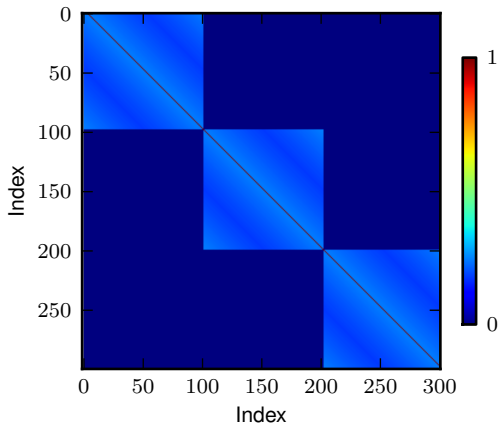

Figure 4: The correlation matrix for a grid code with $N = 300$ neurons and 3 modules of 100 neurons each. The parameters are $\tau = 1$ and $c_0 = 0.25$. The indices are canonically arranged, as explained in the main text. Each neuron is perfectly correlated to itself, therefore the correlation coefficient is 1 along the diagonal. The correlations between modules are zero, so there are three blocks of non-zeros and zeros elsewhere. These blocks are all identical, as the definition of r_{ij} (Eq. 4.5) does not depend on the spatial periods. Due to the equidistantly arranged phases within each module and a periodic stimulus space, it follows that these blocks are circulant matrices, i.e. for the first module: $r_{i,j} = r_{|i-j|,0} = r_{100-|i-j|,0}$ for $i, j \in \{0, 1, \ldots 99\}$.

4.3 RESULTS

We will vary the population size N and the correlation peak c_0 and then compute J. For the simulations, we set the peak rate to $f_{max} = 20$ Hz and the tuning width to $\sigma = \sqrt{2}/2$. Qualitatively these choices are not important, as long as there are enough neurons to cover the space given σ and the peak spike count is larger than one (compare to chapter 2).

4.3.1 Place code

We know that in the absence of correlations, the Fisher information grows linearly in N (chapter 3). For rising correlation amplitude c_0 the Fisher information decreases, yet still grows linearly with N (Figure 5 a). This effect can be explained by considering the two components J_{mean} and J_{cov} individually, as

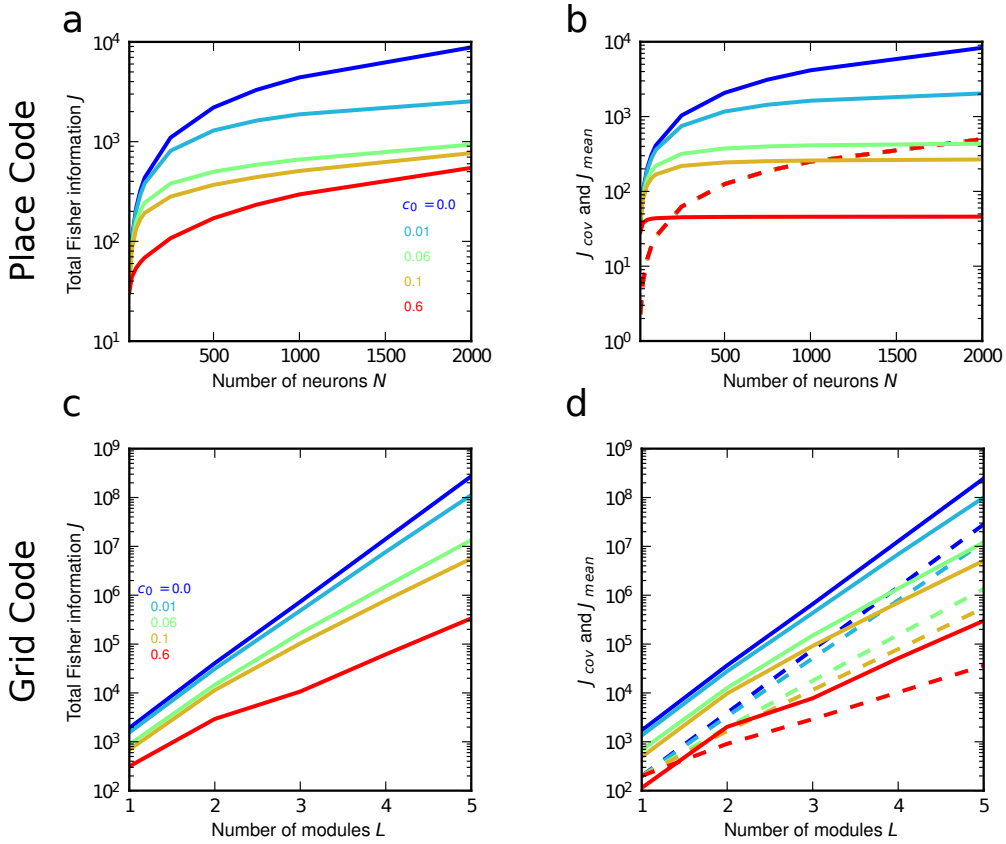

Figure 5: Fisher information for population codes with correlations. We evaluated the Fisher information at position $x = 0$. **a**: The total Fisher information J for a population of N place cells with correlation peak c_0. For zero-correlation the Fisher information grows linearly in N. For larger correlation coefficients the Fisher information falls, but eventually grows linearly in N, as indicated by considering the two components of J individually, see subfigure b. **b**: The same simulation, but the two parts of the Fisher information J_{mean} and J_{cov} are shown separately in solid and dashed lines, respectively. The mean term saturates for increasing correlation peak c_0, but the covariance term grows linearly and is in fact independent of the correlation peak c_0. **c**: Fisher information for grid code without inter-module correlation. The total Fisher information J for a population of L modules and correlation peak c_0. Each module contains $M = 200$ neurons. Even for increasing correlation, the population Fisher information still grows stronger than linearly. The stronger the correlation coefficient becomes the smaller the contraction factor $C/\sqrt{J}$ becomes, and therefore the smaller the growth. **d**: The same simulation, but the two parts of the Fisher information J_{mean} and J_{cov}, are shown separately in solid and dashed lines, respectively.

shown in Fig. 5 b. While the former saturates, the latter grows linearly in N, independently of the degree of correlation. This result is well known, e.g., see Shamir and Sompolinsky [30, 123].

4.3.2 Nested grid code

Let us see how the results just presented for the place code affect grid codes. With increasing peak correlation c_0, each module provides a lower Fisher information. As described in chapter 3, in order for the Fisher information to be

attainable the spatial period should depend on the resolution of the next coarser module. This is the same for modules with intrinsic correlation. All that changes is the "allowed" spatial period – accordingly the spatial periods should obey:

$$\lambda_{k+1} = \frac{C \cdot \lambda_k}{\sqrt{J}}, \tag{4.9}$$

with *safety* factor C and Fisher information of first module J (See chapter 3, Eq. 8 and discussion thereof).

Thus, the population Fisher information of a grid code, despite still growing exponentially, grows more slowly in N for rising c_0. Figure 5 c and d, depict the Fisher information of a grid code with up to 5 modules and $M = 200$ neurons per module.

4.4 CONCLUSION

We demonstrated that, although noise correlations within modules reduce the Fisher information of each module, the exponential scaling of nested grid codes is not qualitatively affected. As presented, this follows from the linear scaling of place codes despite noise correlations.

The spatial phases of grid cells appear to be randomly distributed [55]. This is in strong contrast to the clustered arrangement of orientation preference in the visual system of macaques, for instance, where neighboring cells have similar tuning orientations [21]. Neighboring cells are also more likely to be connected and to receive common input [13, 21]. Thus it has been shown that the cells with similar preferences also have higher noise correlations [29]. For this reason, the effect of limited range correlations is often studied [30, 123], and motivates the function Eq.4.5 in our study. Larger values of the decline parameter τ in Eq.4.5 make the correlation values less dependent on the stimulus preference. For randomly distributed grid cell phases larger

values of τ might be more appropriate. Numerical simulations suggest that almost constant correlation values (τ large) are less detrimental on the Fisher information than limited range correlations (data not shown).

As pointed out in chapter 2 the Fisher information only provides a bound to the resolution of a grid code. For certain cases, like low firing counts per cell, too small spatial periods, etc. this bound is not attainable by maximum likelihood decoding. For nesting in accordance with Eq. 4.9 the attainability is guaranteed by considerations of the posterior distribution (see chapter 3 and 5). Nevertheless, the results should be corroborated by numerical simulations of the maximum likelihood estimator.

Here we assumed that the noise correlations of two neurons in different modules vanish. Given that different modules have different spatial periods and that these modules are spatially separated this assumption appears reasonable [19, 55, 147]. Incorporating such correlations was beyond the scope of this study, because the approach of determining the periodicity of the finer module based on the uncertainty of the coarser one is bound to break down, if there are correlations between the two modules. In such a case the Fisher information of the coarser module itself depends, due to the correlations, on the periodicity of the finer one. To resolve this, a new approach is needed, or numerical simulations have to be done. Two observations motivate further work in this direction. Firstly, recent findings seem to undermine the earlier finding about the spatial distance between grid cells of different scales [132], which would make noise correlations between such cells more likely. Secondly, from a coding theoretical point of view, the effect of these correlations is particularly interesting. The crux of nested grid codes is the specialization of different modules on different scales. This can only be exploited if the scales are *sufficiently* independent. Shedding light on how independent they have to be would be very interesting.[2]

Finally, one upshot of many earlier studies is that for large, heterogeneous populations of unimodal tuning curves, i.e. families with varying tuning widths and peak firing rates, reducing the correlations does not improve encoding accuracy[30, 123, 144]. Grid cells are also highly heterogeneous in their firing rates and

2 For the practical implications of this transition, it is necessary to determine the level of noise correlations in grid cells. Reliably measuring spike correlations, however, is technically challenging [29]. From the reasons given in Ecker et al. the control for internal variables (e.g. short-term memory [24]) and difficulty of single-unit isolation due to low signal-to-noise ratio of extracellular recordings in the entorhinal cortex (E Mankin, personal communication) are particularly valid for grid cells.

tuning parameters [55, 56], and it would be interesting to study the effect of heterogeneity for grid codes as well.

5 THE ENTORHINAL CORTEX OF RODENTS HARBORS AN OPTIMAL GRID CODE FOR SPACE

5.1 SUMMARY

In chapter 2 we show that the optimal grid code on the linear track has nested spatial periods, and that the tuning curves should be self-similar. In this manuscript these two results are generalized to 2D environments.

Maybe the most prominent property of the population of grid cells is that their firing fields are hexagonally arranged. This is especially interesting as hexagonal or almost hexagonal patterns occur throughout nature. Often these arrangements could be motivated by optimality principles. We will show that the hexagonal lattice offers a higher spatial resolution than a quadratic lattice. More specifically, we prove that for unimodal tuning curves the optimal grid cell has a hexagonal periodicity rather than a quadratic one.

These findings are compared to data from the Moser lab, Trondheim and together with other predictions discussed in the light of experimental findings.

5.2 REFERENCE

This work was done under the supervison of Martin Stemmler and Andreas Herz; AM, AH and MS conceived and designed the research. AM performed research. AM, AH and MS discussed the results. AM drafted the current state of the manuscript. Parts were presented as a talk at the Society for Neuroscience meeting in Washington in November 2011.

The Entorhinal Cortex of Rodents Harbors an Optimal Grid Code for Space

Alexander Mathis[1, 2], **Martin Stemmler**[1, 2], **Andreas VM Herz**[1, 2]
[1] Bernstein Center for Computational Neuroscience Munich, 82152 Martinsried, Germany.
[2] Graduate School of Systemic Neuroscience and Division of Neurobiology, Ludwig-Maximilians-Universität München, 82152 Martinsried, Germany.

Abstract

Natural selection pressures animals to use their resources efficiently. For the brain this signifies that neuronal representations are optimized for performance. Path integration in mammals is based on maps that have to be highly precise. A map that has been hypothesized to be formed by grid cells. For this reason, we investigate the system of grid cells in the medial entorhinal cortex under the assumption that this population encodes space with the highest accuracy.

The population of grid cells has curious, yet unexplained characteristics: every cell has multiple spatial firing fields that are arranged like a hexagonal lattice, and these patterns come in different phases and scales. We will show that all these features contribute to the unprecedented precision of such a population code and are indeed an optimal configuration.

1 Introduction

For an animal to survive, reproduce, and thrive it has to efficiently navigate through its hostile environment. This ability is supported by a precise mental representation of space. Many species can indeed precisely keep track of their position, as exemplified in homing experiments. Even after circuitous detours they can home to their nest in a direct way [43, 17, 57, 19]. Mammals also master this task called path integration, and meticulously controlled experiments demonstrated that they achieve this by integrating head direction and speed [43, 18, 19].

Anatomical, physiological, and lesion evidence have implicated the hippocampal formation in path integration. More specifically the grid cells in the medial entorhinal cortex (mEC) are the prime candidate [47, 19, 41, 45], as these cells exhibit spatially modulated firing, receive self-motion signals and keep responding similarly despite experimental manipulations, like turning the lights off [30, 53].

The spatial firing pattern of a grid cell resembles a hexagonal lattice [24, 30]. Yet, at a single cell level, the individual firing fields are indistinguishable [49] and it is therefore the population of grid cells that matters for encoding space. Anatomically neighboring grid cells respond in a spatially shifted way, so that they correspond to different phases of the same lattice, the lattices have inter firing field distances (spatial period) ranging from 30cm to multiple meters that grow along the dorso-ventral axis [30, 10]. Layer three grid cells are additionally modulated by speed and head direction [53, 45].

Hence, this population has a couple of curious properties, most strikingly the hexagonal periodicity and the multiple scales are puzzling, and while much is known about how the mammalian brain encodes space, an answer why this particular design has evolved remains elusive [26]. The optimal coding hypothesis successfully predicts the structure of receptive fields, tuning curves in the cochlear, and the sparseness of neuronal representations in sensory cortices [3, 4, 1, 2, 48, 38]. We investigate the optimality of a population of grid cells (grid code). More specifically, we will derive which features of the grid code endow it with the highest spatial resolution and compare this optimal grid to the properties of grid cells in the mEC.

Other theoretical investigations have mainly studied how grid-like firing patterns arise [22, 41, 12, 32, 11, 50, 64, 42, 26, 13], or how grid fields give rise to place fields [22, 55, 51, 21, 54, 14]. The coding properties of grid cells have received less attention with the notable exception of [20, 56]. Fiete and colleagues interpreted the grid cell activity and emphasized that by modular arithmetic the spatial range can be much longer than the longest spatial period.

We determine the optimal parameters for encoding space with a network of grid cells and compare these values to experimental parameters derived from recordings by the Moser lab, Trondheim. We will show that optimal coding explains the distribution of spatial periods, that they cluster, the size of grid fields, that the size scales with the spatial period and the hexagonality. Furthermore, we will derive that the optimal grid code has a qualitatively remarkable scaling property: the resolution scales exponentially in the number of neurons and thereby offers unprecedented computational benefits for navigation.

2 Materials and Methods

2.1 Theory

2.1.1 Population model

We consider a population of N cells that respond in a stochastic fashion to a stimulus, corresponding to 2D (planar) position $x = (x_1, x_2) \in B \subset \mathbb{R}^2$. Thereby B is the environment of the animal. The firing rate of each cell is given by its tuning curve $\Omega_i(x)$. We will assume that the neuronal response is the spike count $K = (k_0, \cdots, k_N) \in \mathbb{N}^N$, and that it is stochastically dependent on the firing rate of each cell.

Generally, we try to formulate our results as universally as possible and therefore simply denote the stochastic relationship between K and x by some function $\mathcal{P}$,

$$P(K|x) = \mathcal{P}(K, \Omega_i(x)). \tag{1}$$

More specifically, we consider independent Poisson firing,

$$\mathcal{P}(K, \Omega_i(x)) = \prod_i \exp(-\Omega_i(x)) \frac{\Omega_i(x)^{k_i}}{k_i!}. \tag{2}$$

For the tuning curves $\Omega_i(x)$ we mainly work with the general case of functions that are at least twice continuously differentiable ($\mathcal{C}^2$). We often simply assume that these functions are uni- or multimodal. By unimodal we mean that the function has a single, global maximum on its definition domain. Multimodal on the other hand means that the function has multiple peaks.

We will also deploy rotationally symmetric tuning curves, i.e.,

$$\Omega(x) = f_{max} T \cdot \Phi\left(\frac{\|x - c\|^2}{\sigma^2}\right), \tag{3}$$

with mean peak spike count $f_{max}T$ and a monotonically decreasing function $\Phi(s)$ with peak $\Phi(0) = 1$. The expression $\|v\|$ denotes the Euclidean distance, $\|v\| = \sqrt{v_1^2 + v_2^2}$. The tuning width σ scales the tuning curve, while leaving the shape unchanged. A Gaussian tuning curve corresponds to the special case $\Phi(s) = \exp(-s/2)$.

2.1.2 Decoding, Fisher information & Cramer-Rao inequality

The population of neurons encodes the position in a noisy manner. To investigate how precise the representation is, one looks at the performance of a suitable estimator. Due to the stochasticity of the firing, any estimator will make errors, when decoding the position; an estimator $\widehat{x}$ is a method for calculating an estimate of the position based on the noisy spike count K. At a

fixed position x, for each realization the spike count K can be different and hence the estimate $\widehat{x}(K(x))$. This variability can be assessed by the properties of the posterior distribution $p(\widehat{x}|x)$, being the probability distribution of estimates given a fixed position x. The more precise a population code is the more narrow this distribution will be.

For measuring the precision of the posterior we consider the second moment of the posterior, which is the mean square error [52, 7]:

$$\chi^2 = \mathbb{E}\left(\|x - \hat{x}\|^2\right) = \sum_{K \in \mathbb{N}^N} \int_B \|x - \hat{x}(K)\|^2 \cdot P(K|x) dx, \tag{4}$$

The χ^2 error generally depends on the estimator $\hat{x}$. For instance, given a particular population response K, the most likely stimulus that gave rise to it is

$$\hat{x}_{\text{MLE}}(K) = \max_{x \in B} P(x|K), \tag{5}$$

which is known as the maximum likelihood estimate (MLE). The corresponding mean maximum likelihood estimate square error (MMLE) is defined as $\chi^2_{MLE} = \mathbb{E}\left((x - \hat{x}_{MLE})^2\right)$. As the MMLE is numerically expensive to compute for large population sizes, we compare it against a reference that can be computed analytically. The maximum likelihood estimate is both statistically efficient and consistent [35], which means that χ^2_{MLE} asymptotically approaches the mean asymptotic square error (AE) for an increasing number of independent, identically distributed (i.i.d.) observations, which is given by

$$\chi^2_{AE} = \mathbb{E}\left(1/J(x)\right), \tag{6}$$

as shown in [7]. Here $J(x)$ stands for the Fisher information

$$J(x) = \mathbb{E}\left(\left(\frac{\partial}{\partial x} \ln(P(K|x))\right)^2\right). \tag{7}$$

The Cramér-Rao bound gives a limit to the accuracy of any read-out mechanism and is therefore useful for studying the accuracy of stochastic population codes. According to the Cramér-Rao inequality the Fisher information matrix bounds the covariance matrix of any unbiased estimator [35] at position x:

$$\mathbb{E}\left((x - \hat{x}_{MLE})^2 \mid x\right) \geq J(x)^{-1}. \tag{8}$$

For matrices such an inequality means that the difference is positive definite, which in this case, due to symmetry, is equivalent to the difference matrix possessing only positive eigenvalues.

As we are dealing with navigation in arbitrary planar environments the error should be equal in *each* direction for an orthogonal basis, as trading accuracy in one direction for another one is not advantageous. From now on we will always pick the canonical basis, i.e. $x = (x_1, x_2) = x_1(1, 0) + x_2(0, 1)$. In these coordinates the mean square error is given by the sum over the

individual components: $\chi^2 = \chi^2_{x_1} + \chi^2_{x_2}$.

The i, j-th component of the Fisher information matrix is given by:

$$J^{(ij)}(x) = \mathbb{E}\left(\frac{\partial}{\partial x_i} \ln P(K|x) \cdot \frac{\partial}{\partial x_j} \ln P(K|x)\right). \tag{9}$$

The goal $\chi_{x_1} = \chi_{x_2}$ translates into $J(x)$ being a diagonal matrix with equal entries.

As a concrete example, we consider a module of tuning curves with Poisson noise, centers c_i, tuning width σ, and spatial period λ, as given by

$$\Omega_i(x) = f_{\max} \cdot \exp\left(\frac{1}{\sigma^2} \sum_{\alpha=1}^{2} \{\cos\left[2\pi(x_\alpha - c_{i,\alpha})/\lambda\right] - 1\}\right), \tag{10}$$

similar to [44]. If the number of neurons per period λ is $M \gg 1$ and the centers are uniformly distributed, the module's average Fisher information is given by:

$$J^{(ii)} = \frac{M 4\pi^2 f_{\max} T \cdot \exp(-2\sigma^{-2})}{\lambda^2 \sigma^2} \cdot I_1(\sigma^{-2}) \cdot I_0(\sigma^{-2}), \tag{11}$$

with $i = 1, 2$, where $I_n(s)$ is the nth order modified Bessel function of the first kind. The non-diagonal values of the Fisher information vanish [39].

2.1.3 Periodification and planar lattices

For studying the lattice-type dependence let us consider the two equidistant planar lattices: the hexagonal and the square lattice (Figure 1). A planar lattice is a discrete subgroup of the plane $\mathbb{R}^2$, and can therefore be generated by linear combinations with integer coefficients of two basis vectors.

These lattices can be used to construct periodic tilings of the plane and therefore qualify to underlie a grid code. In the following we outline a basic construction for the periodification of a *unimodal* tuning curve given a certain lattice and will later show that under certain assumptions a grid code based on the symmetries of a hexagonal lattice has a higher population Fisher information and therefore offers more spatial resolution.

Let $\Gamma \subset \mathbb{R}^2$ be a planar point lattice [34]:

$$\Gamma = \sum_{\alpha=1}^{2} k_\alpha v_\alpha \qquad \text{for} \qquad k_\alpha \in \mathbb{Z};\ v_\alpha \in \mathbb{R}^2, \tag{12}$$

such that $(v_\alpha)_{1 \le \alpha \le 2}$ is a basis for $\mathbb{R}^2$. For the quadratic and hexagonal lattice it holds that the length of the basis vectors is equal $\|v_1\|_2 = \|v_2\|_2$ and that the angle between $\measuredangle v_1, v_2$ respectively is $90°$ and $120°$.

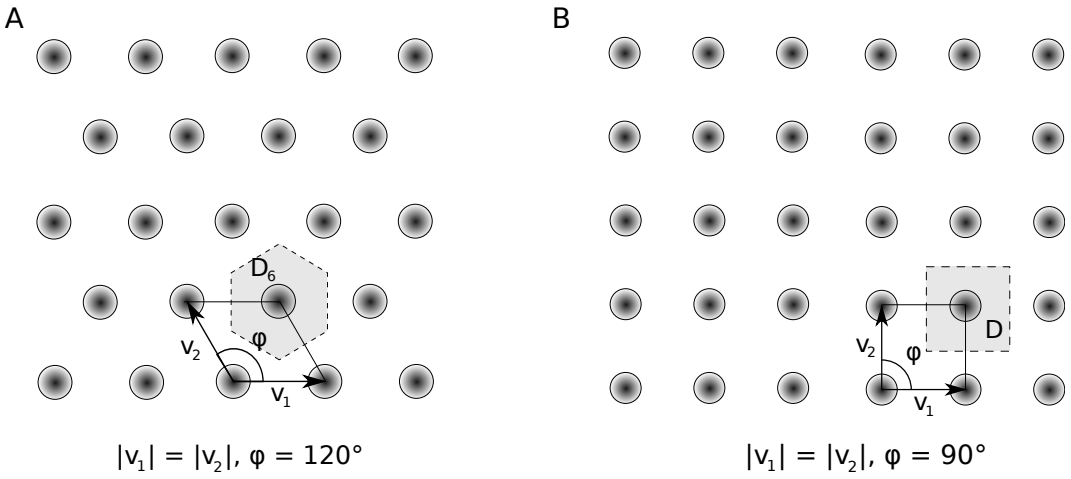

Figure 1: Equidistant planar lattices. **A:** Hexagonal lattice Γ_6 generated by basis vectors v_1 and v_2 of equal length and angle $120°$. The shaded area labeled by D_6 depicts a fundamental domain for this lattice. **B:** Quadratic lattice Γ generated by basis vectors v_1 and v_2 of equal length and angle $90°$. The shaded area labeled by D depicts a fundamental domain for this lattice.

The orbit of a point x in $\mathbb{R}^2$ is the set of elements of $\mathbb{R}^2$ to which x can be moved by the elements of Γ and is denoted by $\Gamma x = \{g + x \mid g \in \Gamma\}$. A fundamental domain of a lattice Γ is a connected subset $D \subset \mathbb{R}^2$ that has the property that the orbits of D under the lattice operation fulfill $\Gamma D = \mathbb{R}^2$ and that it contains exactly one point from each orbit, i.e. $\Gamma x \cap D = x$ for all $x \in D$. Let Γ_6 stand for the hexagonal lattice with fundamental domain being the regular hexagon D_6 (Fig. 1). For the quadratic lattice we pick a square centered around a node as fundamental domain.

Let D be a fundamental domain of lattice Γ and let $\Omega(x)$ be a tuning curve. With the canonical inclusion $\iota : D \to \mathbb{R}^2$ one can define the periodic extension of Ω as

$$\Omega_\Gamma : \mathbb{R}^2 \to \mathbb{R}^+, \qquad x \mapsto \Omega \circ \iota(x \bmod \Gamma). \tag{13}$$

Here $s \bmod \Gamma$ means congruent modulo the lattice Γ, so an element $x \in \mathbb{R}^2$ is mapped to the unique element of the same orbit in D. The definition is illustrated in Fig. 2 and is analogous to the construction of wallpapers, where each motif is placed at any lattice point to define a pattern. Here the restriction of the tuning curve to D is the *motif*.[1]

Having defined the periodic function Ω_Γ, we want to focus our attention on the Fisher information for a population of such neurons. A family of *shifted*, periodic tuning curves $\Omega_\Gamma(x - c_i) =$

[1]This construction yields a function, which everywhere but possible at the boundary of the fundamental domain, has the same differentiability class ($\mathcal{C}^k$) as the initial tuning curve Ω. At the boundary it is at least continuous and can also be smoothed. As a one-dimensional subset of D, the boundary can be neglected when computing the Fisher information.

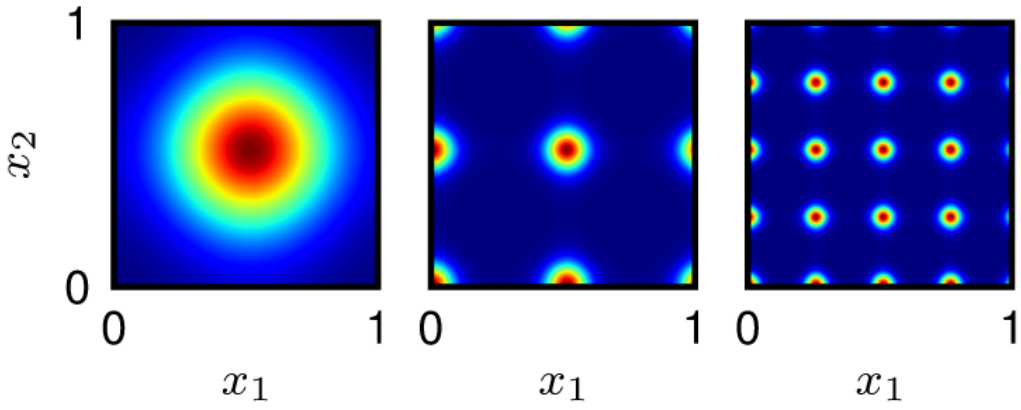

Figure 2: A unimodal tuning curve Ω, shown on the left, can be rescaled and periodically extended using Eqs. (12)-(13). The periodic tuning curves Ω_Γ in the middle and right panels are based on a rectangular lattice Γ spanned by $v_1 = \lambda \cdot (1,0)'$ and $v_2 = \lambda \cdot (0,1)'$. For the middle panel the spatial period is $\lambda = 1/2$, whereas for the right panel $\lambda = 1/4$.

$\Omega\left(\frac{|(x-c_i) \bmod \Gamma|^2}{\sigma^2}\right)$ on the lattice Γ with different centers c_i constitutes a module and is associated with a Fisher information $\overline{J^M_{\Omega,\Gamma}}$. As we assume that all neurons are statistically independent the Fisher information is given by summing over the contributions from all individual cells,

$$\overline{J^M_{\Omega,\Gamma}(x)} = \sum_{i=1}^{M} J_{\Omega_\Gamma}(x - c_i). \tag{14}$$

In the limit of large population with uniformly distributed centers $c \in D$ this finite sum fulfills

$$\left| \frac{\mathrm{vol}D}{M} \cdot \overline{J^M_{\Omega,\Gamma}(x)} - \int_D J_{\Omega_\Gamma}(x - \varphi) \mathrm{d}\varphi \right| \to 0 \tag{15}$$

for $M \to \infty$. As this difference is already tight for decent neuron numbers, we will from now on consider the Fisher information of the *average* cell, which is defined as

$$\overline{J_{\Omega,\Gamma}(x)} := \int_D J_{\Omega_\Gamma}(x - \varphi) \mathrm{d}\varphi \tag{16}$$

For the following theorem let us assume that the initial unimodal tuning curve is radially symmetric. As a first step to compute the Fisher information, we note that

$$\frac{\partial}{\partial x_i} \ln P(K|x) = \frac{\partial}{\partial s} \ln \mathcal{P}(K,s)\Big|_{s=\Omega_\Gamma(x)} \cdot \Phi'(x) \cdot f_{max} T \cdot \frac{2(x_i - c_i)}{\sigma^2}. \tag{17}$$

Together with the definition (9) of the Fisher information this yields

$$J^{(ij)}_{\Omega_\Gamma}(x) = f_{max}^2 T^2 \cdot \frac{4(x_i - c_i)(x_j - c_j)}{\sigma^4} \cdot \Phi'(x)^2 \cdot \underbrace{\sum_K \left(\frac{\partial}{\partial s} \ln \mathcal{P}(K, s)\Big|_{s=\Omega_\Gamma(x)} \right)^2 \cdot \mathcal{P}(K, \Omega_\Gamma(x))}_{=:\mathcal{N}(\|x-c\|^2)} . \tag{18}$$

Note that for $i \neq j$ this function is odd in c around x. As Eq. (16) shows, the population Fisher information is given by averaging these individual contributions over the fundamental domain,

$$\overline{J^{(ij)}_{\Omega,\Gamma}(x)} = \int_D J^{(ij)}_{\Omega_\Gamma}(x - \varphi) \mathrm{d}\varphi. \tag{19}$$

Therefore, as the fundamental domains are symmetric one gets that $\overline{J^{(ij)}_{\Omega,\Gamma}(x)} = 0$ for $i \neq j$. The diagonal entries are all identical and the trace of the Fisher information matrix becomes

$$\mathrm{tr}\left(\overline{J_{\Omega_\Gamma}(x)}\right) = \sum_i \overline{J^{(ii)}_{\Omega_\Gamma}(x)} = \int_D \underbrace{f_{max}^2 T^2 \frac{4\sum_i (x_i - \varphi_i)^2}{\sigma^4} \left(\Phi'_\Gamma \left(\frac{\|x-\varphi\|^2}{\sigma^2} \right) \right)^2 \cdot \mathcal{N}(\|x-\varphi\|^2)}_{=:\mathcal{F}(\|x-\varphi\|^2)} \mathrm{d}\varphi \tag{20}$$

We will use the notation $\overline{B_R(c)} = \{x \in \mathbb{R}^2 \mid \|x - c\|_2 \leq R\}$ for the closed ball of radius R with center c.

3 Results

3.1 Theory

To analyze the Fisher information of a grid code, we start by focusing on its basic building block: the module, a population of grid cells that share the same lattice, but are spatially shifted and represent different (spatial) phases. For a single module we show that the key parameter for improving the resolution is the spatial period of the lattice. In order to harness a small spatial period for a module, the ambiguities of an individual module have to be excluded by the other modules. We will show that this is best done in a nested fashion, which suggests that there should be a progression of grid sizes across modules. Such a code with multiple scales qualitatively changes the scaling behavior of the Fisher information.

Finally, we derive that for a wide range of tuning shapes the Fisher information is maximized by arranging the peaks on a hexagonal lattice rather than on a quadratic lattice. Furthermore, we study the optimal tuning width for such a module. All the model predictions will then be compared to measured characteristics of grid cells.

3.2 Module scaling

For a large number M of phases that densely cover the fundamental domain, the Fisher information of a single module, and therefore the spatial resolution, is independent of the particular location. Thereby, the Fisher information scales like [39]:

$$J_{module} \propto \frac{M \cdot F(\sigma)}{\lambda^2}, \tag{21}$$

with tuning width σ, spatial period λ and F a function of the tuning width. Crucially, for a two dimensional, rotational symmetric tuning curve at the center of the lattice, this function saturates for small widths and is generally bounded [63, 9, 39]. Hence, as the number of neurons is also bounded, the only parameter significantly changing the Fisher information is the spatial period. Indeed, for maximizing the Fisher information the spatial period has to be minimized (Fig. 3a).

As such the smaller the spatial scale the higher the spatial resolution, which is intuitively clear, as rescaling the tuning curves increases their slopes and therefore the ability to discriminate between neighboring locations. Yet this also introduces multiple periods and therefore *large scale* ambiguity - the value of x can only be recovered modulo the lattice Γ, which is illustrated by the posterior distribution of a single module in figure 3b. In the realm of periodic tuning curves resolving this ambiguity requires a multi-scale representation, consisting of multiple modules spanning different spatial periods, and the key questions is, how should these spatial periods be picked?

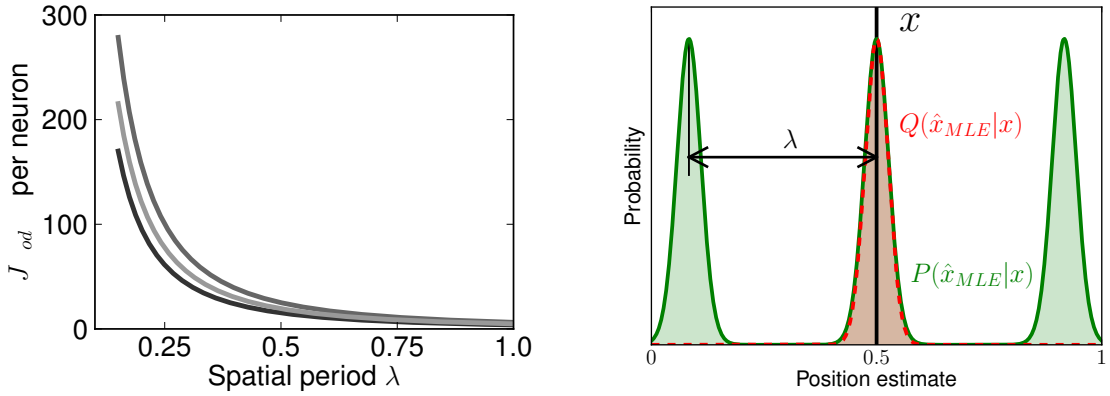

(a) (b)

Figure 3: (a) Average Fisher information for a module over the spatial period λ. The peak firing rate is 1Hz, and three different tuning widths σ are depicted in different gray shades. The Fisher information grows unboundedly for decreasing spatial period, highlighting the advantages of those. (b) Illustration of one-dimensional MLE-posterior $P(\widehat{x}_{MLE}|x)$ for a grid module with spatial period λ. The distribution of estimates $\widehat{x}_{MLE}$ for an animal located at x is shown. Such an estimator can make two types of errors: catastrophic and local ones. The latter are well described by the Fisher information J of the module as shown in (a) and can be captured by $Q(\widehat{x}|x) \propto \exp(-\frac{|\widehat{x}-x|^2}{2J})$. Yet, although $Q(\widehat{x}|x)$ describes the local errors well, it fails to account for catastrophic errors that stem from the inherently periodic nature of the tuning curve: simply put if $\widehat{x}$ is a MLE of x than so is $\widehat{x}+\lambda$, a value that is possibly far from x and therefore results in a catastrophic error. Mathematically this can be seen by assuming $s = \widehat{x}_{MLE}(K)$, then by definition $\max_x P(x|K) = P(s|K)$. Due to the periodicity of all tuning curves, it holds that $P(s|K) = P(s+\lambda|K)$, so also $s+\lambda$ is an estimate and similarly $s+k\cdot\lambda$ for all $k \in \mathbb{Z}$. Although a module with a small spatial period localizes the position better, as can be seen by the Fisher information, it also introduces catastrophic errors — making such modules impractical per se.

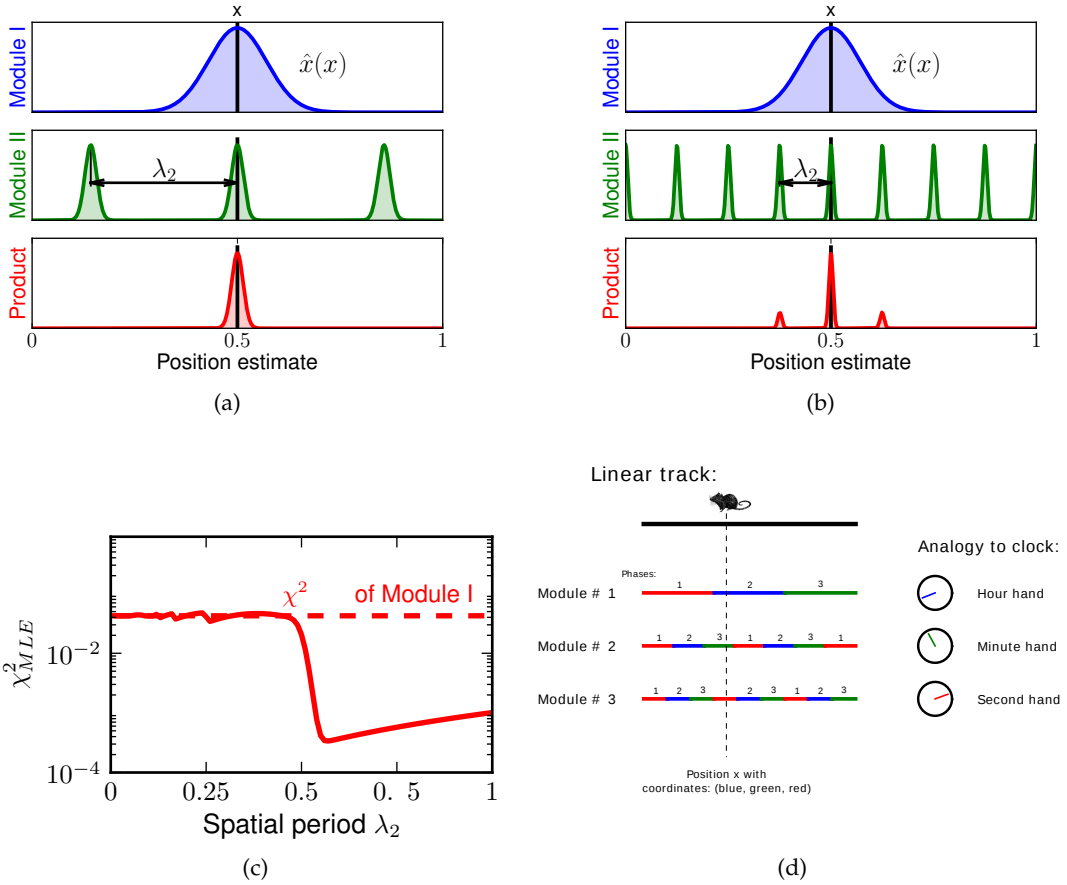

Figure 4: (a) Posterior of two modules as well as the combined grid code. The combined posterior is given by the product of the two module posteriors, due to the vanishing probability of far outliers for module I, these values are also highly unlikely for the product. Consequently this grid code combines the strong localization of module II with the coarse localization of module I, and thereby achieves almost the local discrimination of module II. This effect breaks down for too small spatial periods: (b) The periodicity of module II is larger than the uncertainty of the first module, and therefore the product posterior also has outliers with high incidence, yielding a performance worse than in (a). This suggests that there is an optimal spatial period for the second module, something that is confirmed by panel (c). (c) Mean square error χ^2_{MLE} of combined modules for different spatial periods of the second module λ_2 (solid red) and χ^2_{MLE} of the first module separately (dashed line). For large enough λ_2 the second module improves the accuracy of the population until for values below 0.55 the error grows and eventually falls back to the level of a single module. (d) *Nested interval scheme*: Example with three different spatial periods with three discrete phases each. The first module gives coarse spatial information, that is further subdivided by the other two modules. By themselves the other modules provide ambiguous spatial information on the range; together they effectively subdivide the unit interval. This coding strategy is analogous to the principle of a clock, where each hand further refines time. All three hands code a twelve-hour span down to second precision. Note that due to the high noise in grid cells, the periods are not divisors of each other like in the clock example.

3.3 Nested arrangement outperforms all others

This question can be approached by starting with two modules. For this consideration let us fix the spatial period λ_1 of the first module and consider a slightly smaller spatial period $\lambda_2 < \lambda_1$ for the second module. Due to the smaller spatial period of the second module the Fisher information is larger and therefore the two modules together encode the position more precisely (Fig. 4a). Decreasing the spatial period λ_2 will further increase the Fisher information and seemingly continue to further improve the performance without bound. But this is not the case, if λ_2 becomes smaller than the typical uncertainty of the first module, then there will be no further improvement and eventually even a deterioration (Fig. 4b). Consequently there is a smallest optimal spatial period for the second module given by the coarseness of the first module — this can be seen by the error of the full posterior (Fig. 4c). The uncertainty of the first module is, according to the Cramér-Rao bound, given by a multiple of the inverse Fisher information, i.e.r $\frac{C}{\sqrt{J_1}}$ with safety factor C. The spatial period λ_2 is then given by $\frac{C}{\sqrt{J_1}}$, where we denote the Fisher information of the first module by $J_1 \propto M_1 \cdot F(\sigma_1)$. Subsequently the second module has the following Fisher information:

$$J_2 \propto \frac{M_2 \cdot F(\sigma_2)}{\lambda_2^2} \propto \frac{M_1 \cdot M_2 \cdot F(\sigma_1) \cdot F(\sigma_2)}{C^2}. \tag{22}$$

By induction one arrives at the conclusion that all the modules should have nested spatial periods, where each module further subdivides the preceding ones (Fig. 4d). This intuition has been corroborated by analytical considerations and numerical simulations [40, 39]. Such an arrangement of spatial periods, termed nested coding scheme, yields the highest possible resolution for the population of stochastic grid cells and obeys a qualitatively remarkable scaling property: the resolution scales exponentially in the number of neurons. For seeing this, let us assume that there are L modules, then Eq. 22 generalizes to

$$J_L \propto \prod_{i=1}^{L} M_i \cdot F(\sigma_i), \tag{23}$$

which for equally sized modules becomes proportional to $M^L = M^{N/M}$, with $N = L \cdot M$ being the number of neurons in all modules together. So the Fisher information scales exponentially in the number of neurons N. As a side effect such a code dwarfs a population of cells with spatially localized firing, like place cells, which scales only linearly in the number of neurons [40, 39], and thereby highlights the merits of multiple spatial scales in grid cells. The fact that the largest spatial period λ_1 in our model has the length scale of the encoded domain makes a couple of predictions. Firstly, the relevant behavioral range should be on the order of the largest spatial period λ_1. Secondly, to use the capacity fully, λ_1 including all other spatial periods should adopt to the currently relevant environment of the animal. More generally, the nested coding scheme predicts that the spatial periods of grid cells cluster in multiple discrete groups, and that they should form a geometric progression $\lambda_i = \lambda_1 \cdot const^i$. This implies in

particular that there should be more small spatial periods than large spatial periods present – two predictions that will be discussed in light of the experimental data.

The optimality of these codes has been derived by considerations of the Fisher information and the posterior distribution. In the literature it has been argued that the Cramér-Rao bound, given by the Fisher information is not attainable for low spike counts and small cell numbers [7, 62, 6]. Two conditions that do not apply for the mEC. The attainability of the Cramér-Rao bound by ML-estimation of nested grid codes has been shown [40, 39].

3.4 Self-similarity and area ratio

From the Fisher information of the jth module (23), one gets for the full Fisher information

$$J = \sum_{l=1}^{L} C_l \cdot \prod_{i=1}^{l} M_i \cdot F(\sigma_i), \tag{24}$$

with certain constants C_l. A priori each module could have a different number of phases M_i and tuning widths σ_i, as long as the following constrains are fulfilled: The overall neuron number is constant $\sum_i M_i = N$ and each module contains enough phases and wide enough tuning widths to cover the fundamental domain. By similar means as in [40] for 1D grid codes, one can show that under these constraints the Fisher information is maximized by having approximately the same neuron number per module and consequently, for covering reasons [40], similar relative tuning widths σ.

This constancy of field size to grid size has been pointed out early on in recordings [30, 10], and can also be appreciated in the inset of figure 5. But what range for σ would one expect? In coding theory it is well established that for two dimensional stimulus spaces the Fisher information becomes independent of the tuning width for small values and plateaus [63, 9]; Figure 5 depicts the Fisher information per neuron for a typical tuning curve. The data from the largest environments so far, the 18 m long linear track, [10] have been reanalyzed. The relative tuning width of each recorded grid cell has been estimated and is plotted — these values are distributed within the top $80\% - 100\%$ region of the Fisher information (Fig. 5). There is also a notable trade-off: although smaller spatial tuning widths yield a slightly higher Fisher information per neuron, more neurons are needed to cover the domain and therefore fewer modules exist. But it is the number of modules L that massively improves the resolution.

3.5 Lattice dependence: Hexagonal tops quadratic

Any given radially symmetric tuning curve can be periodically extended to either a rectangular lattice or a hexagonal lattice. But do these choices affect the Fisher information of a module? This question is settled by the following result.

Theorem 3.1. *Consider the set Γ of all planar lattices, whose fundamental domain D has constant area.*

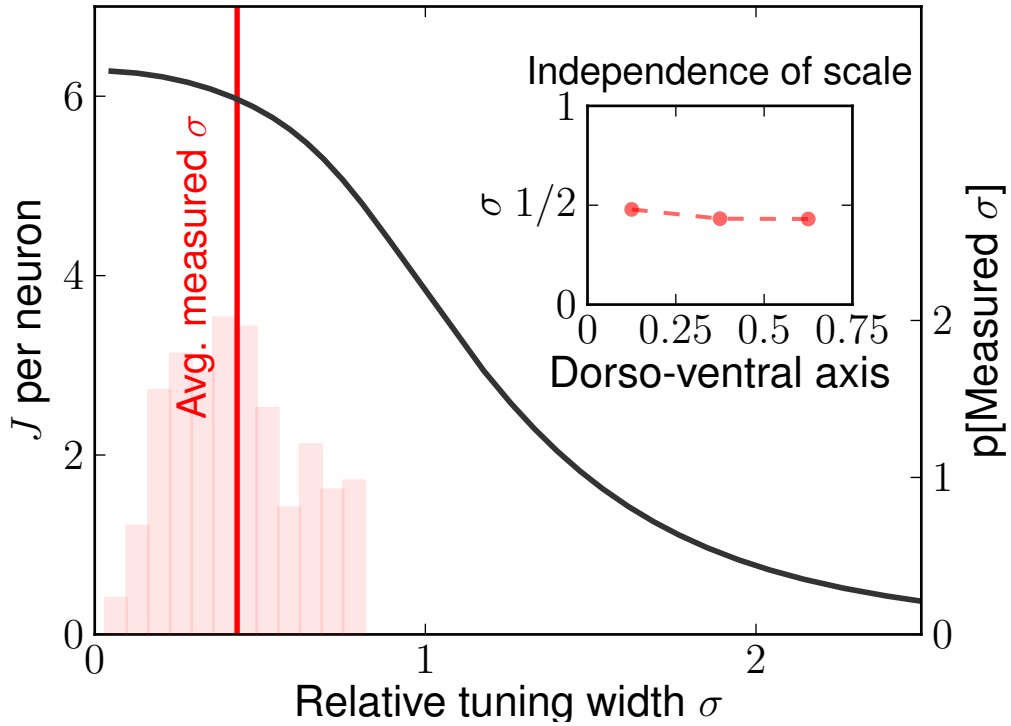

Figure 5: The Fisher information (Eq. (11)) per neuron with tuning curve given by Eq. (10), $f_{max}T = 1$ and spatial period $\lambda = 1$. The Fisher information, shown in black, plateaus for small tuning widths σ, and considerably decreases for large σ. The relative tuning width of grid cell firing patterns on the linear track [10] has been determined and the distribution of values, as well as their average, are shown in red. All experimental widths are close to the peak of the Fisher information. The average measured width along the dorso-ventral axis remains constant, as illustrated in the inset. Each average has been computed from three sets, which were determined according to the recording location of the cells. As the grid sizes increase along this axis [10], this establishes that the relative tuning width is independent of the spatial period.

Let Γ_6 be a hexagonal lattice with fundamental domain D_6 of same area. We assume without loss of generality that D is symmetric around the x-and y-axis. Let $\Omega(x) = f_{max}T \cdot \Phi\left(\frac{|x-c|^2}{\sigma^2}\right)$ be a $\mathcal{C}^2$-radially symmetric tuning curve that has the property that $\mathcal{F}(r)$, as defined above, is non-increasing for $r > R$ for a certain R, with the property that the fundamental domain is longer than $2R$, i.e. $\overline{B_R(0)} \subset D \cap D_6$. The periodically extended tuning curve Ω_Γ for any lattice Γ of this set is associated with a population Fisher information that obeys:

$$\overline{J_{\Omega,\Gamma}} \leq \overline{J_{\Omega,\Gamma_6}}.$$

Proof. We have to show that the eigenvalues of $\overline{J_{\Omega,\Gamma_6}}$ are larger than or equal to those of $\overline{J_{\Omega,\Gamma}}$. These are diagonal matrices with equal terms along the diagonal, therefore it suffices to show this for the traces of the Fisher information matrix. Without loss of generality let us consider $x = 0$. Eq. (20) asserts for the trace $\text{tr}\left(\overline{J_{\Omega_\Gamma}(0)}\right) = \int_D \mathcal{F}(\|\varphi\|^2)d\varphi$, an integral that we can split into contributions of phases with either $\overline{B_R(0)} \cup (D - \overline{B_R(0)}) = D$ as follows:

$$\text{tr}\left(\overline{J_{\Omega_\Gamma}(0)}\right) = \int_{\overline{B_R(0)}} \mathcal{F}(\|\varphi\|^2)d\varphi + \int_{D-\overline{B_R(0)}} \mathcal{F}(\|\varphi\|^2)d\varphi. \tag{25}$$

By definition $\mathcal{F}(s)$ is non-increasing on $D - \overline{B_R(0)}$ and therefore we get by Tóth's theorem of the sums of moments[60, 46, 29] that:

$$\int_{D-\overline{B_R(0)}} \mathcal{F}(\|\varphi\|^2)d\varphi \leq \int_{D_6-\overline{B_R(0)}} \mathcal{F}(\|\varphi\|^2)d\varphi. \tag{26}$$

Since $\mathcal{F}(s)$ is identical on $D \cap \overline{B_R(0)} = D_6 \cap \overline{B_R(0)} = \overline{B_R(0)}$ this establishes the result. □

So far we derived optimal properties for the grid code, in particular nesting, self-similarity, and hexagonality. While the latter have already been discussed nesting will now be checked, in light of published data.

3.6 Predictions and Experimental Observations

We pointed out that the spatial periods should form geometric progressions. This prediction can only be tested by simultaneously recording at multiple sites along the dorso-ventral axis of one animal in a large environment. The jumps that are predicted by the nested arrangement have indeed been observed in a preliminary fashion for two modules in Barry et al. [5], and more rigorously at the SfN conference by Stensola et al. [58]. When pooling over multiple animals and sessions, we expect a strongly skewed distribution, with many more short than long spatial periods. These characteristics are indeed mirrored in the distribution recorded by Brun et al. [10] that is depicted in Fig. 6a.

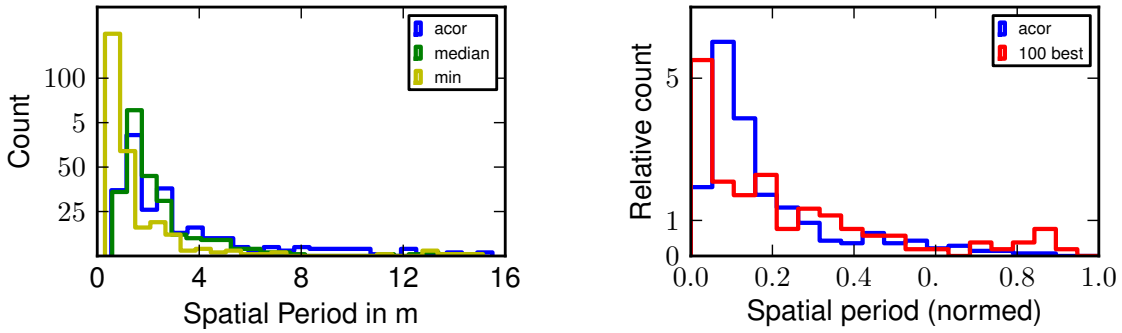

(a) (b)

Figure 6: (a) The distribution of estimated spatial periods from the spatially modulated neurons running on the 18 m long linear track are shown [10]. Brun et al. have determined the spatial periods by different methods, either by taking the *min*imum, or *median* of the pairwise peak to peak distances in the firing map, or by the distance of the first peak in the autocorrelation (*acor*). Different methods were employed, as each rat traversed the track only a few times and the estimation of firing rates was therefore unreliable [10]. Nevertheless, the tendency of few large spatial periods and many small spatial periods can be appreciated. (b) In Mathis et al. the spatial resolution of grid codes with randomly sampled sets of spatial periods was computed [40]. It was noted that although this sampling had no preference in spatial periods, the 100 spatial periods from the grid codes with the highest resolution is significantly skewed — the distribution of these *best* grid sizes is shown in red. The space in this analysis was normalized. The measured grid periods by Brun et al., when normalized by the length of the track show a similar trend [10].

4 Discussion and Conclusion

This paper demonstrated that the parameters of grid cells in the medial entorhinal cortex favor a high spatial resolution. In particular, the optimal grid code is nested with spatial periods obeying geometric progression laws and comprising self-similar tuning curves, and hence constant relative tuning width across modules. Thereby our theory provides a normative justification for the properties of grid cells.

A more quantitative prediction of, for instance, the ratios of spatial periods was beyond the scope of this study for a couple of reasons. Firstly, there is a lack of knowledge about the number of grid cells, their tuning curves, firing variability, correlation structure, etc. These uncertainties could in principle be mediated by providing a range for the predicted ratio, yet there is a more decisive factor: the neuronal decoder is not known, we therefore studied grid cell networks by a more general, information-theoretic measure: the Fisher information and the Cramér-Rao bound. This makes our results more general, but qualitative in nature.

Other studies and models have reported *physiological correlates* of grid firing map properties [27, 13, 22, 31]. For instance, the h-current is correlated with the grid size along the dorso-ventral axis [25]. Thereby, these studies provide a mechanistic explanation for grid cell properties. In that light it is remarkable to note that either the optimal parameters exist "by accident" or that these parameters co-evolved with their physiological correlate.

Optimal quantizers for 2D signals (analog-digital-converters) have hexagonal cells, i.e. the code words are arranged on a hexagonal lattice and, for encoding each analog value, is assigned to the closest lattice point. [28, 46]. A proof for this theorem is based on Fejes Tóth's theorem of the sum of moments, that has also been used in the proof for the optimality of the hexagonal lattice for grid cells in this paper, and that proved to be groundbreaking for packing and covering problems [60, 61]. In this paper we proved the advantage of hexagonal lattices over quadratic ones. Although in earlier studies the perfect hexagonal regularity has always been emphasized [30], recently minor, yet significant deviations have been pointed out and the structure has been described as elliptic grid patterns [59]. Furthermore, Krupic et al. have reported that the majority of cells with high spatial information might not be classical grid cells, but are cells with fewer than three dominant Fourier components, giving rise to band-like cells, and even non-periodic spatial cells [33]. In this paper we stressed that nesting is the key factor for the high resolution, rather than minor changes in tuning widths, peak firing rates, etc. Even further, it is the presence of the multiple scales that empowers nested grid codes with the remarkable exponential scaling, not periodicity. In a nested code the peaks could be distributed between different cells of one module, destroying the periodic structure, but leaving the combinatorial resolution of the population code intact. Therefore, it is important to realize that our assumption that the individual tuning curves are periodic cannot be weakened and therefore not be explained by optimal coding. Similarly, the assumption of modularity cannot be dropped, i.e. that modules of shifted grid cells with the same spatial periods exist. One can devise a nested scheme, where each module comprises only *one* cell with a random phase,

with only small spatial frequency variations between the modules, that due to the higher number of modules performs like a nested *modular* grid code. Such non-periodic or non-modular schemes might be harder to generate with the known models of grid cells [26, 13], and less aesthetic. They could, nevertheless, offer the same spatial resolution.

Investigators of path integration in mammals have emphasized the detrimental effect of noise in the self-motion signals on the accuracy. Path integration is therefore not feasible over longer distances and has to be complemented by other strategies, most crucially by orienting based on landmarks [19]. These behavioral observations are also underpinned by the physiological result that the grid pattern changes and even disappears minutes after inactivating the hippocampus [8], which provides an input that has been implicated to anchor the grid map to salient spatial cues [30, 41].

Other studies on the coding properties of grid cells have suggested that with modular arithmetic the spatial range of the grid code can be much longer than the longest spatial period [20, 56]. This idea crucially depends on reliable, static and global grid patterns, as otherwise the range boost arising from the interference patterns across the multiple cells cannot be exploited. Experimental findings like fragmentation of grid maps in small compartments [16], realignment of grid maps across different mazes [23] and global remapping [37, 36] challenge this requirement. These experimental findings have, however, motivated our assumption that the grid code optimizes the resolution and therefore supports path integration and the metric representation locally — within the range of the largest spatial period. As it has also been suggested by other authors these reliable and precise local *charts* are part of the atlas that forms the manifold like representation of the outside world [15]. The coordinate transformations in this atlas or *initializations* of the grid map within each compartment could be stored in the hippocampus [41].

Finally, from a solely coding theoretical point of view it is interesting to note that both the nested coding strategy and the modular arithmetic strategy for grid cells [20, 56] provide unprecedented coding accuracy for noisy, neuronal representations. Yet, while the latter relies on a network based, error-correction mechanism to achieve exponential scaling, no such mechanism is required for nested grid codes to achieve that feat [39]. In any case, as Sreenivasan and Fiete remark, it is indeed to be expected that other instances of such combinatorial codes will be discovered in the brain.

Acknowledgments

We want to thank May-Britt Moser for discussion, as well was the Moser lab for supporting us with their data. We thank Chun-Wei Yuan and Felix Kempf for comments on the manuscript. This work was supported by the Federal Ministry for Education and Research (through the Bernstein Center for Computational Neuroscience Munich 01GQ0440)

References

[1] JJ Atick. Could information theory provide an ecological theory of sensory processing? *Network: Computation in neural systems*, 3:213–251, 1992.

[2] JJ Atick, Li Zhaoping, and AN Redlich. Understanding Retinal Color Coding from First Principles. *Neural Computation*, 4, 1992.

[3] F Attneave. Some informational aspects of visual perception. *Psychological Review*, 61(3):183–193, 1954.

[4] HB Barlow. Sensory mechanisms, the reduction of redundancy, and intelligence. In *The mechanisation of thought processes*, volume 10, pages 535–539, London, 1959. Her majesty's Stationary Office.

[5] C Barry, R Hayman, N Burgess, and KJ Jeffery. Experience-dependent rescaling of entorhinal grids. *Nature neuroscience*, 10(6):682–4, June 2007.

[6] P Berens, AS Ecker, S Gerwinn, AS Tolias, and M Bethge. Reassessing optimal neural population codes with neurometric functions. *Proceedings of the National Academy of Sciences*, February 2011.

[7] M Bethge, D Rotermund, and K Pawelzik. Optimal short-term population coding: when fisher information fails. *Neural Computation*, 14:2317–2351, 2002.

[8] T Bonnevie, M Fyhn, T Hafting, E Moser, and Moser MB. Misalignment of entorhinal grid fields after hippocampal inactivation. *SfN abstract*, 68.1/BB9, 2006.

[9] WM Brown and A Bäcker. Optimal neuronal tuning for finite stimulus spaces. *Neural computation*, 2006.

[10] VH Brun, T Solstad, KB Kjelstrup, M Fyhn, MP Witter, EI Moser, and MB Moser. Progressive Increase in Grid Scale From Dorsal to Ventral Medial Entorhinal Cortex. *Hippocampus*, 18:1200–1212, 2008.

[11] Y Burak and IR Fiete. Accurate Path Integration in Continuous Attractor Network Models of Grid Cells. *PLoS Computational Biology*, 5(2):1–16, 2009.

[12] N Burgess, C Barry, and J O'Keefe. An Oscillatory Interference Model of Grid Cell Firing. *Hippocampus*, 17:801–812, 2007.

[13] N Burgess and J O'Keefe. Models of place and grid cell firing and theta rhythmicity. *Current Opinion in Neurobiology*, 21:1–11, 2011.

[14] S Cheng and L M Frank. The structure of networks that produce the transformation from grid cells to place cells. *Neuroscience*, 197:293–306, December 2011.

[15] D Derdikman and EI Moser. A manifold of spatial maps in the brain. *Trends in cognitive sciences*, pages 1–9, October 2010.

[16] Dori Derdikman, Jonathan R Whitlock, Albert Tsao, Marianne Fyhn, Torkel Hafting, May-Britt Moser, and Edvard I Moser. Fragmentation of grid cell maps in a multicompartment environment. *Nature neuroscience*, 12(10):1325–32, October 2009.

[17] H Esch and J Burns. Distance estimation by foraging honeybees. *The Journal of experimental biology*, 199:155–62, January 1996.

[18] AS Etienne. The control of short-distance homing in the golden hamster. In *Cognitive Processes and Spatial Orientation in Animals and Man, Vol. I, Experimental Animal Psychology and Ethology*, pages 233–251. Nijhoff, Boston, 1987.

[19] AS Etienne and KJ Jeffery. Path integration in mammals. *Hippocampus*, 14(2):180–92, January 2004.

[20] IR Fiete, Y Burak, and T Brookings. What Grid Cells Convey about Rat Location. *Journal of neurophysiology*, 28(27):6858 – 6871, 2008.

[21] M Franzius, R Vollgraf, and L Wiskott. From grids to places. *J. Computational Neuroscience*, 22:297–299, 2007.

[22] MC Fuhs and DS Touretzky. A Spin Glass Model of Path Integration in Rat Medial Entorhinal Cortex. *Journal of Neuroscience*, 26(16):4266 – 4276, 2006.

[23] M Fyhn, T Hafting, A Treves, MB Moser, and EI Moser. Hippocampal remapping and grid realignment in entorhinal cortex. *Nature*, 446(7132):190–4, March 2007.

[24] M Fyhn, St Molden, MP Witter, EI Moser, and MB Moser. Spatial representation in the entorhinal cortex. *Science (New York, N.Y.)*, 305(5688):1258–64, August 2004.

[25] LM Giocomo, SA Hussaini, F Zheng, ER Kandel, MB Moser, and EI Moser. Grid Cells Use HCN1 Channels for Spatial Scaling. *Cell*, 147(5):1159–1170, November 2011.

[26] LM Giocomo, MB Moser, and EI Moser. Review Computational Models of Grid Cells. *Neuron*, 71(4):589–603, 2011.

[27] LM Giocomo, EA Zilli, E Fransén, and ME Hasselmo. Temporal frequency of subthreshold oscillations scales with entorhinal grid cell field spacing. *Science (New York, N.Y.)*, 315(5819):1719–22, March 2007.

[28] RM Gray and DL Neuhoff. Quantization. *IEEE Transaction on Infromation theory*, 44(6):2325–2383, 1998.

[29] PM Gruber. A short analytic proof of Fejes Tóth's theorem on sums of moments. *Aequationes Mathematicae*, 58:291–295, 1999.

[30] T Hafting, M Fyhn, S Molden, MB Moser, and EI Moser. Microstructure of a spatial map in the entorhinal cortex. *Nature*, 436(7052):801–6, August 2005.

[31] JB Issa and K Zhang. Universal conditions for exact path integration in neural systems. *Proceedings of the National Academy of Sciences*, 109(17):6716–6720, 2012.

[32] E Kropff and A Treves. The Emergence of Grid Cells: Intelligent Design or Just Adaptation ? *Hippocampus*, 18:1256–1269, 2008.

[33] J Krupic, N Burgess, and J O'Keefe. Periodic bands are the building blocks of locational firing in the parahippocampal formation. *SfN abstract*, 729.13/ZZ8, 2011.

[34] S Lang. *Algebraic number theory*. Springer, 2nd edition, 1994.

[35] EL Lehmann. *Theory of Point Estimation.* Springer-Verlag NY, NY, USA, 2nd editio edition, 1998.

[36] JK Leutgeb, S Leutgeb, MB Moser, and EI Moser. Pattern separation in the dentate gyrus and CA3 of the hippocampus. *Science (New York, N.Y.)*, 315(5814):961–6, February 2007.

[37] S Leutgeb, JK Leutgeb, MB Moser, and EI Moser. Place cells, spatial maps and the population code for memory. *Current opinion in neurobiology*, 15(6):738–46, December 2005.

[38] MS Lewicki. Efficient coding of natural sounds. *Nature neuroscience*, 5(4):356–63, April 2002.

[39] A Mathis, AV M Herz, and MB Stemmler. The Resolution of Nested Neuronal Representations can be Exponential in the Number of Neurons. *Physical Review Letters*, 2012.

[40] Alexander Mathis, Andreas V M Herz, and Martin Stemmler. Optimal Population Codes for Space: Grid Cells Outperform Place Cells. *Neural computation*, May 2012.

[41] BL McNaughton, FP Battaglia, O Jensen, EI Moser, and MB Moser. Path integration and the neural basis of the 'cognitive map'. *Nature reviews Neuroscience*, 7(8):663–78, August 2006.

[42] H Mhatre, A Gorchetchnikov, and S Grossberg. Grid cell hexagonal patterns formed by fast self-organized learning within entorhinal cortex. *Hippocampus*, 000, December 2010.

[43] ML Mittelstaedt and H Mittelstaedt. Homing by Path Integration in a Mammal. *Naturwissenschaften*, 67, 1980.

[44] MA Montemurro and S Panzeri. Optimal Tuning Widths in Population Coding of Periodic Variables. *Neural Computation*, 18:1555–1576, 2006.

[45] EI Moser and MB Moser. A Metric for Space. *Hippocampus*, 18:1142–1156, 2008.

[46] DJ Newman. The Hexagon Theorem. *IEEE Transactions on Information Theory*, 28(2):137–139, 1982.

[47] J O'Keefe and L Nadel. *The Hippocampus as a cognitive map*. Oxford University Press, 1978.

[48] BA Olshausen and D Field. Emergence of simple-cell receptive field properties by learning a sparse code for natural images. *Nature*, 381(13), 1996.

[49] E. T. Reifenstein, R. Kempter, S. Schreiber, M. B. Stemmler, and A. V. M. Herz. Grid cells in rat entorhinal cortex encode physical space with independent firing fields and phase precession at the single-trial level. *Proceedings of the National Academy of Sciences*, pages 1–6, April 2012.

[50] MWM Remme, M Lengyel, and BS Gutkin. Democracy-Independence Trade-Off in Oscillating Dendrites and Its Implications for Grid Cells. *Neuron*, 66(3):429–437, May 2010.

[51] ET Rolls, SM Stringer, and T Elliot. Entorhinal cortex grid cells can map to hippocampal place cells by competitive learning. *Network: Computation in Neural Systems*, 447:447–465, 2006.

[52] E Salinas and LF Abbott. Vector reconstruction from firing rates. *J. Computational Neuroscience*, 1:89–107, 1994.

[53] F Sargolini, M Fyhn, T Hafting, BL McNaughton, MP Witter, MB Moser, and EI Moser. Conjunctive representation of position, direction, and velocity in entorhinal cortex. *Science (New York, N.Y.)*, 312(5774):758–62, May 2006.

[54] B Si and A Treves. The role of competitive learning in the generation of DG fields from EC inputs. *Cogn Neurodyn*, 3:177–187, 2009.

[55] T Solstad, EI Moser, and GT Einevoll. From Grid Cells to Place Cells : A Mathematical Model. *Hippocampus*, 16:1026–1031, 2006.

[56] S Sreenivasan and IR Fiete. Grid cells generate an analog error-correcting code for singularly precise neural computation. *Nature neuroscience*, 14:1330–1337, September 2011.

[57] MV Srinivasan, S Zhang, M Altwein, and J Tautz. Honeybee Navigation: Nature and Calibration of the "Odometer". *Science*, 287(5454):851–853, February 2000.

[58] H Stensola, T Stensola, T Solstad, K Froland, MB Moser, and E Moser. Modular organization of grid scale. *SfN abstract*, 726.15/YY6, 2011.

[59] T Stensola, H Stensola, E Moser, and MB Moser. Functional independence of grid cell modules. *SfN abstract*, 726.11/YY5, 2011.

[60] GF Tóth. Sum of Moments of Convex Polygons. *Acta Mathematica Academiae Scientiarum Hungaricae*, 24:417–421, 1973.

[61] LF Tóth. *Lagerungen in der Ebene, auf der Kugel und im Raum*. Springer, 2nd edition, 1972.

[62] S Yaeli and R Meir. Error-based analysis of optimal tuning functions explains phenomena observed in sensory neurons. *Frontiers in computational neuroscience*, 4(October):130, January 2010.

[63] K Zhang and T Sejnowski. Neuronal tuning: to sharpen or broaden. *Neural Computation*, 11(1):75–84, 1999.

[64] EA Zilli and ME Hasselmo. Coupled noisy spiking neurons as velocity-controlled oscillators in a model of grid cell spatial firing. *Journal of Neuroscience*, 30(41):13850–60, October 2010.

6 DISCUSSION AND CONCLUSIONS

> Essentially, all models are wrong,
> but some are useful.
>
> George Edward Pelham Box

In this thesis we study the resolution of neuronal representations of space.[1] In particular, the place cell ensemble (place code) in the hippocampus as well as the grid cell ensemble (grid code) in the medial entorhinal cortex (mEC) of mammals are investigated.

Let us start with place cells. In chapter 2 we show, for homogeneous place codes, that the Fisher information increases linearly with the number of neurons. Thereby, homogeneous refers to a population of neurons with identical tuning curves and tuning widths. This result is well known for general populations of neurons with unimodal tuning curves [14, 39, 82, 144, 152, 153]. Even inhomogeneous populations of place cells, with varying tuning widths and slightly more than one field per cell, scale the same way as a homogeneous place code (chapter 2). Hence, the observed gradient of place field sizes in the hippocampus [70] is not improving the coding precision, if the neurons spike in a statistically independent fashion. This condition is crucial, as we review in chapter 4 that in the presence of high noise correlations, inhomogeneous populations are less affected than homogeneous ones. It has indeed been argued that there are considerable noise correlations among place cells in the hippocampus [152]. Different scales could therefore help to mend the spatial resolution, despite correlations. Another, more speculative explanation is functional: it was pointed out in the introduction that the hippocampus is not solely specialized on space, but is also crucial for episodic memory. Different sizes of place fields might be useful for learning associations to relevant behavioral items [67].

Contrarily, the multiple scales can substantially improve the resolution of a population of grid cells. In chapter 2 and 3 we show this for an arrangement we call nested grid code. In such

1 Here resolution is defined as the accuracy of a maximum likelihood decoder and the Fisher information provides a bound for this accuracy. See chapter 2 or 3 for details.

a code, grid cells with different spatial phases are arranged in modules of the same spatial periods. These modules have staggered spatial periods such that each module further refines the representation of the subsequent module. Thereby, we derive how the optimal spatial period of the refining module can be computed from the noise model of the subsequent module. Such a nested grid code can have a resolution that scales exponentially in the number of neurons, while a place code can only scale linearly in the number of neurons. Thus, a nested grid code can be orders of magnitude more precise than a place code (chapter 2 and 3). We demonstrate that these scalings remain unaltered if one introduces noise correlation between neurons of the same module. As pointed out in chapter 4 the effect of noise correlations between modules was beyond the scope of the current approach, and simulations of estimators as utilized in chapter 2 should be used to elucidate this case.

Yet, it is not simply the multiple scales that endow nested grid codes with exponential scaling. There are many arrangements of the spatial periods that are worse than the best place code of the same number of neurons. For instance, if the spatial periods are all close to each other (chapter 2). Thus, the appropriate nesting of the multiple scales is crucial. By "appropriate" we mean according to the uncertainty of the coarser modules, as defined in (chapter 2 and 3). Yet, although nested grid codes stand out among many other arrangements of spatial periods by their high resolution, some characteristic properties of these nested grid codes are not necessary for this feat. On the one hand, the resolution of these codes is robust to perturbations of the firing maps, like different peak firing rates at different fields, Fano factors of the spiking around one, variable tuning widths, etc. Such robustness is desired for any code, especially for codes in biological systems, where many parameters are highly variable. On the other hand, as pointed out in chapter 5, one can find spatial codes that have non-periodic tuning curves, or have only one phase per module, and still achieve similar resolution levels like nested grid codes. Thus, periodicity and modularity are not necessary implications of optimality.

Among the periodic and modular grid codes, however, *nested grid codes* are optimal. For these nested grid codes we could show that it is best to have an equal amount of neurons per module and that the tuning curves are self-similar across modules. These findings are important, as they appear to be reflected in the properties of grid cells in the mEC ([6, 16, 55, 132], chapter 5).

We could also show in chapter 5 that the hexagonality[2] of grid cells improves the spatial resolution of a grid code. Altogether our results provide a normative justification for the properties of grid cells along the lines of the *optimal coding hypothesis*.

That certain configurations of grid cells provide more spatial information than place cells has also been pointed out by other authors. Guanella and Verschure reported that the resolution of small populations of grid cells is higher than that of small populations of place cells. In particular, they noted the importance of different scales [53]. Fiete and colleagues, on the other hand, argued that the spatial range of the grid code can be much longer than the longest spatial period [18, 42]. Thus, these authors claimed that rats could path integrate over much longer distances than the longest spatial periods of the grid cell population. When these papers were published this had been seen as an important problem, as prior to 2008 the largest spatial period that has been observed was smaller than one meter. Later recordings from environments that were actually substantially larger than the then known periods revealed much longer spatial periods. Periods of at least more than 50% of 18m the linear track were found [16] and the upper limit has still not been determined. As we demonstrate in chapter 2 grid codes that boost the spatial range are prone to catastrophic errors, because the spatial periods are close to each other with respect to the range. Recently Sreenivasan and Fiete suggested an error-correction mechanism that can hamper these catastrophic errors [129]. This mechanism consists of a feedback loop to the population of grid cells. They assume that this network is actually path integrating, so that at each moment the network represents a current position that is updated by small motion increments. The aforementioned loop provides a position signal to the grid cell ensemble. In each cycle, this signal is based on the position before the motion update and thereby *localizes* the novel spatial estimate of the

2 Guanella and Verschure calculated the resolution of small populations of grid cells with different lattice types. They observed for a specific case that hexagonal lattices give a lower error than quadratic lattices and mention that this follows from to the fact that the hexagonal packing is the densest of all circle packings ([53], note that their terminology is different from ours). As such that means that the *effective* spatial period of hexagonal lattices is smaller than that of square lattices. In chapter 5 we show that even if the density is controlled, i.e. the same number of fields per area is considered, a hexagonal arrangement gives at least as much information as a quadratic arrangement for the same radial symmetric tuning curve. Intuitively, this holds because among all regular tilings of the plane with tiles of the same area, the hexagonal tiling can hold the largest inscribed circle. Both results are based on the same mathematical theorem by Tóth [138, 139], which also implies that the optimal quantizer for 2D signals (analog-digital-converter) discretizes space with hexagons [52, 100].

population of grid cells after the motion update. Thereby, it obviates other estimates that are far from the previous position and consequently exclude catastrophic errors. This feedback mechanism is inspired by the the entorhinal-hippocampal loop [129]. In chapter 2 we had not only argued that the spatial representation in the initial model is susceptible to noise, but also that the range is also highly variable with respect to the spatial periods. This problem carries over to the model with error-correction and makes it dependent on reliable, static and global grid patterns. A requirement that is challenged by experimental observations like the fragmentation[3] of grid maps, even within small compartments [26], realignment of grid maps across different mazes [43][4] and global remapping [75, 112].

Our assumption that the grid code optimizes the resolution rather than the range and therefore allows path integration locally has been motivated by these findings. Furthermore, as we review in the introduction, path integration in mammals appears only to be feasible over relatively short distances [36]. In particular, the aforementioned fragmentation of grid patterns in multi-compartmental environments suggests that the mEC encodes space by a collection of regular sub-maps [26]. This division of the environment into sub-maps is remarkable, as it points to a manifold-like representation of the outside world [25]. The anchoring of the individual coordinates for each sub-maps might be stored in the hippocampus [25, 88], and the transformation between these coordinates could happen by computations within the entorhinal-hippocampal loop. This system appears to allow the animal a highly flexible and adaptive spatial representation, that can always be optimized for the current task and environment at hand. Revealing how this mechanistically works is one of the major objectives for understanding navigation in mammals.

3 When Derdikman et al. recorded in environments consisting of multiple compartments the spatial firing pattern of grid cells, which had been identified in open-field environments, ceased to be hexagonal. More specifically, in the hairpin maze, which is a "stack of interconnected, zig-zagged compartments of equal shape and orientation" [26] the grid cell firing patterns were fragmented by the compartment boundaries, and each compartment had its periodic pattern. The experiment suggests that the mEC encodes space by collection of regular sub-maps [25, 26].

4 Fyhn et al. observed that during rate remapping the grid patterns of grid cells remained unaltered. During global remapping the phases of these patterns shifted and/or the grid orientations changed. Crucially, these changes were consistent, so that grid cells recorded from the same tetrode were subject to similar changes. Sometimes also small changes of the spatial periods were observed [25, 43].

From now on we will provide an outlook to related research questions.

OUTLOOK

One upshot of many earlier population coding models with correlation structure is that for large, heterogeneous populations of unimodal tuning curves, i.e. families with varying tuning widths and peak firing rates, reducing the correlations does not improve encoding accuracy [30, 123, 144]. Grid cells are also highly heterogeneous in their firing rates and tuning parameters [55, 56], and it would be interesting to study the effect of heterogeneity for grid codes as well.

Throughout this thesis we consider a *firing code* and assumed that there is a fixed time scale that governs how many spikes each neuron elicits given its spatial firing rate modulation. This time scale is inspired by the periods of the theta rhythm, which has been suggested as the Zeitgeber in the hippocampus ([20], chapter 2). One could incorporate finer time scales in the population coding model, which are indeed present in the hippocampus and the medial entorhinal cortex, like the gamma rhythm or phase precession [20, 104]. For instance, Reifenstein et al. show that for a single grid cell the resolution is about 80% higher, if one considers the theta phase of the individual spikes rather than the spike count [114]. Phase precision could therefore potentially also enhance the resolution of a population of grid cells.

In chapter 2 we argue that the time scale of the theta rhythm is sufficiently short and the velocities sufficiently low that we can as a first approximation consider an immobile animal. This is of course a huge simplification, and moving animals, as well as the precision of the encoded trajectory, could be studied next. For instance, by similar methods to the ones employed by Huys et al. [62].

A major difficulty of navigation studies in mammals is that, although much is known about the cell types that encode space and, as we also discus in this thesis, spatial maps that are formed by these neurons, it is unclear how these maps *mechanistically* give rise to action [36]. One avenue to be taken by modelers would be to suggest how the homing vector can be computed from the path integration system. As this system is, presumably, given by the network of grid cells, one can ask what is necessary to compute the homing vector of the population activity of grid cells. More generally, we discuss in chapter 5 the importance of the specific decoder on the resolution of the grid code. To

provide more quantitative predictions about the grid code, it would be important to learn more about the decoder itself, i.e. the computations that are done with grid cells.

BIBLIOGRAPHY

[1] LF Abbott and P Dayan. The effect of correlated variability on the accuracy of a population code. *Neural Computation*, 11:91–101, 1999.

[2] JJ Atick. Could information theory provide an ecological theory of sensory processing? *Network: Computation in neural systems*, 3:213–251, 1992.

[3] JJ Atick, Z Li, and AN Redlich. Understanding Retinal Color Coding from First Principles. *Neural Computation*, 4, 1992.

[4] F Attneave. Some informational aspects of visual perception. *Psychological Review*, 61(3):183–193, 1954.

[5] HB Barlow. Sensory mechanisms, the reduction of redundancy, and intelligence. In *The mechanisation of thought processes*, volume 10, pages 535–539, London, 1959. Her majesty's Stationary Office.

[6] C Barry, R Hayman, N Burgess, and KJ Jeffery. Experience-dependent rescaling of entorhinal grids. *Nature neuroscience*, 10(6):682–4, June 2007.

[7] S Benhamou, JP Sauve, and P Bovet. Spatial Memory in Large Scale Movements : Efficiency and Limitation of the Egocentric Coding Process. *J. theor. Biol*, 145:1–12, 1990.

[8] P Berens, AS Ecker, S Gerwinn, AS Tolias, and M Bethge. Reassessing optimal neural population codes with neurometric functions. *Proceedings of the National Academy of Sciences*, February 2011.

[9] M Bethge, D Rotermund, and K Pawelzik. Optimal short-term population coding: when fisher information fails. *Neural Computation*, 14:2317–2351, 2002.

[10] E Bloch. *Tübinger Einleitung in die Philosophie I*. Suhrkamp Verlag, Frankfurt am Main, 1963.

[11] O Bobrowski, R Meir, and E Yoninina. Bayesian Filtering in Spiking Neural Networks: Noise, Adaptation, and Multisensory Integration. *Neural Computation*, 21:1277–1320, 2009.

[12] CN Boccara, F Sargolini, VH Thoresen, T Solstad, MP Witter, EI Moser, and MB Moser. Grid cells in pre- and parasubiculum. *Nature neuroscience*, 13(8):987–994, July 2010.

[13] PC Bressloff. Pattern formation and visual cortex. *Les Houches Lectures in Neurophysics*, 2005.

[14] WM Brown and A Bäcker. Optimal neuronal tuning for finite stimulus spaces. *Neural computation*, 2006.

[15] VH Brun, K Otnass, S Molden, HA Steffenach, MP Witter, MB Moser, and EI Moser. Place cells and place recognition maintained by direct entorhinal-hippocampal circuitry. *Science (New York, N.Y.)*, 296(5576):2243–6, June 2002.

[16] VH Brun, T Solstad, KB Kjelstrup, M Fyhn, MP Witter, EI Moser, and MB Moser. Progressive Increase in Grid Scale From Dorsal to Ventral Medial Entorhinal Cortex. *Hippocampus*, 18:1200–1212, 2008.

[17] N Brunel and JP Nadal. Mutual Information, Fisher Information, and Population Coding. *Neural Computation*, 10:1731–1757, 1998.

[18] Y Burak, T Brookings, and I Fiete. Triangular lattice neurons may implement an advanced numeral system to precisely encode rat position over large ranges. *arXiv:q-bio/0606005v1*, 93106:4, June 2006.

[19] A Burgalossi, L Herfst, M von Heimendahl, H Förste, K Haskic, M Schmidt, and M Brecht. Microcircuits of functionally identified neurons in the rat medial entorhinal cortex. *Neuron*, 70(4):773–86, May 2011.

[20] G Buzsaki. *Rhythms of the Brain*. Oxford University Press, USA, 2006.

[21] DB Chklovskii and AA Koulakov. Maps in the brain: what can we learn from them? *Annual Review of Neuroscience*, 27:369–92, January 2004.

[22] MR Cohen and WT Newsome. Context-dependent changes in functional circuitry in visual area MT. *Neuron*, 60(1):162–73, October 2008.

[23] P Dayan and LF Abbott. *Theoretical Neuroscience: Computational and Mathematical Modeling of Neural Systems*. MIT Press, 2001.

[24] L De Almeida, M Idiart, A Villavicencio, and J Lisman. Alternating predictive and short-term memory modes of entorhinal grid cells. *Hippocampus. doi 10.1002/hipo.22030*, May 2012.

[25] D Derdikman and EI Moser. A manifold of spatial maps in the brain. *Trends in Cognitive Sciences*, pages 1–9, October 2010.

[26] D Derdikman, JR Whitlock, A Tsao, M Fyhn, T Hafting, MB Moser, and EI Moser. Fragmentation of grid cell maps in a multicompartment environment. *Nature neuroscience*, 12(10):1325–32, October 2009.

[27] CF Doeller, C Barry, and N Burgess. Evidence for grid cells in a human memory network. *Nature*, 463(7281):657–61, February 2010.

[28] K Doya, S Ishii, A Pouget, and RPN Rao. *Bayesian Brain Probabilistic Approaches to Neural Coding*. MIT Press, 2007.

[29] AS Ecker, P Berens, GA Keliris, M Bethge, NK Logothetis, and AS Tolias. Decorrelated neuronal firing in cortical microcircuits. *Science (New York, N.Y.)*, 327(5965):584–7, January 2010.

[30] AS Ecker, P Berens, AS Tolias, and M Bethge. The Effect of Noise Correlations in Populations of Diversely Tuned Neurons. *Journal of Neuroscience*, 31(40):14272–14283, 2011.

[31] H Eichenbaum. A cortical-hippocampal system for declarative memory. *Nature reviews. Neuroscience*, 1(1):41–50, October 2000.

[32] H Eichenbaum. Hippocampus: mapping or memory? *Current biology*, 10(21):R785–7, November 2000.

[33] AD Ekstrom, MJ Kahana, JB Caplan, TA Fields, EA Isham, EL Newman, and I Fried. Cellular networks underlying human spatial navigation. *Nature*, 425:184–187, 2003.

[34] H Esch and J Burns. Distance estimation by foraging honeybees. *The Journal of Experimental Biology*, 199:155–62, January 1996.

[35] AS Etienne. The control of short-distance homing in the golden hamster. In *Cognitive Processes and Spatial Orientation in Animals and Man, Vol. I, Experimental Animal Psychology and Ethology*, pages 233–251. Nijhoff, Boston, 1987.

[36] AS Etienne and KJ Jeffery. Path integration in mammals. *Hippocampus*, 14(2):180–92, January 2004.

[37] AS Etienne, R Maurer, J Berlie, and B Reverdin. Navigation through vector addition. *Nature*, pages 161–164, 1998.

[38] AS Etienne, R Maurer, and F Saucy. Limitations in the Assessment of Path Dependent Information. *Behaviour*, 106(1/2):81–111, 1988.

[39] CW Eurich and SD Wilke. Multidimensional Encoding Strategy of Spiking Neurons. *Neural Computation*, 12(7):1519–1529, July 2000.

[40] AA Fenton, G Csizmadia, and RU Muller. Conjoint Control of Hippocampal Place Cell Firing by Two Visual Stimuli II. A Vector-field Theory that Predicts Modifications of the Representation of the Environment. *J.Gen.Physiol.*, 116(August):211–221, 2000.

[41] AA Fenton, WW Lytton, JM Barry, PP Lenck-Santini, LE Zinyuk, S Kubík, J Bures, B Poucet, RU Muller, and AV Olypher. Attention-like modulation of hippocampus place cell discharge. *Journal of Neuroscience*, 30(13):4613–25, March 2010.

[42] IR Fiete, Y Burak, and T Brookings. What Grid Cells Convey about Rat Location. *Journal of Neuroscience*, 28(27):6858 – 6871, 2008.

[43] M Fyhn, T Hafting, A Treves, MB Moser, and EI Moser. Hippocampal remapping and grid realignment in entorhinal cortex. *Nature*, 446(7132):190–4, March 2007.

[44] M Fyhn, T Hafting, MP Witter, EI Moser, and MB Moser. Grid cells in mice. *Hippocampus*, 18(12):1230–8, January 2008.

[45] M Fyhn, S Molden, MP Witter, EI Moser, and MB Moser. Spatial representation in the entorhinal cortex. *Science (New York, N.Y.)*, 305(5688):1258–64, August 2004.

[46] CR Gallistel. Insect Navigation: Brains as Symbol-Processing Organs. In S Sternberg and D Scarborough, editors, *Brains as Symbol Processors: The Case of Insect Navigation*, volume 4, pages 1–51. MIT Press, 2 edition, 1998.

[47] TJ Gawne and J Richmond. How independent are the massages carried by adjacent inferior temporal cortical neurons? *Journal of Neuroscience*, 13(7):2758–2771, 1993.

[48] A Georgopoulos, A Schwartz, and R Kettner. Neuronal population coding of movement direction. *Science*, 233(4771):1416–1419, September 1986.

[49] ED Gershon, MC Wiener, PE Latham, and BJ Richmond. Coding Strategies in Monkey V1 and Inferior Temporal Cortices. *Journal of Neurophysiology*, 79(3):1135–1144, 1998.

[50] LM Giocomo, MB Moser, and EI Moser. Review Computational Models of Grid Cells. *Neuron*, 71(4):589–603, 2011.

[51] KM Gothard, WE Skaggs, and BL McNaughton. Dynamics of mismatch correction in the hippocampal ensemble code for space: interaction between path integration and environmental cues. *Journal of Neuroscience*, 16(24):8027–40, December 1996.

[52] RM Gray and DL Neuhoff. Quantization. *IEEE Transaction on Infromation theory*, 44(6):2325–2383, 1998.

[53] A Guanella and P Verschure. Prediction of the Position of an Animal Based on Populations of Grid and Place Cells: A Comparative Study. *Journal of Integrative Neuroscience*, 6(3):433–446, 2007.

[54] T Hafting, M Fyhn, T Bonnevie, MB Moser, and EI Moser. Hippocampus-independent phase precession in entorhinal grid cells. *Nature*, 453(7199):1248–52, June 2008.

[55] T Hafting, M Fyhn, S Molden, MB Moser, and EI Moser. Microstructure of a spatial map in the entorhinal cortex. *Nature*, 436(7052):801–6, August 2005.

[56] AVM Herz, C Kluger, A Mathis, and M Stemmler. Variability of grid cell firing on a trial-to-trial basis. In *Ninth Göttingen Meeting of the German Neuroscience Society*, pages T26–15C, 2011.

[57] JJ Hopfield. Neural networks and physical systems with emergent collective computational abilities. *Proceedings of the National Academy of Sciences*, 79:2554–2558, 1982.

[58] JJ Hopfield. Neurodynamics of mental exploration. *Proceedings of the National Academy of Sciences*, 107(4):1648–53, January 2010.

[59] DH Hubel and TN Wiesel. Receptive fields and functional architecture of monkey striate cortex. *Journal of Physiology*, 195(1):215–43, March 1968.

[60] TN Hubel, DH and Wiesel. Receptive Fields of Single Neurons in the Cat's Striate Cortex. *Journal of Physiology*, 148:574–591, 1959.

[61] NE Humphries, N Queiroz, JRM Dyer, NG Pade, MK Musyl, KM Schaefer, DW Fuller, JM Brunnschweiler, TK Doyle, JDR Houghton, GC Hays, CS Jones, LR Noble, VJ Wearmouth, EJ. Southall, and DW Sims. Environmental context explains Lévy and Brownian movement patterns of marine predators. *Nature*, 465(7301):1066–1069, June 2010.

[62] QJM Huys, RS Zemel, R Natarajan, and P Dayan. Fast population coding. *Neural Computation*, 19(2):404–441, 2007.

[63] JB Issa and K Zhang. Universal conditions for exact path integration in neural systems. *Proceedings of the National Academy of Sciences*, 109(17):6716–6720, 2012.

[64] J Jackson and AD Redish. Network Dynamics of Hippocampal Cell-Assemblies Resemble Multiple Spatial Maps Within Single Tasks. *Hippocampus*, 17:1209–1229, 2007.

[65] K Jezek, EJ Henriksen, A Treves, EI Moser, and MB Moser. Theta-paced flickering between place-cell maps in the hippocampus. *Nature*, 478(7368):246–9, October 2011.

[66] RS Johansson and JR Flanagan. Coding and use of tactile signals from the fingertips in object manipulation tasks. *Nature reviews. Neuroscience*, 10(5):345–59, May 2009.

[67] MW Jung, SI Wiener, and BL McNaughton. Comparison of Spatial Firing Characteristics Ventral Hippocampus of the Rat. *Journal of Neuroscience*, 74(12):7347–7456, 1994.

[68] I Kant. *Kritik der reinen Vernunft*. Suhrkamp-Taschenbuch Wissenschaft, Frankfurt am Main, 14 edition, 2000.

[69] SM Kay. *Fundamentals of Statistical Signal Processing: Estimation Theory*. Prentice Hall, Upper Saddle River, New Jersey, 1993.

[70] KB Kjelstrup, T Solstad, VH Brun, T Hafting, S Leutgeb, MP Witter, EI Moser, and MB Moser. Finite scale of spatial representation in the hippocampus. *Science (New York, N.Y.)*, 321(5885):140–3, July 2008.

[71] JL Kubie, A Fenton, N Novikov, D Touretzky, and RU Muller. Changes in goal selection induced by cue conflicts are in register with predictions from changes in place cell field locations. *Behavioral Neuroscience*, 121(4):751–763, 2007.

[72] RF Langston, JA Ainge, JJ Couey, CB Canto, TL Bjerknes, MP Witter, EI Moser, and MB Moser. Development of the spatial representation system in the rat. *Science (New York, N.Y.)*, 328(5985):1576–80, June 2010.

[73] C Leibold and R Kempter. Memory Capacity for Sequences in a Recurrent Network with. *Neural Computation*, 18:904–941, 2006.

[74] JK Leutgeb, S Leutgeb, MB Moser, and EI Moser. Pattern separation in the dentate gyrus and CA3 of the hippocampus. *Science (New York, N.Y.)*, 315(5814):961–6, February 2007.

[75] S Leutgeb, JK Leutgeb, CA Barnes, EI Moser, BL McNaughton, and MB Moser. Independent codes for spatial and episodic memory in hippocampal neuronal ensembles. *Science (New York, N.Y.)*, 309(5734):619–23, July 2005.

[76] C Lever, S Burton, A Jeewajee, J O'Keefe, and N Burgess. Boundary vector cells in the subiculum of the hippocampal formation. *Journal of Neuroscience*, 29(31):9771–7, August 2009.

[77] MS Lewicki. Efficient coding of natural sounds. *Nature neuroscience*, 5(4):356–63, April 2002.

[78] EA Maguire, N Burgess, JG Donnett, RSJ Frackowiak, DF Frith, and J O'Keefe. Knowing Where and Getting There: A Human Navigation Network. *Science*, 280(5365):921–924, May 1998.

[79] EA Maguire, DG Gadian, IS Johnsrude, CD Good, J Ashburner, RS Frackowiak, and CD Frith. Navigation-related structural change in the hippocampi of taxi drivers. *Proceedings of the National Academy of Sciences*, 97(8):4398–403, April 2000.

[80] D Marr. Simple Memory: A Theory for Archicortex. *Philosophical Transactions of the Royal Society of London*, 262(841):23–81, 1971.

[81] A Mathis, AVM Herz, and M Stemmler. How Good is Grid Coding versus Place Coding for Navigation Using Noisy, Spiking Neurons? *Frontiers in Computational Neuroscience. Conference Abstract: Bernstein Conference on Computational Neuroscience*, 4(2010):3389–3389, 2010.

[82] A Mathis, AVM Herz, and M Stemmler. Optimal Population Codes for Space: Grid Cells Outperform Place Cells. *Neural Computation*, 9(24):2280–2317, May 2012.

[83] A Mathis, M Stemmler, and A Herz. How good is grid coding versus place coding for navigation using noisy, spiking neurons? *BMC Neuroscience*, 11(Suppl 1):O20, 2010.

[84] A Mathis, MB Stemmler, and AVM Herz. Exponential Scaling of Nested Neuronal Representations. *Front. Comput. Neurosci. Conference Abstract: BC11 : Computational Neuroscience & Neurotechnology Bernstein Conference & Neurex Annual Meeting*, 2011.

[85] T Maudlin. *Philosophy of Physics: Space and Time*. Princeton University Press, Princeton, 2012.

[86] BL McNaughton, A Barnes, J Meltzer, and J Sutherland. Hippocampal granule cells are necessary for normal spatial learning but not for spatially-selective pyramidal cell discharge. *Experimental Brain Research*, 76:485–496, 1989.

[87] BL McNaughton, CA Barnes, JL Gerrard, K Gothard, MW Jung, JJ Knierim, H Kudrimoti, Y Qin, WE Skaggs, M Suster, and KL Weaver. Deciphering the hippocampal polyglot: the hippocampus as a path integration system. *The Journal of Experimental Biology*, 199:173–85, January 1996.

[88] BL McNaughton, FP Battaglia, O Jensen, EI Moser, and MB Moser. Path integration and the neural basis of the 'cognitive map'. *Nature reviews Neuroscience*, 7(8):663–78, August 2006.

[89] R Menzel, K Geiger, L Chittka, J Joerges, and J Kunze. The knowledge base of bee navigation. *The Journal of Experimental Biology*, 146:141–146, 1996.

[90] R Menzel, U Greggers, A Smith, S Berger, R Brandt, S Brunke, G Bundrock, T Plu, F Schaupp, E Schu, S Stach, J Stindt, N Stollhoff, and S Watzl. Honey bees navigate according to a map-like spatial memory. *Proceedings of the National Academy of Sciences*, 102(8), 2005.

[91] G Miesenböck. Optogenetic Control of Cells and Circuits. *Annual Review of Cell and Developmental Biology*, 27:731–758, 2011.

[92] ML Mittelstaedt and H Mittelstaedt. Homing by Path Integration in a Mammal. *Naturwissenschaften*, 67, 1980.

[93] MA Montemurro and S Panzeri. Optimal Tuning Widths in Population Coding of Periodic Variables. *Neural Computation*, 18:1555–1576, 2006.

[94] RGM Morris, P Garrud, JNP Rawlins, and J O'Keefe. Place navigation impaired in rats with hippocampal lesions. *Nature*, 297, 1982.

[95] EI Moser, E Kropff, and MB Moser. Place cells, grid cells, and the brain's spatial representation system. *Annual Review of Neuroscience*, 31:69–89, January 2008.

[96] EI Moser and MB Moser. A Metric for Space. *Hippocampus*, 18:1142–1156, 2008.

[97] VB Mountcastle. The columnar organization of the neocortex. *Brain*, 120:701–22, April 1997.

[98] RU Muller and JL Kubie. The Effects of Changes in the Environment Hippocampal Cells on the Spatial Firing of. *Journal of Neuroscience*, 7(7):1951–1968, 1987.

[99] L Nadel. The hippocampus and space revisited. *Hippocampus*, 1(3):221–9, July 1991.

[100] DJ Newman. The Hexagon Theorem. *IEEE Transactions on Information Theory*, 28(2):137–139, 1982.

[101] J O'Keefe and N Burgess. Geometric determinants of the place fields of hippocampal neurons. *Nature*, 381, 1996.

[102] J O'Keefe and J Dostrovsky. The hippocampus as a spatial map: Preliminary evidence from unit activity in the freely-moving rat. *Brain research*, 34:171–175, 1971.

[103] J O'Keefe and L Nadel. *The Hippocampus as a cognitive map*. Oxford University Press, 1978.

[104] J O'Keefe and ML Recce. Phase relationship between hippocampal place units and the EEG theta rhythm. *Hippocampus*, 3(3):317–30, July 1993.

[105] BA Olshausen and D Field. Emergence of simple-cell receptive field properties by learning a sparse code for natural images. *Nature*, 381(13), 1996.

[106] M A Paradiso. A Theory for the Use of Visual Orientation Information which Exploits the Columnar Structure of Striate Cortex. *Biological Cybernetics*, 58:35–49, May 1988.

[107] E Park, D Dvorak, and AA Fenton. Ensemble Place Codes in Hippocampus: CA1, CA3, and Dentate Gyrus Place Cells Have Multiple Place Fields in Large Environments. *PloS one*, 6(7):e22349, January 2011.

[108] C Parron and E Save. Evidence for entorhinal and parietal cortices involvement in path integration in the rat. *Experimental brain research. Experimentelle Hirnforschung. Expérimentation cérébrale*, 159(3):349–59, December 2004.

[109] S Pouget, S Deneve, JC Ducom, and PE Latham. Narrow versus wide tuning curves: What's best for a population code? *Neural Computation*, 11(1):85–90, January 1999.

[110] AD Redish. *Beyond the Cognitive Map: From Place Cells to Episodic Memory*. MIT Press, February 1999.

[111] AD Redish, FP Battaglia, MK Chawla, AD Ekstrom, JL Gerrard, P Lipa, ES Rosenzweig, PF Worley, JF Guzowski, BL McNaughton, and CA Barnes. Independence of Firing Correlates of Anatomically Proximate Hippocampal Pyramidal Cells. *Journal of Neuroscience*, 21(RC134):1–6, 2001.

[112] AD Redish, ES Rosenzweig, JD Bohanick, BL McNaughton, and CA Barnes. Dynamics of Hippocampal Ensemble Activity Realignment : Time versus Space. *Journal of Neuroscience*, 20(24):9298–9309, 2000.

[113] DS Reich, F Mechler, and JD Victor. Independent and redundant information in nearby cortical neurons. *Science (New York, N.Y.)*, 294(5551):2566–8, December 2001.

[114] ET Reifenstein, R Kempter, S Schreiber, MB Stemmler, and AVM Herz. Grid cells in rat entorhinal cortex encode physical space with independent firing fields and phase precession at the single-trial level. *Proceedings of the National Academy of Sciences*, pages 1–6, April 2012.

[115] AM Reynolds, AD Smith, R Menzel, U Greggers, DR Reynolds, and JR Riley. Displaced honey bees perform optimal scale-free search flights. *Ecology*, 88(8):1955–61, August 2007.

[116] F Sargolini, M Fyhn, T Hafting, BL McNaughton, MP Witter, MB Moser, and EI Moser. Conjunctive representation of position, direction, and velocity in entorhinal cortex. *Science (New York, N.Y.)*, 312(5774):758–62, May 2006.

[117] F Savelli, D Yoganarasimha, and JJ Knierim. Influence of Boundary Removal on the Spatial Representations of the Medial Entorhinal Cortex. *Hippocampus*, 1282:1270–1282, 2008.

[118] R Schmidt, K Diba, C Leibold, D Schmitz, G Buzsáki, and R Kempter. Single-trial phase precession in the hippocampus. *Journal of Neuroscience*, 29(42):13232–41, October 2009.

[119] WB Scoville and B Milner. Loss of Recent Memory After Bilateral Hippocampal Lesions. *The Journal of Neurology, Neurosurgery and Psychiatry*, 20:11–21, 1957.

[120] HS Seung and H Sompolinsky. Simple models for reading neuronal population codes. *Proceedings of the National Academy of Sciences*, 90(22):10749–53, November 1993.

[121] MN Shadlen and WT Newsome. The variable discharge of cortical neurons: implications for connectivity, computation, and information coding. *Journal of Neuroscience*, 18(10):3870–96, May 1998.

[122] M Shamir and H Sompolinsky. Correlation Codes in Neuronal Networks. *NIPS*, 15:277–284, 2001.

[123] M Shamir and H Sompolinsky. Implications of neuronal diversity on population coding. *Neural Computation*, 18(8):1951–86, August 2006.

[124] PE Sharp. Complimentary roles for hippocampal versus subicular/entorhinal place cells in coding place, context, and events. *Hippocampus*, 9(4):432–43, January 1999.

[125] EP Simoncelli. Natural image statistics and neural representation. *Annual Review of Neuroscience*, 24:1193–216, 2001.

[126] MA Smith and A Kohn. Spatial and temporal scales of neuronal correlation in primary visual cortex. *Journal of Neuroscience*, 28(48):12591–603, November 2008.

[127] T Solstad, CN Boccara, E Kropff, MB Moser, and EI Moser. Representation of geometric borders in the entorhinal cortex. *Science (New York, N.Y.)*, 322(5909):1865–8, December 2008.

[128] LR Squire. Memory systems of the brain: A brief history and current perspective. *Neurobiology of Learning and Memory*, 82(3):171–7, November 2004.

[129] S Sreenivasan and IR Fiete. Grid cells generate an analog error-correcting code for singularly precise neural computation. *Nature neuroscience*, 14:1330–1337, September 2011.

[130] MV Srinivasan, S Zhang, M Altwein, and J Tautz. Honeybee Navigation: Nature and Calibration of the "Odometer". *Science*, 287(5454):851–853, February 2000.

[131] HA Steffenach, M Witter, MB Moser, and EI Moser. Spatial memory in the rat requires the dorsolateral band of the entorhinal cortex. *Neuron*, 45(2):301–13, January 2005.

[132] H Stensola, T Stensola, T Solstad, K Froland, MB Moser, and E Moser. Modular organization of grid scale. *SfN abstract*, 726.15/YY6, 2011.

[133] J Stillwell. *Mathematics and its History*. Springer, New York, 2nd edition, 2002.

[134] JS Taube. The head direction signal: origins and sensory-motor integration. *Annual Review of Neuroscience*, 30:181–207, January 2007.

[135] JS Taube, RU Muller, and JB Ranck. Head-direction cells recorded from the postsubiculum in freely moving rats. I. Description and quantitative analysis. *Journal of Neuroscience*, 10(2):420–35, February 1990.

[136] JS Taube, RU Muller, and JB Ranck. Head-direction cells recorded from the postsubiculum in freely moving rats. II. Effects of environmental manipulations. *Journal of Neuroscience*, 10(2):436–47, February 1990.

[137] EC Tolman. Cognitive maps in rats and men. *Psychological Review*, 55(4):189–208, July 1948.

[138] GF Tóth. Sum of Moments of Convex Polygons. *Acta Mathematica Academiae Scientiarum Hungaricae*, 24:417–421, 1973.

[139] LF Tóth. *Lagerungen in der Ebene, auf der Kugel und im Raum*. Springer, 2nd edition, 1972.

[140] DS Touretzky and AD Redish. Theory of rodent navigation based on interacting representations of space. *Hippocampus*, 6:247–70, January 1996.

[141] NM van Strien, NLM Cappaert, and MP Witter. The anatomy of memory: an interactive overview of the parahippocampal-hippocampal network. *Nature reviews. Neuroscience*, 10(4):272–82, April 2009.

[142] C van Vreeswijk. What is the neural code? In L van Hemmen and TJ Sejnowski, editors, *23 Problems in Systemic Neuroscience*. Oxford University Press, 2006.

[143] R Wehner and M Srinivasan. Path integration in insects. In KJ Jeffery, editor, *The Neurobiology of Spatial Behaviour*. Oxford University Press, Oxford, 2003.

[144] SD Wilke and CW Eurich. Representational Accuracy of Stochastic Neural Populations. *Neural Computation*, 189:155–189, 2001.

[145] TJ Wills, F Cacucci, N Burgess, and J O'Keefe. Development of the hippocampal cognitive map in preweanling rats. *Science (New York, N.Y.)*, 328(5985):1573–6, June 2010.

[146] MA Wilson and BL McNaughton. Dynamics of the hippocampal ensemble code for space. *Science (New York, N.Y.)*, 261(5124):1055–8, August 1993.

[147] MP Witter and EI Moser. Spatial representation and the architecture of the entorhinal cortex. *Trends in Neurosciences*, 29(12):671–8, December 2006.

[148] MP Witter, PA Naber, T van Haeften, WC Machielsen, SA Rombouts, F Barkhof, P Scheltens, and FH Lopes da Silva. Cortico-hippocampal communication by way of parallel parahippocampal-subicular pathways. *Hippocampus*, 10(4):398–410, January 2000.

[149] M Wittlinger, R Wehner, and H Wolf. The ant odometer: stepping on stilts and stumps. *Science (New York, N.Y.)*, 312(5782):1965–7, June 2006.

[150] MM Yartsev, MP Witter, and N Ulanovsky. Grid cells without theta oscillations in the entorhinal cortex of bats. *Nature*, 479(7371):103–107, 2011.

[151] J Zeil, A Kelber, and R Voss. Structure and function of learning flights in bees and wasps. *The Journal of Experimental Biology*, 199:245–252, 1996.

[152] K Zhang, I Ginzburg, BL McNaughton, and TJ Sejnowski. Interpreting neuronal population activity by reconstruction: unified framework with application to hippocampal

place cells. *Journal of Neurophysiology*, 79(2):1017–44, February 1998.

[153] K Zhang and T Sejnowski. Neuronal tuning: to sharpen or broaden. *Neural Computation*, 11(1):75–84, 1999.

[154] E Zohary, MN Shadlen, and WT Newsome. Correlated neuronal discharge rate and its implications for psychophysical performance. *Nature*, 1994.

ACKNOWLEDGEMENTS

> This paper has proved to be controversial.
>
> Anonymous reviewer.

First and foremost, I would like to thank my supervisors, Andreas and Martin. When I had just started working with them, they gave me, a topologist, a guided tour of the fascinating world of Neuroscience and granted me the freedom to explore ever since. I am thankful for their enthusiasm, scrutiny and guidance. It was a pleasure to work with them. Recently I learned that Martin is a high-energy physicist by training, a term that also describes his personality quite literally.

I am grateful to Mark Hübener for his contributions in the TAC meetings.

The Herz lab and all the neighboring labs were a great place to work, discuss and learn. With Eric, I shared a table which was too long for a time which was unfortunately too short – als Berliner Original mußte er früh ebendahin zurückkehren. Later came Dinu, and our "night shifts" were essential for finishing this thesis and some parts of the manuscripts it contains. Grazie a Gio for bringing this LaTeX-classicthesis-design to my attention. I also want to extend my thanks to all other former and current members of the Herz lab.

Thanks as well to all other colleagues in the BCCN, the GSN and the Biocenter. In particular, I highly appreciated the direct and unembellished discussions with Christian, his style of bouncing around ideas was very refreshing. Furthermore, thanks to Axel for our swift collaboration.

Over the past few years, also many scientists outside of Munich also had an impact on me. Thanks to the members of the Center for Neurobiology and Behavior, Columbia University and the Computational Neuroscience Lab, Tsinghua University for their hospitality during my brief summer visits. The conferences and summer schools I attended were highly informative and captivating. In particular, I would like to thank Dave Redish for all he told me about the hippocampus.

I am grateful to all proof readers of various parts of the thesis: Alex, Álvaro, Audrey, Chun, Dinu and Felix.

Last but not least, I would like to thank my family and my adorable fiancée for all their love and support through all these years.

PUBLICATION LIST

A Mathis, AVM Herz, and M Stemmler: "The Resolution of Nested Neuronal Representations can be Exponential in the Number of Neurons". *Physical Review Letters*, 109 (1), 018103, 2012.

A Mathis, AVM Herz, and M Stemmler: "Optimal Population Codes for Space: Grid Cells Outperform Place Cells". *Neural Computation*, 24 (9):2280-2317, 2012.

A Mathis, M Stemmler, and AVM Herz: "The Entorhinal Cortex of Rodents Harbors an Optimal Grid Code for Space", in preparation

A Mathis, AVM Herz and M Stemmler: "The Effect of Correlations on Nested Grid Codes", in preparation

A Kammerer, A Mathis, M Stemmler, AVM Herz, C Leibold: "A Physiologically Inspired Model for Global Remapping in the Hippocampus", in preparation

Conference Contributions:

A Hartz, M Stemmler, A Mathis and AV Herz (2012) "Finite Size Effects in Grid-Cell Attractor Models for Spatial Navigation". *Front. Comput. Neurosci. Conference Abstract: Bernstein Conference*, Munich.

AJ Kammerer, A Mathis, Stemmler M, AV Herz and C Leibold (2012) "A Physiologically Inspired Model for Global Remapping in the Hippocampus". *Front. Comput. Neurosci. Conference Abstract: Bernstein Conference*, Munich.

J Nagele, D Patirniche, A Mathis, M Stemmler and AV Herz (2012) "Grid cells discharge with less variability than place cells". *Front. Comput. Neurosci. Conference Abstract: Bernstein Conference*, Munich.

FM Kempf, A Mathis, M Stemmler and AV Herz (2012) "Neural Representation of Space: Relation between one- and two-dimensional Environments". *Front. Comput. Neurosci. Conference Abstract: Bernstein Conference*, Munich.

A Mathis, A Herz and M Stemmler (2011) "How grid codes optimally encode space". *Society for Neuroscience Conference*, Washington.

A Mathis, A Herz and M Stemmler (2011) "Exponential Scaling of Nested Neuronal Representations", *Front. Comput. Neurosci. Conference Abstract: Bernstein Conference*, Freiburg.

A Mathis, A Herz and M Stemmler (2011) "Optimal Distribution of Spatial Periods for Grid Cell Ensembles on Finite Space". *9th Göttingen Meeting of the German Neurscience Society.*

D Patirniche, A Mathis, M Stemmler, A Herz (2011) "A Parametric Free Method for Estimating High Dimensional Tuning Curves". *9th Göttingen Meeting of the German Neuroscience Society.*

A Herz, C Kluger, A Mathis, M Stemmler (2011) "Variability of Grid Cell Firing On a Trial-To-Trial Basis". *9th Göttingen Meeting of the German Neuroscience Society.*

A Kammerer, A Mathis, M Stemmler, A Herz, C Leibold (2011) "A Physiologically Inspired Model for Global Remapping in the Hippocampus". *Computational Neuroscience Meeting CNS*2011*, Stockholm.

A Mathis, M Stemmler, A Herz (2010) "How Good is Grid Coding versus Place Coding for Navigation Using Noisy, Spiking Neurons?" *Front. Comput. Neurosci. Conference Abstract: Bernstein Conference*, Berlin.

C Kluger, A Mathis, M Stemmler and A Herz (2010) "Movement Related Statistics of Grid Cell Firing". *Front. Comput. Neurosci. Conference Abstract: Bernstein Conference*, Berlin.

A Mathis, M Stemmler, A Herz (2010) "How good is grid coding versus place coding for navigation using noisy, spiking neurons?" *Computational Neuroscience Meeting CNS*2010*, San Antonio.

A Mathis, M Stemmler, A Herz (2010) "How good is grid coding versus place coding for navigation using noisy, spiking neurons?" *AREADNE Research in Encoding and Decoding of Neural Ensembles*, Santorini.

EIDESSTATTLICHE ERKLÄRUNG

Ich versichere hiermit an Eides statt, dass die vorgelegte kumulative Dissertation von mir, wo nicht anderweitig gekennzeichnet, selbständig und ohne unerlaubte Hilfe angefertigt ist. Die Beiträge zu den Manuskripten waren wie folgt:

Die Erstellung der Veröffentlichung "A Mathis, AVM Herz, and M Stemmler: Optimal Population Codes for Space: Grid Cells Outperform Place Cells. Neural Computation, accepted February 7, 2012" unterlag folgender Arbeitsteilung: AM, AH and MS conceived and designed the research. AM performed research. AM, AH and MS discussed the results and wrote the paper.

Die Erstellung der Veröffentlichung "A Mathis, AVM Herz, and M Stemmler: The Resolution of Nested Neuronal Representations can be Exponential in the Num- ber of Neurons. PRL, accepted, April 18, 2012" unterlag folgender Arbeitsteilung: AM, AH and MS conceived and designed the research. AM performed research, MS did numerical simulation of estimator errors in Fig. 2c/d. AM, AH and MS discussed the results and wrote the paper.

Die Arbeit zum Manuskript "A Mathis, M Stemmler, and AVM Herz: The Entorhinal Cortex of Rodents Harbors an Optimal Grid Code for Space, preprint" unterlag folgender Arbeitsteilung: AM, AH and MS conceived and designed the research. AM performed research. AM, AH and MS discussed the results. AM drafted the current state of the manuscript.

München, Juni 2012

Alexander Mathis

Hiermit bestätigen die Mitautoren die von Herrn Mathis angegebenen Beiträge zu den einzelnen Publikationen.

München, Juni 2012

Martin Stemmler Andreas Herz